UNIVERSIDADE FEDERAL DE UBERLÂNDIA

CHEMISTRY INSTITUTE

Graduate Program in Chemistry
Laboratory of Photochemistry and Material Science

LEANDRO AUGUSTO FAUSTINO

Spectroscopic and electrochemical characterization of a terpyridine-based Ru(II) complex with 2-pyridylacetate as ancillary ligand

Uberlândia – MG

2022

LEANDRO AUGUSTO FAUSTINO

Spectroscopic and electrochemical characterization of a terpyridine-based Ru(II) complex with 2-pyridylacetate as ancillary ligand

Manuscript submitted to the Graduate Program in Chemistry from the Universidade Federal de Uberlândia as partial fulfillment of the requirements for the PhD degree in Chemistry.

Supervisor: Dr. Antonio Otavio de Toledo Patrocinio

Uberlândia – MG

2022

ATA

Programa de Pós-Graduação em:	Química				
Defesa de:	Tese de Doutorado Acadêmico, 126, PPGQUI				
Data:	Trinta e um de março de dois mil e vinte e dois	Hora de início:	13:30	Hora de encerramento:	18:00
Matrícula do Discente:	11813QMI008				
Nome do Discente:	Leandro Augusto Faustino				
Título do Trabalho:	Spectroscopic and electrochemical characterization of a terpyridine-based Ru(II) complex with 2-pyridylacetate as ancillary ligand				
Área de concentração:	Química				
Linha de pesquisa:	Química Bioinorgânica, Fotoquímica e Fotobiologia				
Projeto de Pesquisa de vinculação:	Estudo espectroeletroquímico de fotocatalisadores híbridos para aplicações em conversão de energia solar em combustíveis				

Reuniu-se por meio de webconferência, Plataforma Maicrosoft Teams, link https://teams.microsoft.com/dl/launcher/launcher.html? url=%2F_%23%2Fl%2Fmeetup-join%2F19%3A6V4Vpf-SwYAt9lGBwv0XOnvgU9WjiqCLIiEEMuBzqrk1%40thread.tacv2%2F 1643663366963%3Fcontext%3D%257B%2522Tid%2522%253A%2522cd5e6d23cb99-4189-88ab-1a9021a0c451%2522%252C%2522Oid%2522%253A%2522244beae2-a3e1-4a65-8320-88b2e06d3952%2522%257D%26anon%3Dtrue&type=meetupjoin&deeplinkId=32e406bd-4d9e-4b57-b344-862d275cbd68&directDl=true&msLaunch=true&enableMobilePage=true& suppressPrompt=true, a Banca Examinadora, designada pelo Colegiado do Programa de Pós-graduação em Química, assim composta: Professores Doutores: Lucas Carvalho Veloso Rodrigues, da Universidade de São Paulo; André Luiz Barboza Formiga, da Universidade Estadual de Campinas; André Luiz Bogado e Gustavo Von Poelhsitz, da Universidade Federal de Uberlândia e Antonio Otavio de Toledo Patrocinio, orientador do candidato.

Iniciando os trabalhos o presidente da mesa, Dr. Antonio Otavio de Toledo Patrocinio, apresentou a Comissão Examinadora e o candidato, agradeceu a presença do público, e concedeu ao Discente a palavra para a exposição do seu trabalho. A duração da apresentação do Discente e o tempo de arguição e resposta foram conforme as normas do Programa.

A seguir o senhor(a) presidente concedeu a palavra, pela ordem sucessivamente, aos(às) examinadores(as), que passaram a arguir o(a) candidato(a). Ultimada a arguição, que se desenvolveu dentro dos termos regimentais, a Banca, em sessão secreta, atribuiu o resultado final, considerando o(a) candidato(a):

Aprovado.

Esta defesa faz parte dos requisitos necessários à obtenção do título de Doutor.

O competente diploma será expedido após cumprimento dos demais requisitos, conforme as normas do Programa, a legislação pertinente e a regulamentação interna da UFU.

Referência: Processo nº 23117.015216/2022-81   SEI nº 3496563

I dedicated this project to my parents, Idivana and Antonio, for being my light. To my brother, Evandro, my best friend. To my fiancé Kenepher for all the love.

"Science is not only a disciple of reason but, also, one

of romance and passion"

Stephen Hawking

ACKNOWLEDGEMENTS

TABLE OF CONTENTS

RESUMO

Compostos de coordenação são capazes de catalisar reações de grande interesse tecnológico, como por exemplo, a oxidação da água ou a redução de CO_2. Neste trabalho, o novo complexo de Ru(II) [RuCl(trpy)(acpy)], trpy = 2,2':6',2"-terpiridina, acpy = 2-piridilacetato foi sintetizado e suas propriedades espectroscópicas, eletroquímicas e catalíticas exploradas em detalhe. Espectros de ressonância magnética nuclear de hidrogênio e espectroscopia vibracional no infravermelho foram empregados para comprovação estrutural do composto e sugerem a coordenação bidentada do ligante acpy. Ensaios espectrofotométricos, corroborados por simulações teóricas, revelam que as transições eletrônicas de menor energia são dominadas por transferências de carga do metal para o ligante (MLCT). Ensaios eletroquímicos revelam que em potenciais anódicos, o pico redox observado em 0.006 V *vs* Fc/Fc$^+$, corresponde ao par redox Ru$^{II/III}$. Em potenciais catódicos, dois picos de redução são observados em -1.95 V e -2.20 V *vs* Fc/Fc$^+$ sendo atribuídos à redução do ligante trpy e do centro metálico, respectivamente. Sob condições anidras e atmosfera de CO_2 o complexo apresentou atividade eletrocatalítica convertendo CO_2 à CO com um TON$_{CO}$ = 12 e k$_{cat}$ = 1.5 s^{-1}. Na presença de 1% de água (v/v), os valores de TON$_{CO}$ = 21 e k$_{cat}$ = 2.0 s^{-1} foram encontrados e, adicionalmente, formato foi detectado com um TON$_{HCOO^-}$ = 7. As eficiências faradaicas obtidas com 1% de água foram de 76% e 20%, respectivamente para CO e formato. Experimentos de espectroeletroquímica na região do infravermelho e sob atmosfera de CO_2 revelam a possível formação do metalocarboxilato (Ru-COO$^-$). Na presença de água a possível quebra do quelato foi observada.

Palavras-chave: catalisadores homogêneos, compostos de coordenação, eletrorredução de CO_2, complexos de rutênio, transferência eletrônica.

ABSTRACT

Coordination compounds are capable of catalysing reactions of great technological interest, for example, the watter splitting or the CO_2 reduction. In this project, the new Ru(II) complex, [RuCl(trpy)(acpy)], trpy = 2,2':6',2"-terpyridine, acpy = 2-pyridylacetate was synthesized and its spectroscopic, electrochemical and catalytic properties explored in detail. Hydrogen nuclear magnetic resonance and vibrational infrared spectra were used to prove the structure of compound and suggest the bidentated coordination of acpy ligand. Spectrophotometric essays, corroborated by theoretical simulations, reveal that lower electronic transitions are dominated by metal-ligand charge transfer (MLCT). Electrochemical studies revealed that in anodic potentials the peak observed at 0.006 V *vs* Fc/Fc$^+$ correspond to the redox pair Ru$^{II/III}$. In cathodic potentials, two reduction peaks were detected at -1.95 V and -2.20 V *vs* Fc/Fc$^+$, being attributed to the trpy and metal center reductions respectively. Under anhydrous conditions and a CO_2 atmosphere, the complex presented an electrocatalytic activity converting CO_2 to CO with a TON$_{CO}$ = 12 and k$_{cat}$ = 1.5 s^{-1}. In the presence of 1% water (v/v), the TON$_{CO}$ = 21 and k$_{cat}$ = 2.0 s^{-1} were obtained and, additionally, formate was detected with TON$_{HCOO^-}$ = 7. The faradaic efficiencies obtained with 1% water were 76% and 20%, respectively for CO and formate. Spectroelectrochemical experiments in the infrared range and under a CO_2 atmosphere reveal the possible formation of the metallocarboxylate (Ru-COO$^-$). In the presence of water the possible chelate breakdown was observed.

Keywords: homogeneous catalysts, coordination compounds, CO_2 electrorreduction, ruthenium complexes, electron transfer.

ABBREVIATIONS AND SYMBOLS

MLCT	Metal-Ligand Charge Transfer;
LLCT	Ligand-Ligand Charge Transfer;
ILCT	Intraligand Charge Transfer;
TLC	Thin Layer Chromatography;
λ	Wavelength (nm);
ε	Extinction Molar Coefficient (L mol^{-1} cm^{-1});
Δt	Time Variation (s).
CV	Cyclic Voltammetry
WE	Working Electrode
CE	Counterelectrode
RE	Reference Electrode
FTIR	Fourier Transform Infrared Absorption Spectroscopy
SEC	Spectroelectrochemistry
BE	Bulk Electrolysis
GC	Gas Chromatography
^{1}H NMR	Hydrogen Nuclear Magnetic Ressonance
H-H Cosy	Bidimensional Hydrogen Correlation Spectroscopy
d	Doublet
s	Singlet
t	Triplet

dd	Double Doublet
Fc/Fc$^+$	Ferrocene/Ferrocenium
HOMO	Highest Occupied Molecular Orbital
LUMO	Lowest Unoccupied Molecular Orbital
SOMO	Singly Occupied Molecular Orbital
ppm	Parts per million
TON	Turnover Number

LIST OF FIGURES

LIST OF TABLES

1. INTRODUCTION

The population growth associated with the development of new technologies in the past decades has led to an increase in the energy demand worldwide. The energy consumption in 1950 was around 28.5 TW h^{-1} contrasting to 173.3 TW h^{-1} in 2019 (RITCHIE; ROSER, 2020). The demand is expected to be even higher in the following years. Moreover, different countries around the world have as major energy source fossil fuels, such as natural gas, oil and coal (MOHSIN, MUHAMMAD et al., 2021).

A series of problems can be attributed to the use of those fuels, but the high emission rates of greenhouse gases, such as CO_2, are of special concern (OMRI et al., 2015; AYE; EDOJA, 2017; ZAFAR et al., 2019; KHAN; KHAN; REHAN, 2020; HUSSAIN; REHMAN, 2021). According to the bulletin of the World Meteorological Organization (WMO), in 2020 a new record of greenhouse gases trapped in the atmosphere was reached, 413.2 ppm, which corresponds to 149% of the pre-industrial level. One more consideration that must be taken is that, in 2020, the world faced the COVID-19 pandemics. During this time with, the economic slowdown, it was expected a decreasing in the CO_2 emission rates but, in fact such a decrease was not observed according tho the WMO bulletin (BASSO et al., 2021). The high concentrations of CO_2 in the atmosphere have associations with climate changes as it induces an increase of global temperature average. Consequently, other problems begin to arise such as ocean acidification, glacier melting which increase the sea level, leading to the extinction of several species (ZHANG, R.-Z. et al., 2020).

As long the concentration of CO_2 continue to arise, the world will still face the problems of global warming. Thus, to overcome the greenhouse gases

emission and solve the energy challenges, strategies for the development of new renewable and less aggressive energy sources are needed to promote a sustainable development (MOHSIN, M. et al., 2018; SHAH et al., 2019). Sunlight is pointed as a key alternative for green energy production as it is available wordwide and in large quantities. It must be absorbed and converted to be further distributed and used on demand. Natural photosynthesis is an example of these processes as radiant energy drives the conversion of low energy and Earth abundant species (H_2O and CO_2) on high-energetic species (sugars) and O_2, through biomolecules, Equation 1.

$$6\,H_2O + 6\,CO_2 \xrightarrow{h\nu} C_6H_{12}O_6 + O_2$$
<div align="right">Equation 1</div>
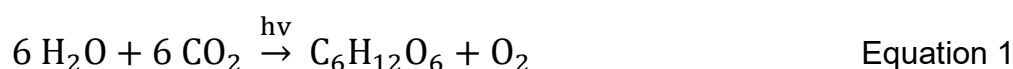
In the natural photosynthesis, the water molecule is split into protons, electrons and molecular oxygen. Protons and electrons are combined with CO_2 to yield glycose. It is estimated that this process produces 100 billion tons of dry biomass, which corresponds to an energy supply around 100 TW (BARBER, 2009). Therefore, solar-to-fuels energy conversion is a necessary tool for change our current dependence on fossil fuels.

Mechanistically the photosynthetic process is more complicated than it sounds. Two different photosystems are involved: PSI and PSII. In PSII, the so-called Kok cycle takes place and the water molecules are photooxidized into molecular oxygen releasing protons and redox equivalents. This reaction is catalyzed by a well studied *oxygen evolving center*, a cluster containing four Mn ions binded by oxo bridges and exhibit different redox during the catalytic cycle, Figure 1 (SCHMIDT; HUSTED, 2019).

Figure 1. General represenation of the Kok cycle in PSII.
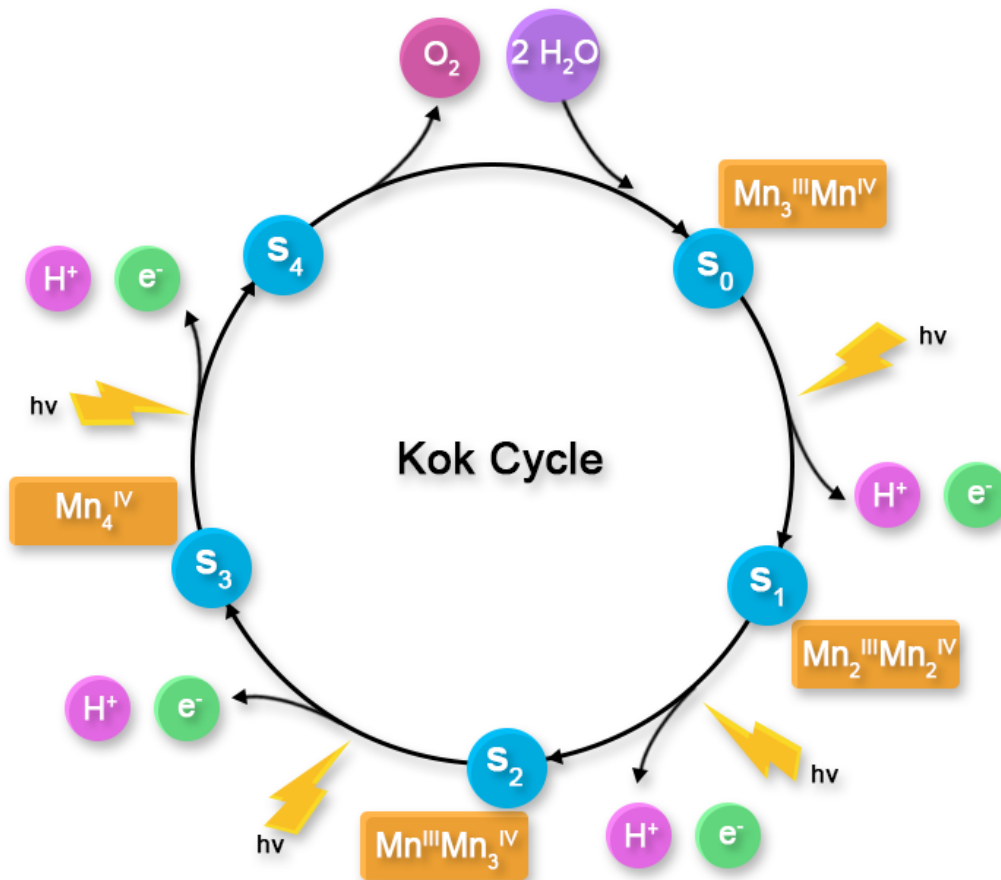
Adapted from (KÄRKÄS et al., 2014; SCHMIDT; HUSTED, 2019)

The protons and redox equivalents formed in the PSII are transferred to PSI through molecules of ATP (adenosine triphosphate) and NADPH (nicotinamide adenine dinucleotide phosphate), where in the Calvin cycle the CO_2 reduction occurs (KOK; FORBUSH; MCGLOIN, 1970; RAINES, 2003), Figure 2. In the Calvin cycle, CO_2 fixation occurs through the association with ribulose 1,5-bisphosphate (RuBP) aided by the ribulose-1,5-biphosphate carboxylase/oxygenase protein (RuBisCO). After it, ATP and NADPH molecules are used as reducing agents producing species which will be converted into carbohydrates.

Figure 2. General representation of Calvin cycle in PSI.
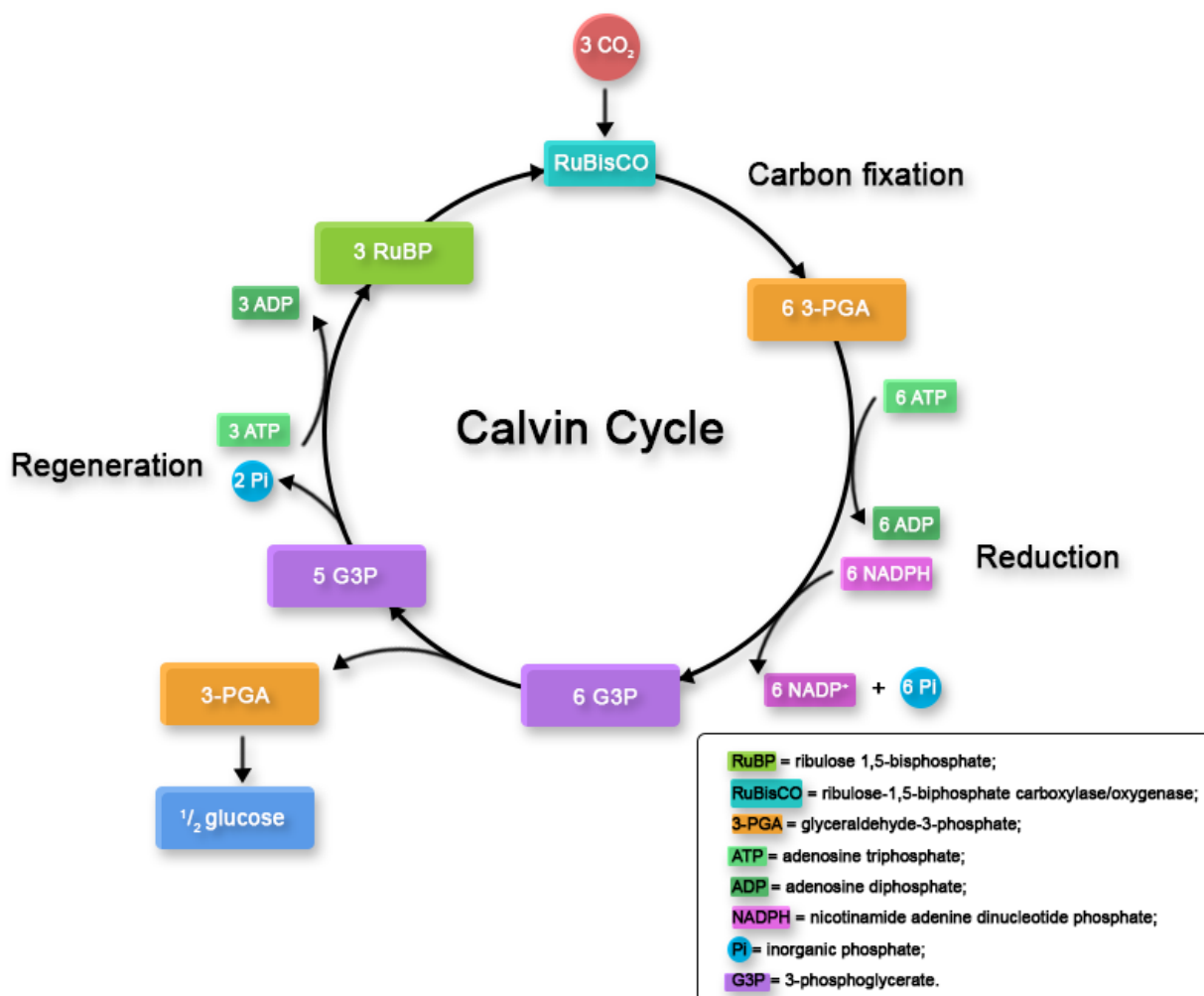
Adapted from (VECCHI et al., 2020)

Mimicking the natural photosynthetic process is challenging. The whole photosynthetic process involves several steps with different kinetic regimes, as shown in Figures 1 and 2. One way to study and optimize it is by focusing on a single process independently, separating the water oxidation reactions from the CO_2 reduction (BERARDI et al., 2014). As a result of multiple studies on the catalytic sites of the natural photosynthesis, coordination compounds are identified as potential candidates to act as arficial catalysts for CO_2 reduction and

water oxidation and, therefore, have attracted great attention in the last few decades (ANDREIADIS et al., 2011; KÄRKÄS et al., 2014; KNÖR, 2015; KIM; EDRI; FREI, 2016; ZHANG; SUN, 2019; BOUTIN et al., 2020).

This interest has emerged from the fact that these compounds have multiple redox states, which can be accessed at relatively low overpotentials by susceptible electron and proton transfers (LOUIS et al., 2019). Moreover, it is necessary to highlight the feasibility of tuning their properties by varying ligands through concepts of molecular engineering (HORVÁTH et al., 1998; ZHANG, S. et al., 2020). The selection of ligands is an important approach in the catalytic process, leading to changes in the electronic and steric effects, which can tune the reactivity, selectivity and stability of these inorganic catalysts (NAKAMURA et al., 2015; COSTENTIN; SAVÉANT, 2017; RAMAKRISHNAN; CHIDSEY, 2017).

1.1. CO_2 reduction mediated by coordination compounds

As described in the previous section, the emission of CO_2 in the atmosphere is a major environmental concern and its capture and conversion into other products are urgent. CO_2 reduction is an endergonic and non-spontaneous process. The one-electron reduction of CO_2 to $CO_2^{\bullet-}$ requires a potential of $E^0 = -1.85$ V *vs* NHE (aqueous solution pH = 7) (KOPPENOL; RUSH, 1987; YIN et al., 2020). Additionally, considerable overpotentials are observed given the symmetry and low polarity of the CO_2 molecule. Multi-electron proton transfer can reduce the kinetic and thermodynamic barriers, leading to several products according to Table 1 (CHANG; WANG; GONG, 2016; ULMER et al., 2019; SILVA et al., 2021).

Table 1. Possible CO_2 reduction processes in aqueous solution with the respectives potentials reductions *vs* NHE at pH = 7.

Equation	E^0 (V)
$CO_2 + e^- \rightarrow CO_2^{\bullet-}$	-1.85
$CO_2 + 2\ H^+ + 2\ e^- \rightarrow HCOOH$	-0.61
$CO_2 + 2\ H^+ + 2\ e^- \rightarrow CO + H_2O$	-0.53
$CO_2 + 4\ H^+ + 4\ e^- \rightarrow HCHO + H_2O$	-0.48
$CO_2 + 6\ H^+ + 6\ e^- \rightarrow CH_3OH + H_2O$	-0.38
$CO_2 + 8\ H^+ + 8\ e^- \rightarrow CH_4 + 2\ H_2O$	-0.24

(SHEN et al., 2020)

The CO_2 reduction driven by a two-electron transfer results in the formation of HCOOH or CO. The formation of HCOOH is an advantage since it can be used as a molecular hydrogen storage (LAURENCZY; DYSON, 2014; KANEGA et al., 2020). The interest in hydrogen as a green fuel has raised exponentially in the recent years (JAIN, 2009; PAL et al., 2018; ATILHAN et al., 2021; OLIVEIRA; BESWICK; YAN, 2021). On the other hand, CO is also well-kown feedstock in the chemical industry and is typically produced by the reverve Water Gas Shift Reaction (WGSR). The CO resulting from this catalytic process is an useful input for industrial chemistry, taking place of the so-called Fischer-Tropsch processes and also in the production of alcohols, such as, methanol (STEYNBERG, 2004; HILDEBRANDT et al., 2009; GONZÁLEZ-CASTAÑO; DORNEANU; ARELLANO-GARCÍA, 2021).

Considering the importance of the possible products formed by multi-electron reduction of CO_2, it is clear that this process requires catalysts to accelerate these reactions. Such catalysts must have the suitable properties to

be activated at low overpotentials. Different classes of catalysts have been studied during the past years being both heterogenous or homogenous catalysts.

Inside the class homogenous catalysts, molecular catalysts have attracted attention due to the fact that it is possible to tune their electronic and structural properties. For example, in the case of catalysts based on coordination compounds, the electronic density over the metal center can be tuned by the selection of ligands incorporating groups with electron-donating or even electron-withdrawing character (SUN et al., 2011; JOHNSON et al., 2016b; SUNG et al., 2017). In addition, the focus on the influence of the second coordination sphere have been gained attention. Some examples reported in the literature include strategies that the ligand can trigger the catalytic process by a steric bulk effect or even by intramolecular interactions via hydrogen bonds, facilitating the interaction with substrate (SCHMEIER et al., 2011; SEU et al., 2012; AGARWAL et al., 2015; COSTENTIN et al., 2015; NERI et al., 2016; SAMPSON; KUBIAK, 2016; NGO et al., 2017; SUNG et al., 2017).

In most cases, catalyst is synthesized in an inactive form and must be activated by an external source of energy, which can be provided in different ways. Thus, CO_2 reduction mediated by homogeneous catalysts can occur by diverses routes (SCHAUB; PACIELLO, 2011; KREIMEYER, 2013; ROHMANN et al., 2016; LOGEMANN et al., 2021). Here the focus will be in the photochemical and electrochemical routes (FAUSTINO et al., 2018; SOUZA et al., 2020).

The photochemical CO_2 reduction mechanism mediated by metal complexes is still under discussion by several researchers, but this process usually involves the reductive quenching of a ^{3}MLCT (metal-ligand charge transfer) state (SOUSA, S. F. et al., 2014; PRADO et al., 2017). In this case, the

catalyst or photosensitizer absorbs the light generating a ^{3}MLCT excited state, which is quenched by a sacrificial donor (MÜLLER et al., 2017). After that, the reduced catalyst interacts with CO_2 leading to aducts which are reduced again and CO is released to restart the catalytic cycle (TAKEDA et al., 2008). The electrochemical process has several steps in common with the photochemical one, but no quencher is used in it (SOUSA, SINVAL F; PATROCINIO, 2014). In this case the activation of catalyst is initiated by the electron transfer between the electrode surface and the catalyst. After it the reduced catalyst interacts with CO_2 as in the photochemical pathway. A general catalytic cycle based on different literature reports can be observed in Figure 3 (SILVA et al., 2021).

Figure 3. Pathways proposed for CO_2 reduction through photo and electrocatalysis by metal carbonyl complexes.
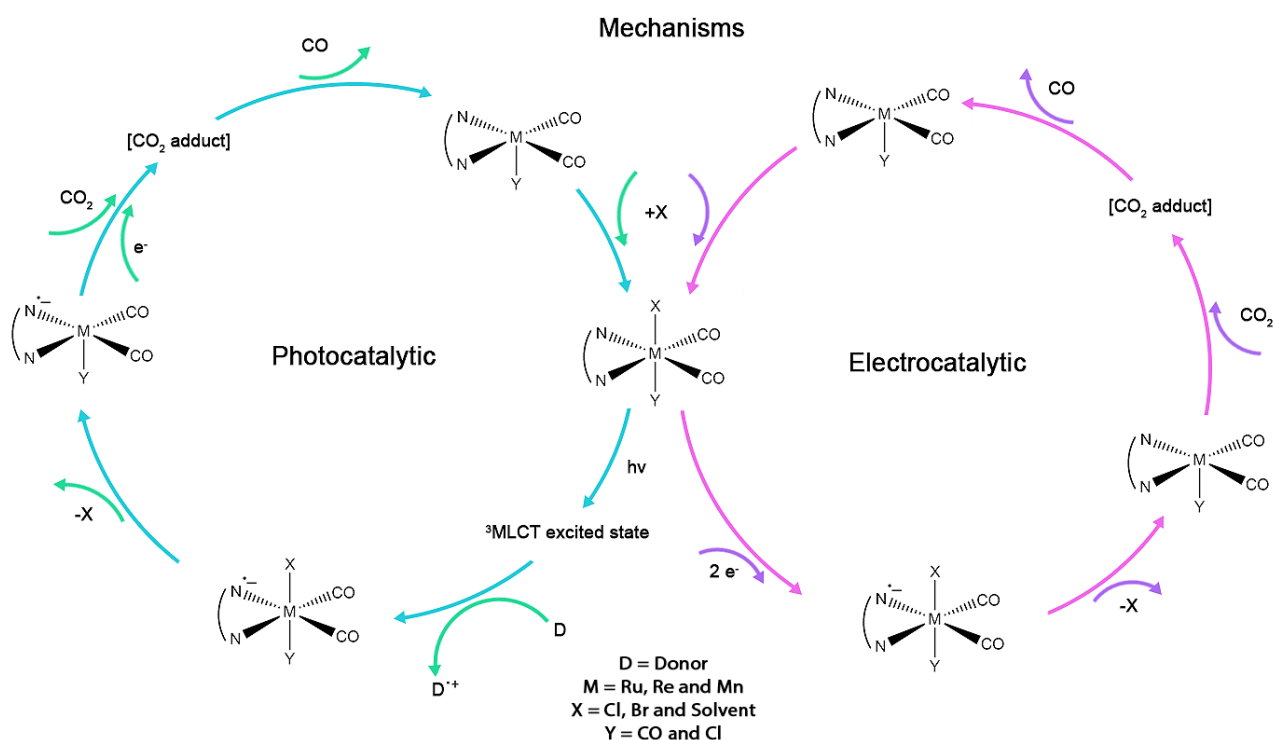
Adapted from (SILVA et al., 2021)

Different Ir(III), Re(I), Mn(I) and Ru(II) complexes, d^6 configuration, have been studied as catalysts for CO_2 reduction. Usually their designs are based on structures containing polypyridyl ligands and a monodentade ligand which ensure the catalytic site. Also, there are differences in the catalytic pathways according to the metal and ligands. For example, Ir(III) complexes have shown great turnover numbers (TONs) ranging from 222 000 and 3 500 000 for HCOOH as reported by Himeda, Tanaka and collaborators (HIMEDA et al., 2007; TANAKA, R.; YAMASHITA; NOZAKI, 2009). If on the one hand they present high values for HCOOH formation, in the case of these Ir(III) complexes, the disadvantage is that extreme conditions, such as high temperature and pressure, are necessary. Furthermore, iridium is a non-abundant metal and, consenquetly, it is expensive (SILVA et al., 2021). Likewise, Re(I) complexes have shown high selectivities for CO production, although the synthetic costs are high when compared with their Mn(I) analogs, which have shown a catalytic response with lower overpotentials (SINOPOLI et al., 2018). The use of catalysts based on first row transition metals have been investigated just in the recent years. In the past it was believed that the lower robustness of catalysts base on the first row transition metals could be a problem when compared with compounds based on noble metals (ALIG; FRITZ; SCHNEIDER, 2019). Catalysts based specifically on ruthenium complexes will be discussed in the next section.

1.2. Ruthenium complexes as electrocatalysts for CO_2 reduction

Ruthenium complexes are among the most studied species due to their versatility (ARENDS; KODAMA; SHELDON, 2004; DAS et al., 2017). Such interest may be due to the possibility of accessing many oxidation states

(MÄGERLEIN et al., 2007), varying from -II, which the metal center has the configuration d^{10}, up to +VIII, configuration d^0 (TAKEUCHI et al., 1983). Another characteristic is that ruthenium can accommodate a vast class of ligands with different coordination modes (ADENIYI; AJIBADE, 2016). Thereby, several Ru(II)-based complexes were studied as electrocatalysts for CO_2 reduction.

The first studies about Ru(II) complexes as electrocatalysts for CO_2 reduction were made by Tanaka and collaborators using the compounds shown in Figure 4 (TANAKA, K.; MORIMOTO; TANAKA, 1983; ISHIDA; TANAKA; TANAKA, 1987).

Figure 4. First reported Ru(II) electrocatalysts for CO_2 reduction.

$[Ru(bpy)_2(CO)_2]^{2+}$ $\qquad$ $[Ru(bpy)_2(CO)Cl]^+$
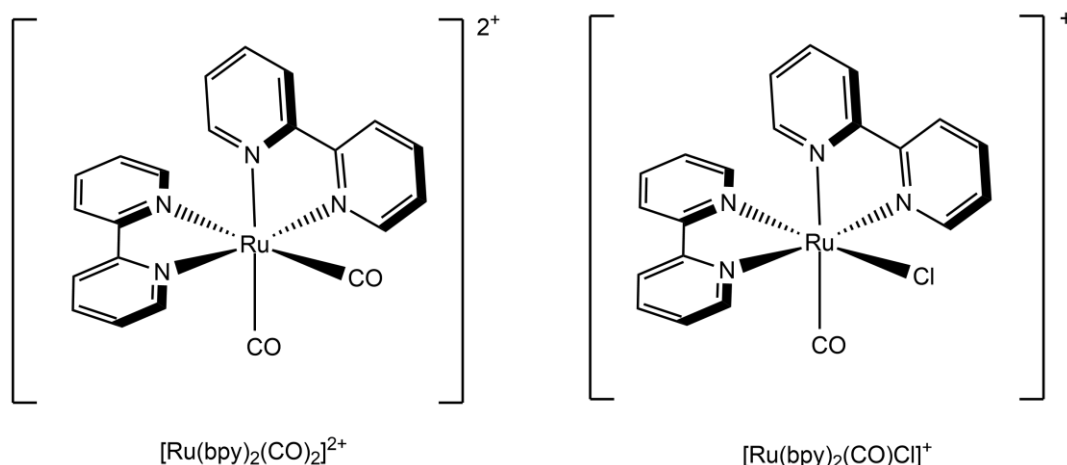
Adapted from (TANAKA, K.; MORIMOTO; TANAKA, 1983; ISHIDA; TANAKA; TANAKA, 1987).

In these studies, the authors evaluated the best catalytic conditions, products, selectivity and insights about the reaction mechanism. They observed that the pH is closely connected to the different products formed during the process. For example, in low pHs the major product formed was CO (TON_{CO} ~ 26 DMF/H_2O 1:1 for both complexes) and H_2. By contrast, at high pHs $HCOO^-$ was the major product (TON_{HCOO^-} = 18 for $[Ru(bpy)_2(CO)_2]^{2+}$ and TON_{HCOO^-} = 11

for $[Ru(bpy)_2(CO)Cl]^+$ DMF/H_2O 1:1) (ISHIDA et al., 1987; ELGRISHI et al., 2017). In the perspective of mechanistic insights, it was observed that after 2-electron reduction, one of the bpy ligand tends to labilize with further electropolymerization through Ru-Ru bonds at the electrode surface. As a consequence, the deactivation of the catalyst occurs (COLLOMB-DUNAND-SAUTHIER; DERONZIER; ZIESSEL, 1994; WANG et al., 2015). In order to prevent the electropolymerization, it was proposed that one of the bpy ligands could be replaced by a trpy ligand, Figure 5 (NAGAO; MIZUKAWA; TANAKA, 1994; CHEN et al., 2011; CHEN et al., 2014; DAS et al., 2017).

Figure 5. Molecular structure reported of $[Ru(trpy)(bpy)(CH_3CN)]^{2+}$
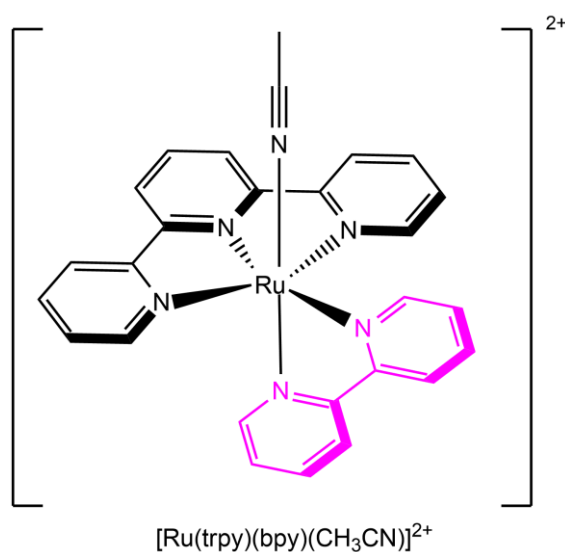
$[Ru(trpy)(bpy)(CH_3CN)]^{2+}$

Adapted from (NAGAO; MIZUKAWA; TANAKA, 1994; CHEN et al., 2011; CHEN et al., 2014; DAS et al., 2017)

The $[Ru(trpy)(bpy)(CH_3CN)]^{2+}$ hindered the electropolymerization, but it was still unstable under typical reaction conditions. Comparing the TON_{CO} for $[Ru(bpy)_2(CO)_2]^{2+}$ and $[Ru(bpy)_2(CO)Cl]^+$ with the $[Ru(trpy)(bpy)(CH_3CN)]^{2+}$, the value obtained for the latter was even smaller (TON_{CO} = 7 CH_3CN/H_2O 9:1)

(CHEN et al., 2014). This can be explained by the strong CO coordination to the metal center, difficulting its release, and consequently inhibiting the catalytic process (PETERSON; NØRSKOV, 2012; AKHADE et al., 2014; RAMAKRISHNAN; CHIDSEY, 2017).

In order to increase the catalytic activity of ruthenium trpy-based complexes, studies about the influence of bidentade ligands are under way. One of the strategies that have been studied consists in the use of the so-called *trans* effect to decrease the stability of the metal carbonyl intermediate, easing the release of CO. Using this strategy, a ligand with a strong σ-donor character is positioned *trans* to the coordination site where CO_2 is expected to bind (CHEN et al., 2011; GONELL et al., 2020). Based on this approach different research groups have proposed different Ru(II)-trpy complexes to evaluate how the coordination site *trans* to the CO_2 binding site, Figure 6, can affect the electrocatalytic properties (LEE et al., 2018; GONELL et al., 2020).

Figure 6. Molecular structure reported of $[Ru(trpy)(Mebim-py)(CH_3CN)]^{2+}$ and $[Ru(trpy)(pqn)(CH_3CN)]^{2+}$.

$[Ru(trpy)(Mebim-py)(CH_3CN)]^{2+}$ $[Ru(trpy)(pqn)(CH_3CN)]^{2+}$
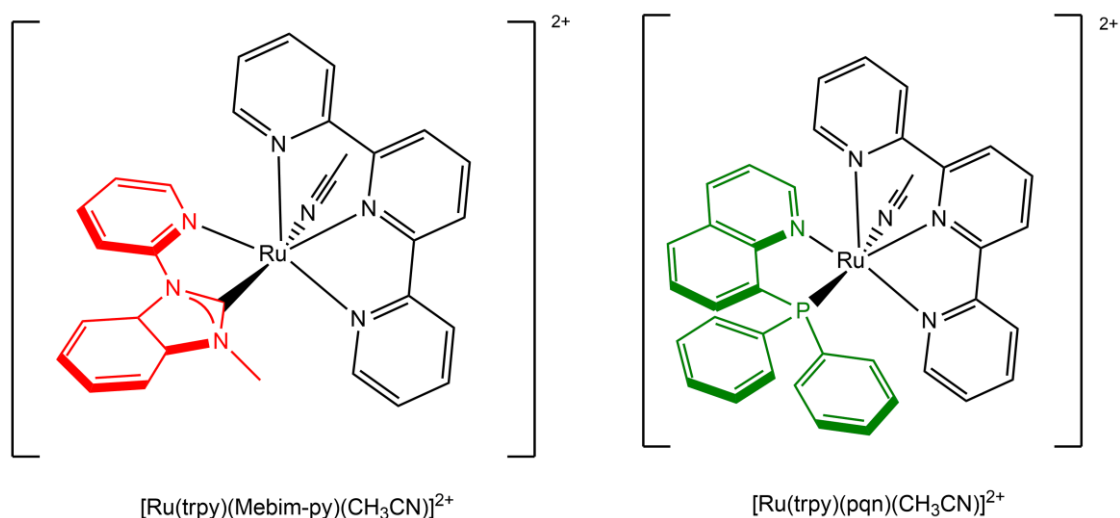
Adapted from (LEE et al., 2018; GONELL et al., 2019)

In Figure 6, it is possible to observe that two different ligands are positioned *trans* to the possible coordination site of CO_2. The N-heterocyclic carbene is expected to have a higher σ-donor character than the phosphine ligand. The strong σ-donor character increases the electronic density of the metal center and as consequence, an increase in the bond distance between the ligand positioned *trans* to the σ-donor is observed. As a consequence, in the activated state, it destabilizes the carbonyl complex releasing CO. In the case of [Ru(trpy)(Mebim-py(CH$_3$CN)]$^{2+}$ the TON reached in the bulk electrolisys experiments was 30 (CH$_3$CN/H$_2$O 95:1), while for the [Ru(trpy)(pqn)(CH$_3$CN)]$^{2+}$ it was 2. It shows that the M-CO bond is strongly influenced by the *trans* effect.

Based on that, the focus of this project was to employ a ligand with a moderate *trans* effect, acpy = 2-pyridylacetate, and evaluate how it can affect the catalytic properties of its corresponding complex, [RuCl(trpy)(acpy)], Figure 7.

Figure 7. Possible bond isomers for [RuCl(trpy)(acpy)].
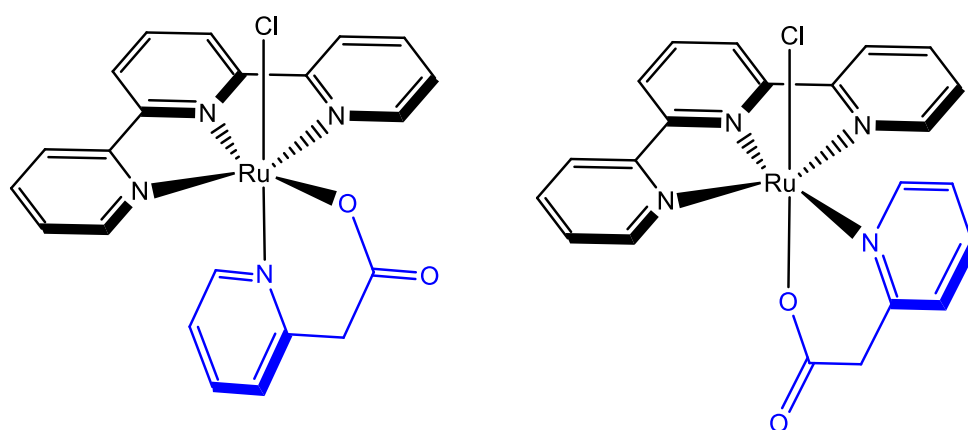
2. OBJECTIVES

The main objective of this work was to synthesize a new ruthenium(II) complex following by a detailed spectroscopic and electrochemical characterization to investigate its potential as electrocatalyst for CO_2 reduction. For that, some specific objectives were proposed:

- Carry out UV-Vis and IR spectroelectrochemical experiments in order to identify key reaction intermediates;

- Evaluate the influence of adding H_2O as a Brønsted acid on the product selectivity;

- Investigate the stability of the Ru-acpy chelate as a function of the metal oxidation state.

3.   MATERIALS AND METHODS

3.1.   Preparation and purification of materials

3.1.1. Trichloride(2,2':6',2"-terpyridine)ruthenium(III) – [RuCl$_3$(trpy)]

The complex was synthesized according to previous procedures described in the literature (SULLIVAN; CALVERT; MEYER, 1980; NILLES et al., 2018). In a round bottom flask 0.562 g (2.41 mmol) of RuCl$_3$.xH$_2$O (Aldrich) and 0.500 g (2.41 mmol) of 2,2':6',2"-terpyridine (Aldrich) were added in 30 mL of absolute ethanol (Vetec). The mixture was refluxed for 3 hours under argon atmosphere and monitored by thin layer chromatography in methanol saturated with NaCl. The mixture was cooled to room temperature. The brown solid formed was filtered under vacuum and washed with 3 portions of ethanol (30 mL) (Vetec) and 3 portions of ether (30 mL) (Vetec).   The material was dried under reduced pressure. 0.623 g (1,41 mmol) of product were obtained, corresponding to a yield of 58%.

3.1.2. Chloride   2-pyridylacetate(2,2':6',2"-terpyridine)ruthenium(II)   – [RuCl(trpy)(acpy)]

The complex was synthesized based on procedures reported in the literature for similar complexes (LLOBET; DOPPELT; MEYER, 1988; CHOWDHURY et al., 2011). In a round bottom flask 0.400 g (0.91 mmol) of [RuCl$_3$(trpy)], 2 mL (14 mmol) of triethylamine (Aldrich) and 0.395 g (2.27 mmol)

of 2-pyridylacetic acid hydrochloride (Aldrich) were added in 30 mL of absolute ethanol (Vetec). The mixture was stirred for 1.5 hours under argon atmosphere, and protected from the light at room temperature monitored by thin layer chromatography in dichloromethane:methanol (20:1) saturated with NaCl. After the procedure, the mixture was filtered under vacuum. A dark purple powder was collected and washed with portions of water and ether (Vetec). The material was dried under reduced pressure. 0.320 g (0.632 mmol) were obtained, corresponding to a yield of 69%.

^{1}H NMR (DMSO-d_6): 9.84 (1H, d, J = 8.0 Hz); 8.61 (4H, d, J = 8.0 Hz); 8.34 (2H, d, J = 8.0 Hz); 8.07 (1H, td, J_1 = 4.0 Hz, J_2 = 8.0 Hz, J_3 = 20.0 Hz); 7.96 (2H; td, J_1 = 4.0 Hz, J_2 = 8.0 Hz, J_3 = 16.0 Hz); 7.87 (1H, t, J_1 = 8.0 Hz, J_2 = 16.0 Hz); 7.75, t, (J_1 = 8.0 Hz, J_2 = 16.0 Hz); 7.68 (1H, d, J = 8.0 Hz); 7.55 (2H, td, J_1 = 4.0 Hz, J_2 = 8.0 Hz, J_3 = 12.0 Hz); 3.61 (2H, s). ESI-MS analysis: theoretical (*m/z*+H) = 507.015 (100%); *found*: (*m/z*+H) = 507.015. Elemental analysis for $C_{22}H_{17}ClN_4O_2Ru.(2.H_2O)$, calculated: C, 48.76%; H, 3.91%; N, 10.34%; obtained: C, 48.84%; H, 3.84%; N, 10.31%.

3.2.   Methods

The syntheses of the complexes were monitored by thin layer chromatography (TLC). The samples were placed in chromatographic plates covered with silica (Aldrich), which contains a luminescent indicator. The mobile phase used was dichloromethane:methanol (20:1) saturated with NaCl. The observation of stains happened in a dark chamber (Spectroline, model CM-10A) under UV lighthing at 254 and 365 nm.

Elemental analysis were performed in a elemental analyzer CHNS/O (PerkinElmer, model 2400).

Electronic absorption spectra were recorded with a single-beam spectrophotometer (Thermo-Scientific, model Evolution 201) and rectangular quartz cuvettes with optical paths of 1.000 or 0.100 cm were used.

Attenuated total reflectance fourier transform infrared (ATR-FTIR) spectra were recorded on a spectrometer (PerkinElmer, model FT-IR Frontier Single Range - MIR Spectra) equipped with a diamond crystal plate, using 16 scans at a resolution of 4 cm^{-1}.

^{1}H NMR spectra were recorded with a DRX-400 Bruker Ascend 400 MHz spectrometer at 298 K. Residual solvent signals were used as internal standards.

Mass spectra were recorded in a high resolution spectrometer QTOF (Agillent®, model 6520 B), with ionization by electrospray. The spectrometers were located in the Nanobiotechnology Laboratory (IBTC) at Universidade Federal de Uberlândia and in the Artificial Photosynthesis Group (APG) at Brookhaven National Laboratory. The samples were solvated in the methanol/water (4:1) mixture and introduced in the equipment using a syringe (100 μL) and a direct infusion pump with a flow of 200 μL h^{-1} was used. The ionization was performed with a nebulizer gas (20 psi), the drying gas was heated to 200 ºC with flows of 8.0 L min^{-1} and a tension of 4.5 kV was applied to the capillary. The spectra were acquired in the positive mode. The values of mass/charge calculated for the charged ion were obtained from ChemDraw Ultra 12.0 software.

Electrochemical measurements were carried out in a potentiostat (Metrohm Autolab, model PGSTAT204) employing a glassy carbon working

electrode (WE), a platinum wire as the counterelectrode (CE) and Ag/AgCl (3 mol L^{-1}) as the pseudo-reference (RE). Potentials were recorded using ferrocene as the internal standard. 0.1 mol L^{-1} TBAPF$_6$ solutions in anhydrous acetonitrile or dichloromethane were employed as the supporting electrolyte. All the potentials are represented *versus* Fc/Fc$^+$ (E^0 = 0.48 V *vs* Ag/AgCl).

The spectroelectrochemical experiments (SEC) were performed in the UV-Vis and FTIR ranges. In the UV-Vis experiments, a quartz cuvett coupled with three electrodes was used. The electrodes used were an Ag/AgCl wire as the pseudo-referece electrode (RE), a platinum wire as the counterelectrode (CE) and a platium grid as the working electrode (WE) connected to a potentiostat (Metrohm Autolab, model PGSTAT 204). Controlled potentials were applied and the spectra were recorded by an optical fiber based spectrophotometer (Ocean Optics, model SD2000). Experiments in the IR region were performed using a transmission cell adapted as described by Harlt and collaborators (KREJČIK; DANĚK; HARTL, 1991). The working, counterelectrode and pseudo-reference electrodes were melt-sealed in a polyethylene spacer. This spacer/electrode assembly was constructed by first inserting the three electrodes between two polyethylene foils and then fusing the polymer at 100 °C under slight pressure. This assembly combined with Teflon® spacers (0.5 total thickness) was placed between two CaF$_2$ windows. Controlled potentials were applied by the potentiostat and the spectra were recorded with a spectrometer (PerkinElmer, model FT-IR Frontier Single Range – MIR Spectra).

Bulk electrolysis experiments were performed using an H-cell. The cell was designed with a system of O-rings and septa in order to minimize gas leaks, and to allow the collection of headspace samples with a syringe. A porous

membrane was employed as separator to allow electric current to flow between the catholyte and anolyte. In the catholyte, an Ag wire coupled in a luggin was used as the pseudo-reference electrode, and a graphite electrode (4.0 cm^2) was used as the working electrode. In the anolyte, a platinum grid was used as the counterelectrode. The system was sealed and aliquots from the catholyte headspace were collected at different times and analyzed by gas chromatography (GC)

The evolution of CO was analyzed by a gas chromatograph (Shimadzu, model GC-2014) employing a system equipped with a flame ionization detector (FID), a methanizer and a packed column (ShinCarbon-ST 2 m of length and 1.0 of mm diameter). The column was submitted initially to 40 ºC for 4 minutes, then the temperature was raised to 200 ºC at a pace of 8 ºC min^{-1} and held for 10 minutes. The carried gas used was H_2 with a flow of 10 mL min^{-1}. The methanizer was kept at 400 ºC, the FID at 200 ºC and the injector at 100 ºC. The evolution of H_2 was analyzed by a gas chromatograph (PerkinElmer, model Clarus 580) equipped with a packed column (Porapak N), molecular sieve and a thermal conductivity detector (TCD). The injector was kept at 120 ºC, the column at 35 ºC and the detector at 150 ºC, using argon as carrier gas with a flow of 30 mL min^{-1}. The quantification of gases was done with calibration curves obtained from the analyses of known volumes of respective gases in the cell.

The theoretical calculations were perfomed by Dr. Antonio Eduardo da Hora Machado. All geometries were fully optimized at the M06 level of density functional theory (DFT). Time-dependent density functional theory (TD-DFT) calculations were performed to predict the UV-Vis electronic excitations of structures. In this case the functional density used was the CAM-B3LYP. In all

calculations the basis set used was DZP-DKH, and the solvents were described by the IEFPCM model (JORGE et al., 2009; BARROS et al., 2010).

4. RESULTS AND DISCUSSION

4.1. Spectral properties of [RuCl(trpy)(acpy)]

To confirm the product structures, ^{1}H NMR and H-H Cosy experiments were performed, Figure 8 and 9, respectively. In Figure 8, it is possible to observe that the compound contains 17 hydrogens atoms, as expected. The determined chemical shifts are listed in Table 2. For the signals in the aromatic range a tentative assignment was performed based on the integrals, couplings constants and multiplicity. Hydrogens H_3 and H_4 were attributed to the signal at 8.61 ppm, presenting a coupling constant of 8.0 Hz, the integral corresponds to 4 hydrogens. The hydrogen H_6 correspond to 2 hydrogens atoms and its multiplicity is a doublet as expected. For H_5, triple doublet is observed as expected and an integral value of 2. Hydrogens $H_{3'/3''}$ and $H_{4'}$ appear as triple doublets, with shifts of 7.50 and 8.07 ppm respectively, and coupling constants of 4.0 and 8.0 Hz. The integrals match, as expected. H_a, H_b and H_c show shifts of 7.68, 7.75 and 7.87 ppm and coupling constants of 8.0 Hz, and therefore the multiplicity meets the expectations for the proposed structure with a doublet in relation to H_a and triplet in relation to H_b and H_c. H_d shows a doublet signal at 9.84 ppm and the integral corresponds to one hydrogen atom, and it is also coupled with H_c at 8.0 Hz. At 3.61 ppm is possible to observe a singlet signal which corresponds to the hydrogens of CH_2 group in the acpy ligand. In a previous study conducted by our

group, it was observed that, for the complex $[Ru(bpy)_2(acpy)]^+$ the methylene protons in the coordinated acpy exhibit a diastereotopic effect with a coupling constant of 16.5 Hz (SOUSA, S. F., 2019; SOUSA, S. F. et al., 2021). In the case of [RuCl(trpy)(acpy)], the behavior differs from the one previously observed by Sousa. This suggests that the geometric and electronic properties change as trpy replaces bpy in the complex.

Figure 8. ^{1}H NMR spectrum in DMSO-d_6 of [RuCl(trpy)(acpy)], 298 K and 400 MHz.
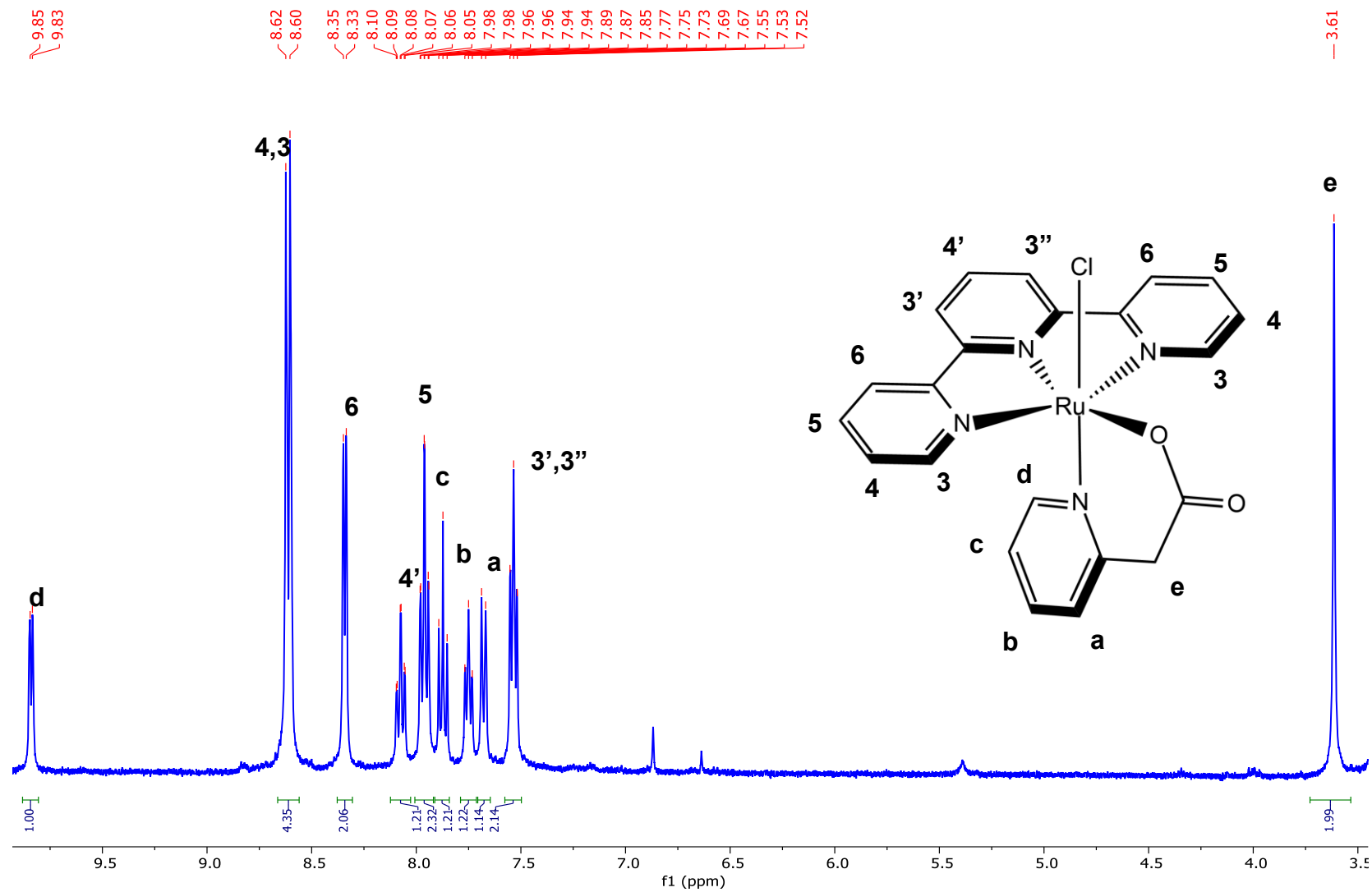
Figure 9. Cosy spectrum in DMSO-d₆ of [RuCl(trpy)(acpy)], 298 K and 400 MHz.
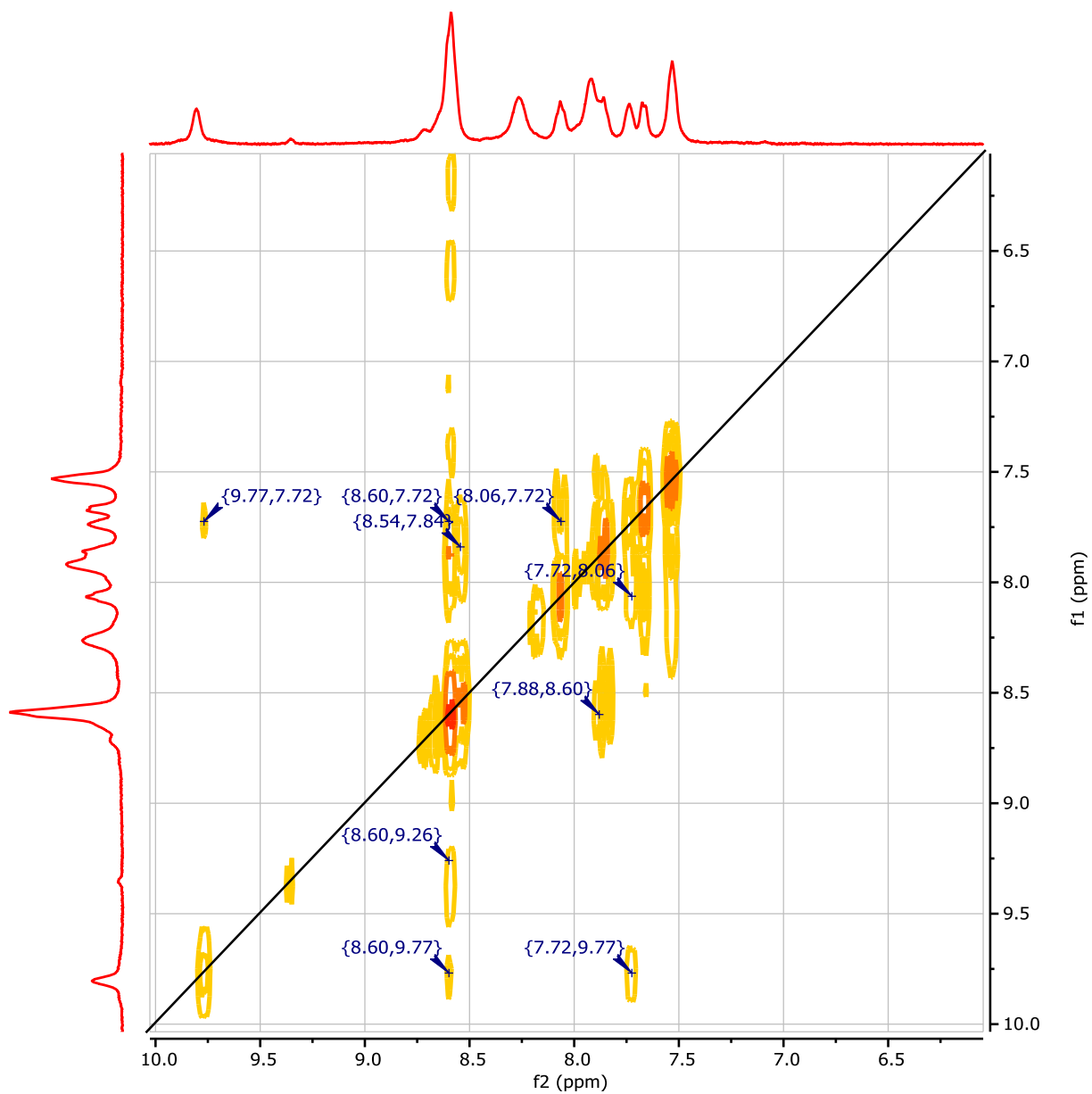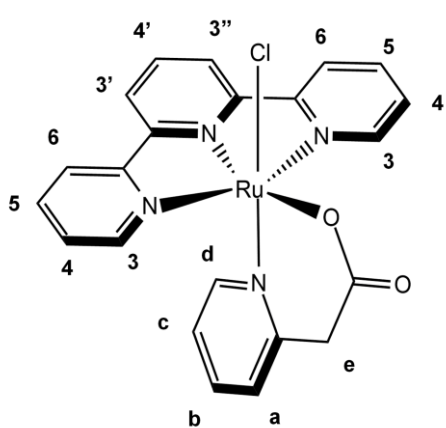
Table 2. ^{1}H NMR Chemical shifts and coupling constants of [RuCl(trpy)(acpy)].

Structure	Proton		δ / ppm	J / Hz
	H$_3$	d	8.61	8.0
	H$_4$	d	8.61	8.0
	H$_5$	td	7.96	4.0 / 8.0 / 16.0
	H$_6$	d	8.34	8.0
	H$_{3'/3''}$	td	7.55	4.0 / 8.0 / 12.0
	H$_{4'}$	td	8.07	4.0 / 8.0 / 20.0
	H$_a$	d	7.68	8.0
	H$_b$	t	7.75	8.0 / 16.0
	H$_c$	t	7.87	8.0 / 16.0
	H$_d$	d	9.84	8.0
	H$_e$	s	3.61	-

d= doublet, td = triple doublet, t = triplet, s = singlet.

Experiments of mass spectrometry were performed in the positive mode to further evidence purity of the as-synthesized complex, Figure 10. Two sets of signals were observed with their highest peaks at M^+ = 507.015 and 528.997, respectively. The first value corresponds to the protonated complex since the compound is neutral, and the second one corresponds to the complex interacting with a sodium ion. The production of sodium cluster ions in electrospray mass spectrometry is commonly observed even in the presence of small amounts of Na^+ (ZHOU; HAMBURGER, 1996). The observed isotopic distributions for each set of signals are in accordance with simulations for [RuCl(trpy)(acpy)]H^+ or [RuCl(trpy)(acpy)]Na^+.

Figure 10. Mass spectrum of [RuCl(trpy)(acpy)] in methanol/water (4:1).

C:\Users\leand...L\080620\R1.RAW Injection 1 FTMS + p ESI F...0000-2000.0000] MS + spectrum 1.63
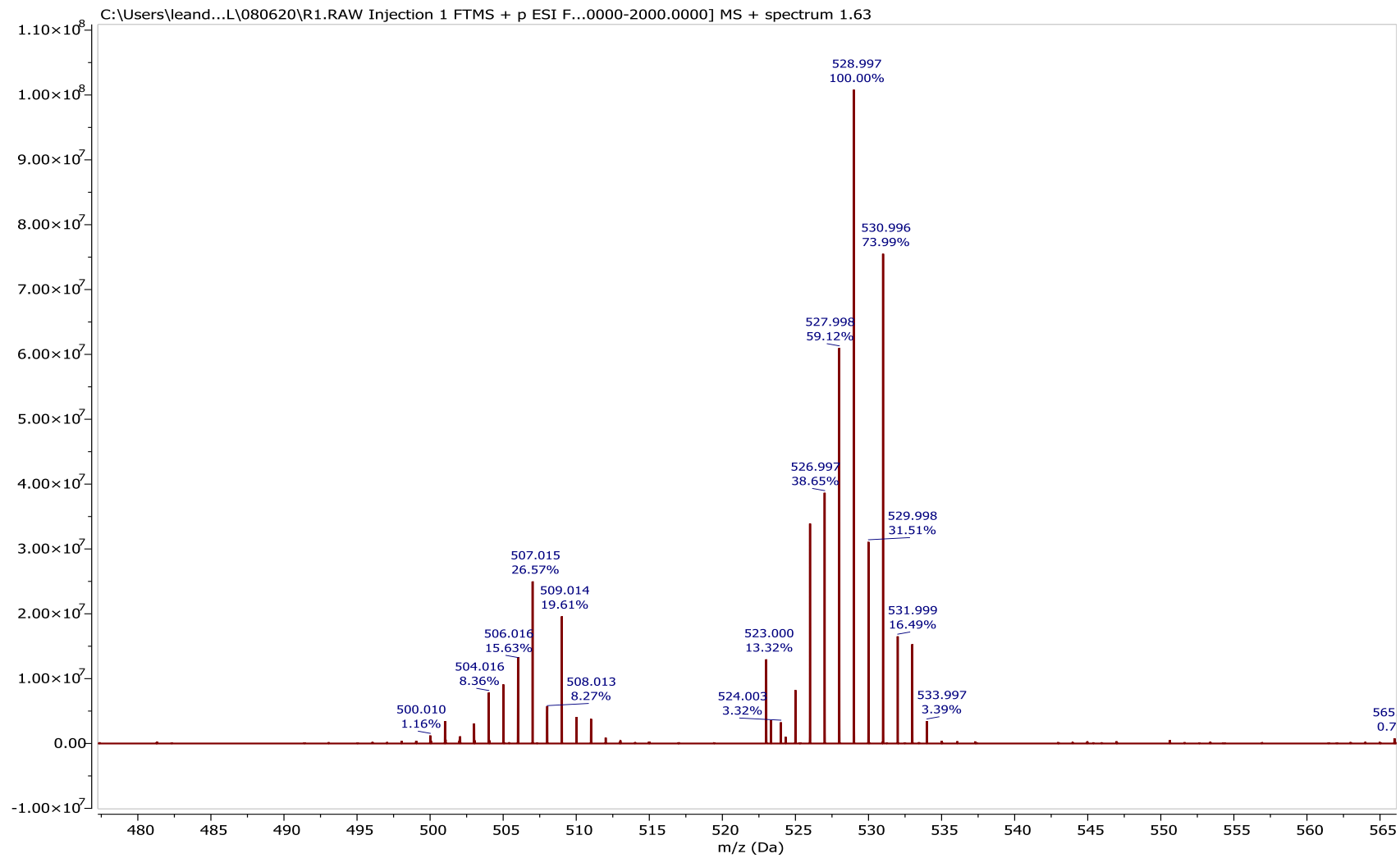
Due to the planarity of the trpy ligand and the asymmetry of the acpy ligand, two bond isomers can be expected for the complex with the chlorido ligand *trans* to the pyridil or the carboxylic groups of acpy. The ^{1}H NMR spectrum suggests that one isomer is probably favored during the complexation of the acpy ligand, due to the fact that no splits are observed in the signals. This behavior is reported on the complex $[Ru(trpy)(pic)(OH_2)]^+$ (pic = picolinate) in which the absence of resonance in low field confirm that the pyridyl ring in pic ligand is *trans* to the coordinated H_2O (CHATTERJEE; SENGUPTA; MITRA, 2007). For the investigated complex, theoretical calculations were performed to analyze the relative energies of each isomer considering acetonitrile as a solvent. The optimized structures are shown in Figure 11.

Figure 11. Isomers expected to [RuCl(trpy)(acpy)].

1   2
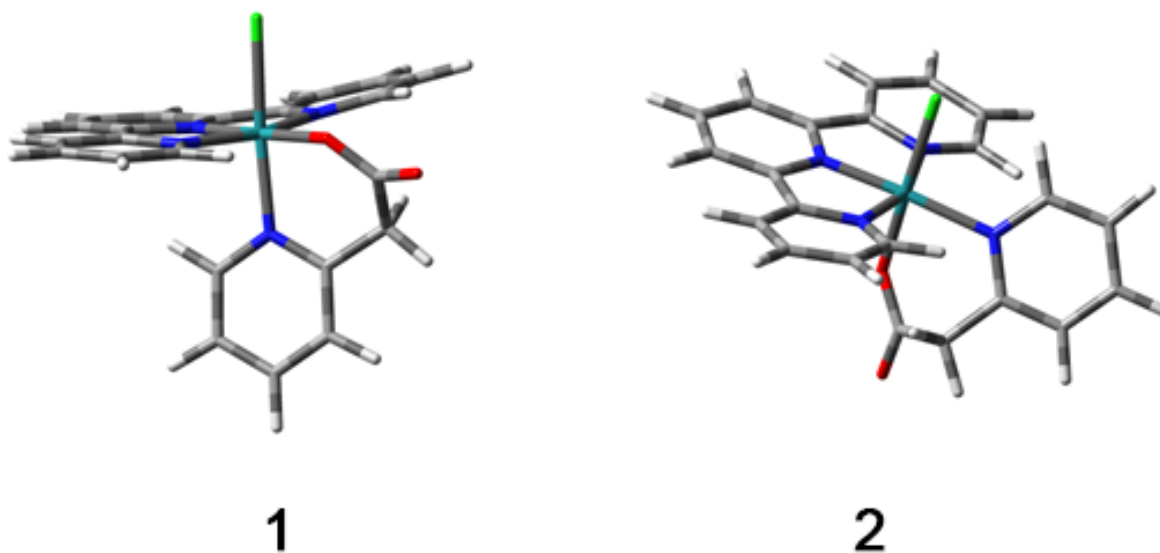
The calculated free energy values show that, in the CH_3CN, the isomer number 1 is more stable than 2 by a considerable difference ($\Delta G = \Delta G_{isomer(1)} - \Delta G_{isomer(2)}$; ΔG = -1.76 kJ mol^{-1}). Despite all indication for the formation of single

isomer, conclusive experimental evidence of the geometry of [RuCl(trpy)(acpy)] requires single crystal diffractometry.

The formation of a single isomer meets the expectations for the employed synthetic scheme, i.e., starting from [Ru(trpy)Cl$_3$], after the reduction of metal center by triethylamine, the coordination of acpy should occur first by the N-atom in the pyridyl ligand in the axial position in relation to the trpy ligand, so O-site at the carboxylate group could be *trans* to trpy. Such observations are in line with other examples in the literature about the stereorentetive synthesis of ruthenium complexes. This is the case of [Ru(pap$_2$)(pic)]$^+$ and [Ru(pap$_3$)]$^{2+}$, in which pap = 2-phenylazopyridine and pic, 2-picolinate (GOSWAMI; MUKHERJEE; CHAKRAVORTY, 1983; GHATAK; CHAKRAVARTY; BHATTACHARYA, 1995) for example. Even with the possibility of generating several isomers due to the asymmetrical structure of these ligands, only one isomer is observed. The complex was also characterized by FTIR experiments and compared to the free ligands, Figure 12.

Figure 12. ATR infrared spectra of free ligands, [RuCl$_3$(trpy)] and [RuCl(trpy)(acpy)].
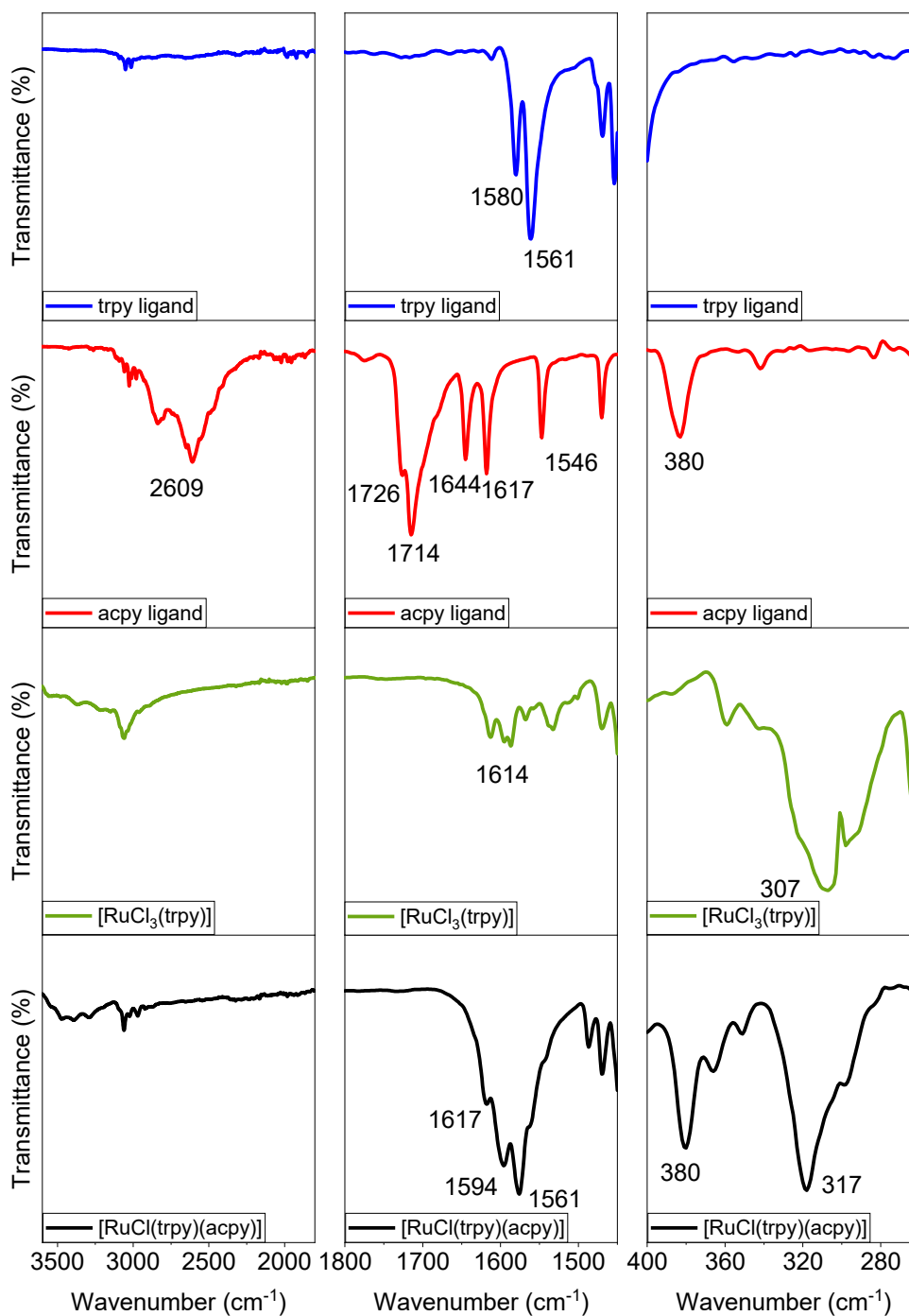
In the infrared spectra it is possible to observe that the non-coordinated

ligand acpy shows an O-H stretch around 2609 cm^{-1}, ascribed to the protonated

carboxylic acid group. This signal is lost a after reaction with the metal center, corroborating with the conclusion that acpy is coordinated in a bidentate N-O fashion. Between 1800 and 1500 cm^{-1}, for the free acpy ligand, it is also possible to observe two stretching vibrations at 1726 and 1714 cm^{-1}, which correspond to the C=O of the carboxylic group. The peaks at 1644, 1617 and 1546 cm^{-1} are associated to the C=C vibration from the pyridine ring. For the free trpy ligand, the peaks at 1580 and 1561 cm^1 correspond to the C=C stretches from aromatic rings (SILVERSTEIN; WEBSTER; KIEMLE, 2005). The spectrum of [RuCl(trpy)(acpy)] in this region exhibits at least three overlapped stretchings at 1617, 1594 and 1561 cm^{-1}, evidencing a shift of ν(C=O) to shorter wavenumbers in comparison to the free acpy. In the region, between 400 and 260 cm^{-1} for [RuCl(trpy)(acpy)], the stretch at 317 cm^{-1} appears shifted for higher wavenumbers when compared to the stretching at 307 cm^{-1} for the precursor [RuCl$_3$(trpy)]. This region is associated to the Ru-N and Ru-Cl stretchings (NAKAMOTO, 2009). The FTIR data corroborates with the proposed structure for [RuCl(trpy)(acpy)] with acpy coordinated to the Ru(II) center in a bidentade mode.

The electronic transitions in the UV-Vis region were investigated and compared to the theoretical spectra obtained by TD-DFT, Figure 13.

Figure 13. Absorption spectra of [RuCl(trpy)(acpy)] in acetonitrile.
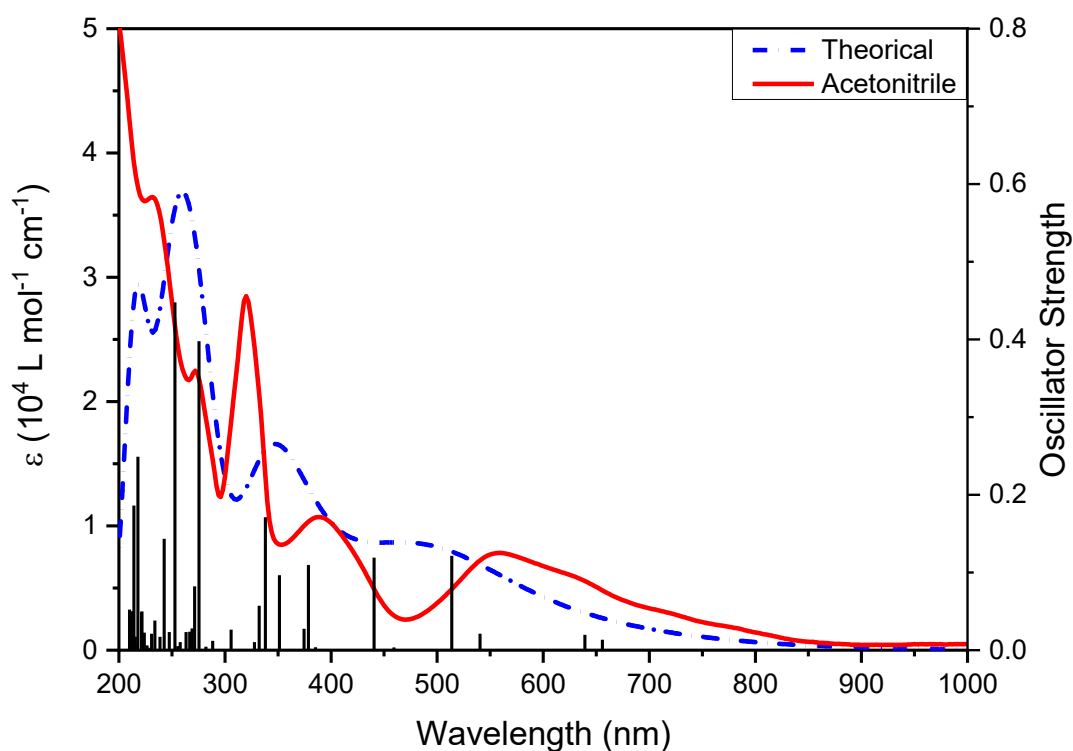
In the experimental UV-Vis spectrum it is possible to observe absorption bands at 390 nm and 560 nm. These bands have molar absorption coefficients (ε) with an order of magnitude around 10^3 cm^{-1} mol^{-1} L and are attributed to Metal-Ligand Charge Transfer (MLCT) transitions. Other absorption bands can be observed below 350 nm and are attributed to Intra-Ligand Charge Transfer (ILCT) or Ligand-to-Ligand Charge Transfer (LLCT) transitions. Further information on the character of the electronic transitions was obtained through theoretical TD-DFT calculations. TD-DFT calculation is an important tool, particularly for transition metal complexes, since it can be used to estimate the HOMO and LUMO energies and their respective electron densities (MORIGAKII et al., 2009).

The calculated orbitals are shown in Figure 14 and the respective transitions are listed in Table 3.

Figure 14. Representatives images of electronic transitions of [RuCl(trpy)(acpy)] in acetonitrile.

| LUMO | LUMO+1 | LUMO+2 | LUMO+3 | LUMO+6 |

| HOMO | HOMO-1 | HOMO-2 | HOMO-3 | HOMO-4 | HOMO-7 |
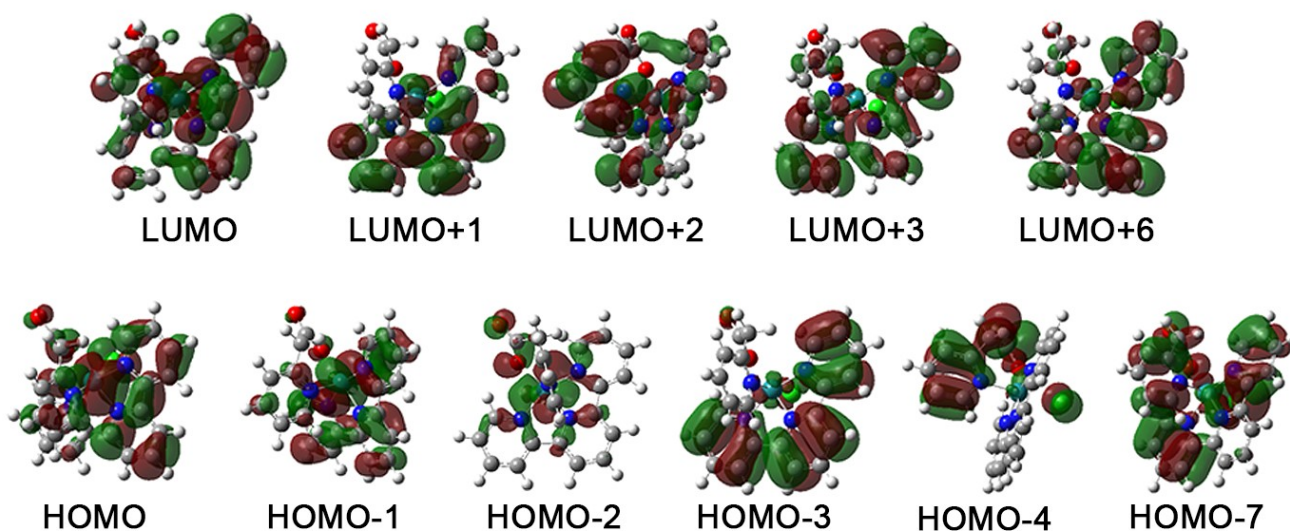
Table 3. Eletronic transitions of [RuCl(trpy)(acpy)] and the correspondent oscillator strength.
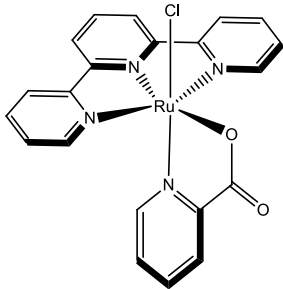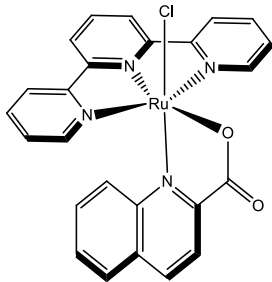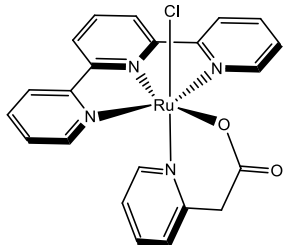
λ nm (eV)	Oscillator Strength	Transition	Nature
655.67 (1.89)	0.0137	H-2→L (39.4%) H-1→L (32.4%) H→L (7.5%)	MLCT $_{d\,Ru→\pi\,tpy}$
639.27 (1.94)	0.0199	H-2→L (40.3%) H-1→L (21.5%) H→L (16.%)	MLCT $_{d\,Ru→\pi\,tpy}$
540.43 (2.29)	0.0214	H-1→L (40.0%) H→L (24.3%) H→L+1 (30.5%)	MLCT $_{d\,Ru→\pi\,tpy}$
513.65 (2.41)	0.1216	H-1→L+1 (13.3%) H→L (27.6%) H→L+1 (56.8%)	MLCT $_{d\,Ru→\pi\,tpy}$

459.29 (2.70)	0.0038	H-2→L (15.8%) H-2→L+1 (72.0%)	MLCT $_{\text{d Ru}→π\text{ tpy}}$
440.50 (2.81)	0.1192	H-1→L+1 (64.3%) H→L (24.3%)	MLCT $_{\text{d Ru}→π\text{ tpy}}$ IL $_{π\text{ tpy}→π^*\text{ tpy}}$
378.67 (3.27)	0.1100	H-2→L+2 (10.2%) H-1→L+2 (46.9%) H→L+2 (39.0%)	MLCT $_{\text{d Ru}→π^*\text{acpy}}$ LLCT $_{π\text{ tpy}→π^*\text{ acpy}}$
351.26 (3.53)	0.0966	H→L+3 (100%)	MLCT $_{\text{d Ru}→π\text{ tpy}}$ IL $_{π\text{ tpy}→π^*\text{ tpy}}$
338.02 (3.67)	0.1712	H-2→L+3 (20.4%) H-1→L+3 (79.6%)	MLCT $_{\text{d Ru}→π\text{ tpy}}$ IL $_{π\text{ tpy}→π^*\text{ tpy}}$
275.53 (4.50)	0.3978	H-3→L (54.7%) H-1→L+6 (22.1%) H→L+6 (13.3%)	MLCT $_{\text{d Ru}→π\text{ tpy}}$ IL $_{π\text{ tpy}→π^*\text{ tpy}}$
252.71 (4.90)	0.4477	H-3→L (9.6%) H-3→L+1 (56.3%) H-2→L+6 (9.9%) H→L+6 (8.5%)	MLCT $_{\text{d Ru}→π\text{ tpy}}$ IL $_{π\text{ tpy}→π^*\text{ tpy}}$
242.61 (5.11)	0.1436	H-4→L (77.9%) H-4→L+2 (14.3%)	LLCT $_{π\text{ acpy}→π^*\text{ tpy}}$ LLCT $_{\text{n Cl}→π^*\text{ tpy/acpy}}$ IL $_{π\text{ acpy}→π^*\text{ acpy}}$
217.80 (5.69)	0.2491	H-4→L+1 (26.8%) H-3→L+3 (42.3%)	IL $_{π\text{ tpy}→π^*\text{ tpy}}$ LLCT $_{π\text{ acpy}→π^*\text{ tpy}}$ LLCT $_{\text{n Cl}→π\text{ tpy}}$
214.07 (5.79)	0.1863	H-7→L (18.4%) H-4→L+1 (29.7%) H-3→L+3 (12.6%)	IL $_{π\text{ tpy}→π^*\text{ tpy}}$ LLCT $_{π\text{ acpy}→π^*\text{ tpy}}$

The calculations show that transitions between 655.67 nm – 338.02 nm are MLCT in nature, with electrons being transferred from d orbitals in the metal

center to π* orbitals at the trpy, MLCT$_{d - \pi*trpy}$. They involve transitions from the HOMO (H), H-1 and H-2 to LUMO (L) and L+1 states. While the HOMO-2 is centered at the d orbitals in the Ru(II) center, in the HOMO and HOMO-1 states the electron density is distributed between the Ru(II) and trpy orbitals showing the strong interaction between the ligand and the metal center. Charge transfer to the acpy ligand occurs with the population of L+2 orbital only at 378 nm. Below 280 nm, light absorption is dominated by IL or LLCT transitions. The calculations agree well with the behavior already reported for other ruthenium(II) terpyridine-based complexes, such as [RuCl(trpy)(bpy)], in which the HOMO is essentially formed by t$_{2g}$ orbitals of Ru(II) with small contribuitions of π orbitals from terpyridine and bipyridine (JAKUBIKOVA et al., 2009). An interesting comparison can be made between the electronic spectrum of [RuCl(trpy)(acpy)] and those previous reported for Ru(II)-trpy complexes containing other N-O ligands, Table 4. The lowest MLCT absorption band in [RuCl(trpy)(acpy) is red-shifted in comparison to the other two complexes, which means the electron density in the metal center is higher in the complex with acpy. The higher electron density in the [RuCl(trpy)(acpy)] is likely correlated to the lower stabitly of the six-ring chelate formed by the acpy ligand compared to the five-ring structure of pic or quin ligands.

Table 4. Comparative values of wavelength and molar absorption coefficient to other ruthenium complexes in acetonitrile.

Compound	λ_{max} (nm) $(\varepsilon/10^4$ (L.mol^{-1}.cm^{-1})	Reference
	519 (0,36) and 389 (0,48)	(LLOBET; DOPPELT; MEYER, 1988)
	533 (1,4) and 378 (1,1)	(CHOWDHURY et al., 2011)
	558 (0,08) and 388 (0,1)	This Work

4.2. Stability of [RuCl(trpy)(acpy)] in aerobic conditions

In our previous work with the [Ru(bpy)$_2$(acpy)]$^+$ complex, the aerobic oxidation of the methylene group in the coordinated acpy ligand was observed, Figure 15 and, based on a detailed experimental/theoretical studies, the formation of Ru$^{(IV)}$=O species were proposed to be responsible for the C-H activation (SOUSA, S. F. et al., 2021).

Figure 15. Reaction of the [Ru(bpy)2(acpy)]+ with molecular oxygen resulting into a new complex.

[Ru(bpy)$_2$(acpy)]$^+$ [Ru(bpy)$_2$(acpyox)]$^+$
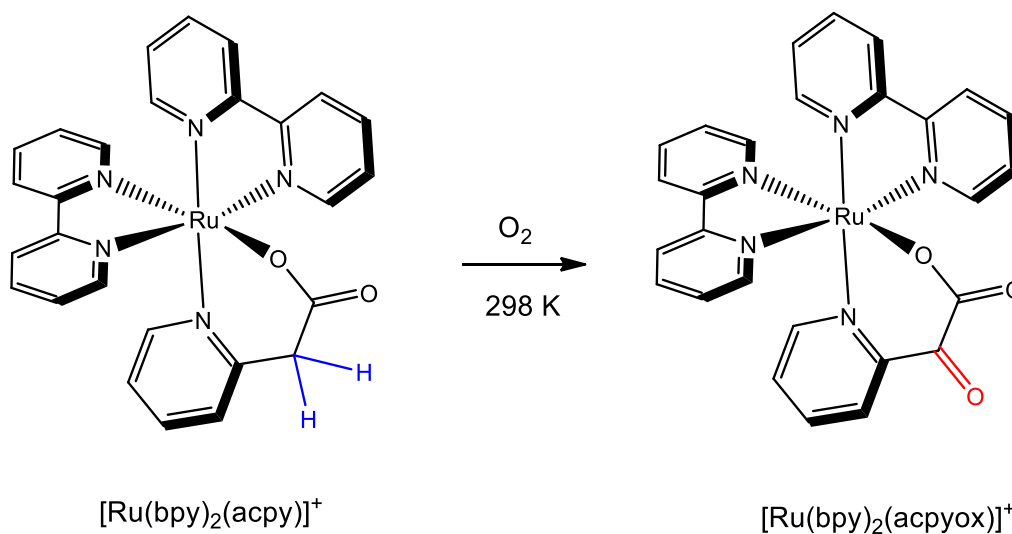
Adapted from (SOUSA, S. F., 2019)

The employment of molecular oxygen as a single oxidant in the dehydrogenation of organic substrates has been thoroughly studied, due to its potential to be an alternative to the traditional oxidation methods, which employ hazardous or toxic reagents (ABAD et al., 2006; GLIGORICH; SIGMAN, 2009; SOUSA, S. F. et al., 2021). In the case of [Ru(bpy)$_2$(acpy)]$^+$, the free ligand does not undergo any reactions with the molecular oxygen, but after a complexation with the metal center, the CH$_2$ group is oxidized into the α-keto derivative (SOUSA, S. F., 2019). This behavior of the [Ru(bpy)$_2$(acpy)]$^+$ complex was one of the motivations of this study.

In order to verify if the [RuCl(trpy)(acpy)] manifests the same behavior as [Ru(bpy)$_2$(acpy)]$^+$, experiments under the same aerobic conditions were carried out. The complex [RuCl(trpy)(acpy)] was dissolved in a mixture of acetone:water (1:1) and stirred under an oxygen atmosphere for 50 hours. Then, the solution

was rotaevaporated, and the crude product was analysed by ^{1}H NMR and FTIR, Figures 16 and 17, respectively.

Figure 16. ^{1}H NMR of [RuCl(trpy)(acpy)] in CD_6CO before and after exposed to aerobic conditions, 298 K and 400 MHz.
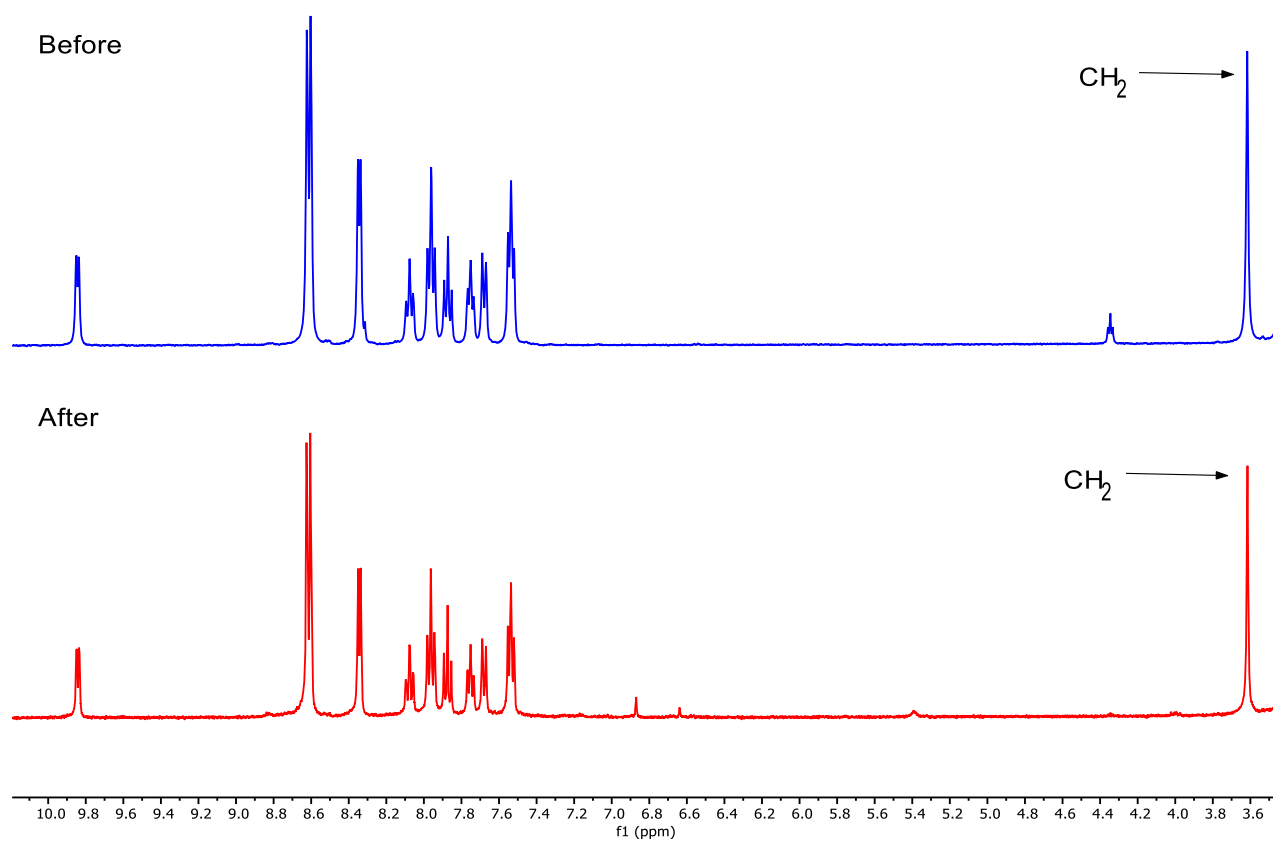
Figure 17. FTIR of [RuCl(trpy)(acpy)] before and after aerobic test oxidation.
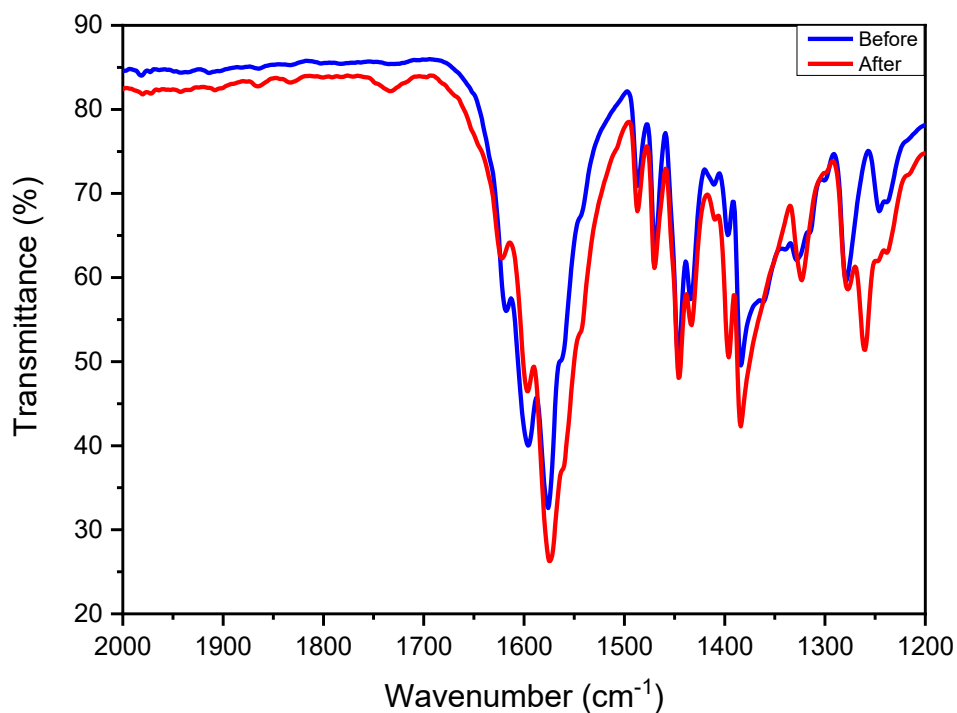
In the ^{1}H NMR spectra it is possible to observe that the correspondent signal to the CH_2 group in the acpy ligand remains even after 50 hours of exposure to oxygen. No significant changes were observed in the aromatic signals. The integrity of the complex was subsequently confirmed by FTIR spectra, in which no significant changes were observed. It is possible to infer that the new complex, [RuCl(trpy)(acpy)], is stable under aerobic conditions. To understand such stability, we can look at the proposed reaction mechanism for [Ru(bpy)$_2$(acpy)]$^+$, Figure 18.

Figure 18. Free energy profile of the proposed mechanism for the O_2 reduction by $[Ru(bpy)_2(acpy)]^+$ and C-H activation to yield the $[Ru^{II}(bpy)_2(S\text{-}\alpha\text{-}OH\text{-}acpy)^+$. Bpy groups are omitted for clarity.
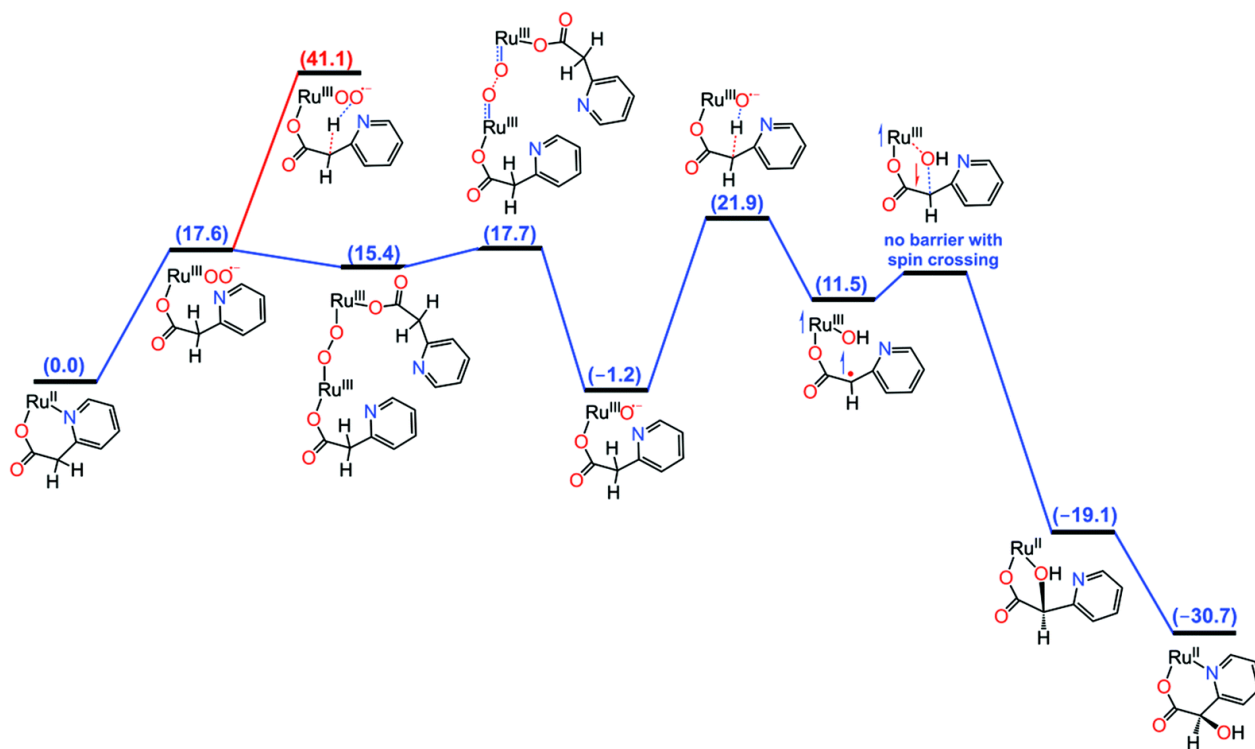
(SOUSA, S. F. et al., 2021)

The nucleophilic attack by O_2 is facilitated by the relative instability of the six-ring chelate formed by the acpy ligand. C-H activation requires the formation of $Ru^{IV}=O$ species, which occurs through a diruthenium µ-peroxo intermediate $[(Ru^{III}(bpy)_2(O\text{-}acpy)_2O_2]^{2+}$. Afterwards, the $Ru^{IV}=O$ (or $Ru^{III}\text{-}O^{\cdot -}$) center can promote the C-H activation with relative low activation energies resulting in the formation of $Ru^{III}\text{-}OH$, $[Ru^{III}(bpy)_2(O\text{-}acpy^{\cdot})OH]^+$. Then, the hydroxo group is transferred to the α-C radical, forming the $[Ru^{II}(bpy)_2(\alpha\text{-}OH\text{-}acpy)]^+$. Further investigations revealed that $[Ru^{IV}(bpy)_2(O\text{-}\alpha\text{-}OH\text{-}acpy)]^+$ species are formed from the $[Ru^{II}(bpy)_2(\alpha\text{-}OH\text{-}acpy)]^+$, leading to the final α-keto derivative $[Ru(bpy)_2(acpyox)]^+$.

As trpy is a stronger π-acceptor than bpy, in the [RuCl(trpy)(acpy)] the six-ring acpy chelate seems to be more stable, hindering the nucleophilic attack by O_2. Another fact that ensures the stability of this complex under O_2 is the monodentade ligand, Cl⁻. It is expected that the most probable reaction in the solution would be the eventual labilization of the chloride ligand following the oxidation of the metal center.

In fact, as it will be shown by electrochemical experiments, $Ru^{II/III}$ oxidation in [RuCl(trpy)(acpy)] occurs at lower potentials than in $[Ru(bpy)_2(acpy)]^+$, but no further oxidation to yield Ru^{IV} species is observed at the investigated potentials.

4.3. Electrochemical properties and spectroelectrochemical studies

The electrochemical properties of [RuCl(trpy)(acpy)] were evaluated by cyclic voltammetry and spectroelectrochemistry in the UV-Vis and IR regions. The voltammetric experiments were performed using acetronitrile as a solvent and 0.1 M of $TBAPF_6$ (tetrabutylammonium hexafluorophosphate) as a supporting electrolyte. The studies were separated into two different regions, first considering anodic potentials and, later, cathodic potentials.

4.3.1. Anodic range

In the anodic range the electrochemical experiments were performed considering the range of -0.4 to +1.0 V *vs* Fc/Fc⁺ (0.48 V *vs* NHE). Voltammograms in this range are shown in Figure 19 as a function of the scan rate and the determined electrochemical parameters are listed in Table 5.

Figure 19. Cyclic voltammetries of 1 mM [RuCl(trpy)(acpy)] in 0.1 M TBAPF$_6$/CH$_3$CN under argon atmosphere at different scan rates.
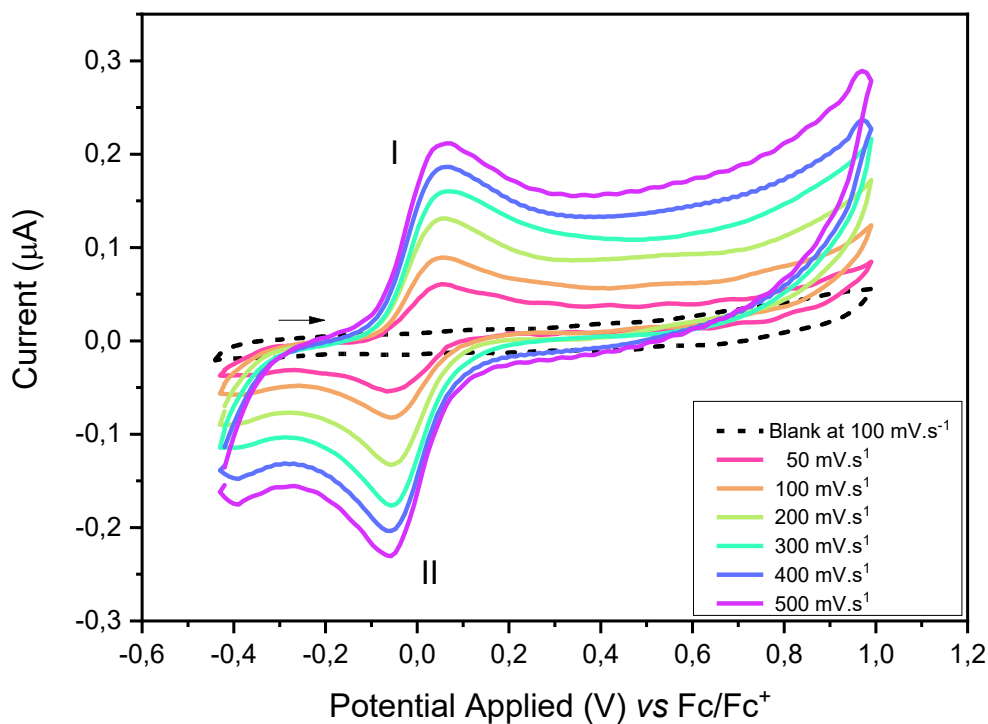
Table 5. Electrochemical parameters of [RuCl(trpy)(acpy)] in 0.1 TBAPF$_6$ acetonitrile solution compared to data for ferrocene under the same experimental conditions.

Compound	ν (mV s^{-1})	I_{pa} (μA)	I_{pc} (μA)	E_{pa} (V)	E_{pc} (V)	$E_{1/2}$ (V)	ΔE_p (V)	$|E_{pa}-E_{1/2}|$ (V)	I_{pa}/I_{pc}
Ferrocene	100	37.90	-33.20	0.48	0.37	0.36	0.110	0.06	1.14
	50	5.00	-4.19	0.006	-0.11	-0.04	0.116	0.07	1.03
	100	6.94	-6.10	0.006	-0.11	-0.04	0.116	0.07	0.95
	200	10.40	-8.88	0.006	-0.11	-0.04	0.116	0.07	1.04
[RuCl(trpy)(acpy)]	300	12.70	-12.10	0.006	-0.11	-0.04	0.116	0.07	1.18
	400	13.50	-14.20	0.006	-0.11	-0.04	0.116	0.07	1.13
	500	15.30	-14.80	0.006	-0.11	-0.04	0.116	0.07	1.19

In the voltammograms in Figure 19 it is possible to observe a redox couple with $E_{1/2}$ = -0.04 *vs* Fc/Fc$^+$. Analyzing the difference between the oxidation and reduction potential peaks (ΔE_p) for [RuCl(trpy)(acpy)], the value obtained was 116 mV. Under the same conditions, the value for the Fc/Fc$^+$ couple was 110 mV. The latter is known to exhibit an 1e$^-$ reversible redox couple in this region (TSIERKEZOS, 2007; PAUL et al., 2019). Thus, it is possible to conclude that the number of electrons involved in the oxidation of [RuCl(trpy)(acpy) is one, i.e., Ru$^{II/III}$, Equation 2.

$$[Ru^{II}Cl(trpy)(acpy)] \rightarrow [Ru^{III}(Cl)(trpy)(acpy)]^+ + e^- \qquad \text{Equation 2}$$

Some reversibility criteria were evaluated for this redox couple (BARD; FAULKNER, 2002; SKOOG et al., 2006; ELGRISHI et al., 2018). They are described below:

- The ratio between the anodic and cathodic peak currents should be approximately one unit (I_{pa}/I_{pc});

- The anodic and cathodic potentials should be independent from the scan rate;

- The difference between the anodic peak potential and the half-wave ($E_{pa} - E_{1/2}$) should be approximately 59/n mV, in which n represents the number of electrons in the redox process;

- The anodic and cathodic peak currents should be proportional to the square root of the scan rate ($I_p \propto \sqrt{v}$).

When analyzing the first criterion, it is possible to observe that values obtained for the ratio I_{pa}/I_{pc} were close to 1. The second condition is also met as

observed in Table 5, i.e., both oxidation and reduction potentials are independent from the scan rate. The third criterion, which states that $(E_{pa}-E_{1/2})$ should be equal to 59/n, is also met for $n \cong 1$. For the fourth criterion, it can be observed in Figure 20 that I_p varies linearly with $\sqrt{\nu}$, which confirms that the process is controlled by the difusion of species.

Figure 20. The linear behavior of I_p versus $\sqrt{\nu}$ (■) oxidation (■) reduction.
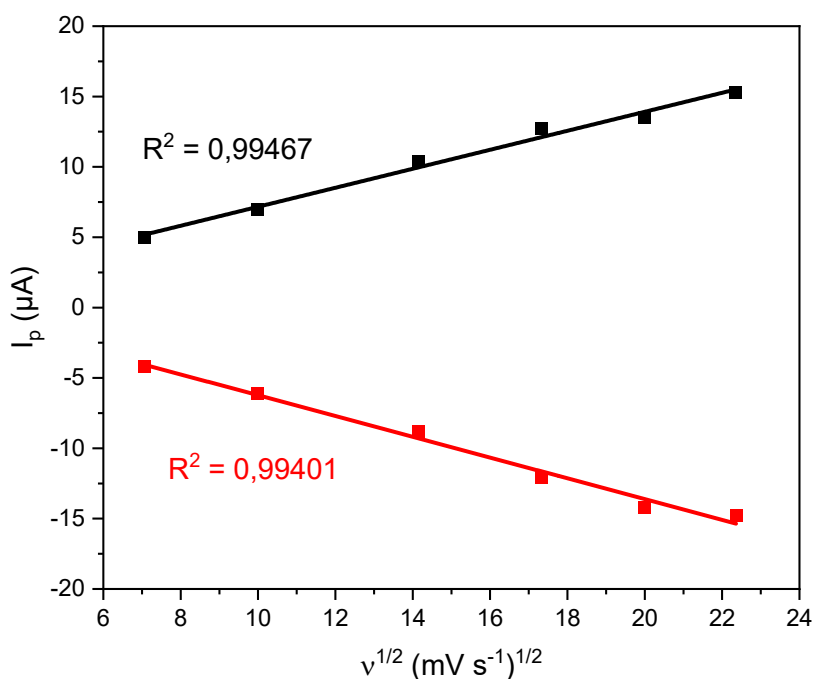
The oxidation of the Ru^{II} center was confirmed by UV-Vis espectroelectrochemical experiments (UV-Vis SEC) under the same conditions as the voltammetries. Spectroelechemical experiments are an important tool, making it possible to generate species with different oxidation states *in situ* and observe them spectroscopically (D'ALESSANDRO; USOV, 2021). In Figure 21,

spectral changes when 0.12 V *vs* Fc/Fc$^+$ is applied are shown as a function of time.

Figure 21. Changes in the UV-Vis spectra of 0.1 mM [RuCl(trpy)(acpy)] during spectroelectrochemistry in 0.1 M TBAPF$_6$/CH$_3$CN applying 0.12 V vs Fc/Fc$^+$, Δt = 10 s.
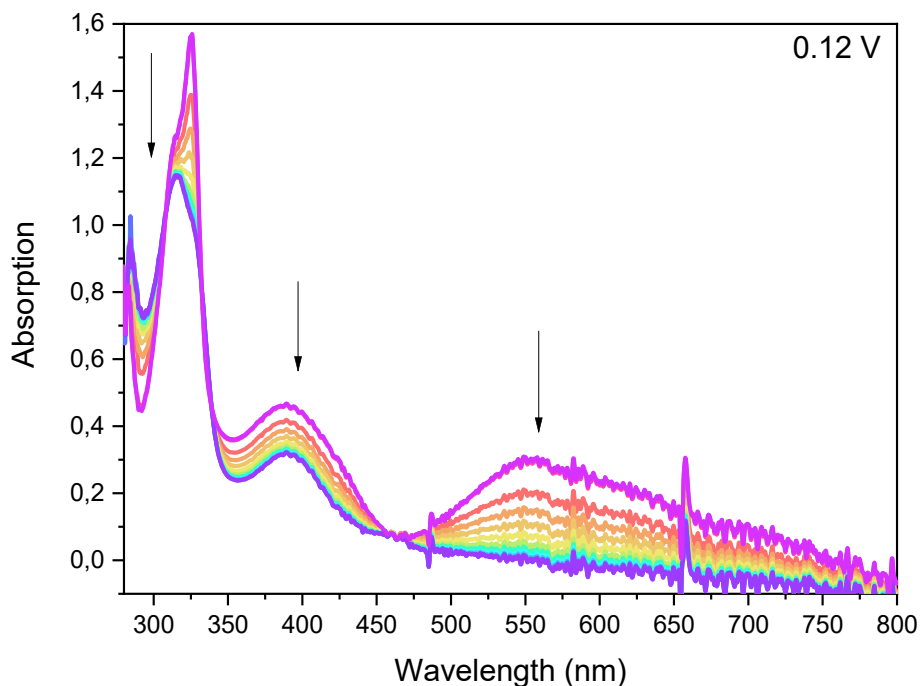
In the spectra of Figure 19 it is possible to observe a loss of MLCT as a function of time (Δt = 10 s). In the applied potential, the Ru^{II} center is oxidized to Ru^{III}. As a result, a bleaching of the MLCT band is observed. The same observations were reported for other ruthenium complexes in the literature (PAULA, 1994; SHERBORNE; SCOTT; GORDON, 1997).

The oxidation potential observed for [RuCl(trpy)(acpy)], E$_{1/2}$ = -0.04 V *vs* Fc/Fc$^+$, is close to the ones reported for *trans*-[RuCl(trpy)(pic)] and *cis*-[RuCl(trpy)(pic)] (2-picolinate), E$_{1/2}$ = -0.02 and 0.07 *vs* Fc/Fc$^+$, respectively. These oxidation potentials are lower when compared to other ruthenium

complexes, such as $[Ru(bpy)_2(acpy)]^+$, 0.88 V *vs* Fc/Fc^+ (SOUSA, S. F. et al., 2021) and others Ru(II) trpy-based complexes (WHITE; MAJI; OTT, 2014). These lower oxidation potentials result from fact that the carboxylate ligands are capable of stabilizing high oxidation states (DUAN et al., 2012).

The potentials described above attest that the concepts of molecular engineering can be used to tune the properties of the complex accordingly and reach the desired properties. Furthermore they can be used to predict the probabilty of some reactions occur employing this complex as catalyst. In the case of this new complex, the initial approach was to study its ability to act as a catalyst for the *water splitting* reaction by replacing the chloride ligand by an H_2O ligand (KAMDAR; GROTJAHN, 2019). This replacement is used to increase solubility and also to reduce the oxidation potential of Ru^{II} reaching the catalytic state, $Ru^{IV}=O$ or $Ru^{V}=O$, through proton coupled electro transfer (PCET) steps. An example of that was in case of the complexes $[Ru(bpy)_2Cl_2]$ and $[Ru(bpy)_2(py)(OH_2)]^{2+}$. In the first one, the $Ru^{II/III}$ and $Ru^{III/IV}$ redox pair occur at 0 and 1.78 V *vs* NHE, in contrast, the same couples are observed at 0.67 and 0.78 V *vs* NHE in the aquo complex (MOYER; MEYER, 1981; MEYER; HUYNH, 2003; KAMDAR; GROTJAHN, 2019). However, several attempts to synthesize $[Ru(OH_2)(trpy)(acpy)]^+$ were not successful, as a considerable number of side products were formed. Hence, a different approach employing different precursors must be used but the implementation was not possible in the time course of this work.

4.3.2. Cathodic range

The electrochemical properties in the cathodic range, from -0.4 to -2.48 V *vs* Fc/Fc⁺, were also evaluated. The cyclic voltammograms at different scan rates are shown in Figure 22.

Figure 22. Cyclic voltammetries of 1 mM [RuCl(trpy)(acpy)] in 0.1 M TBAPF$_6$/CH$_3$CN under argon atmosphere at different scan rates.
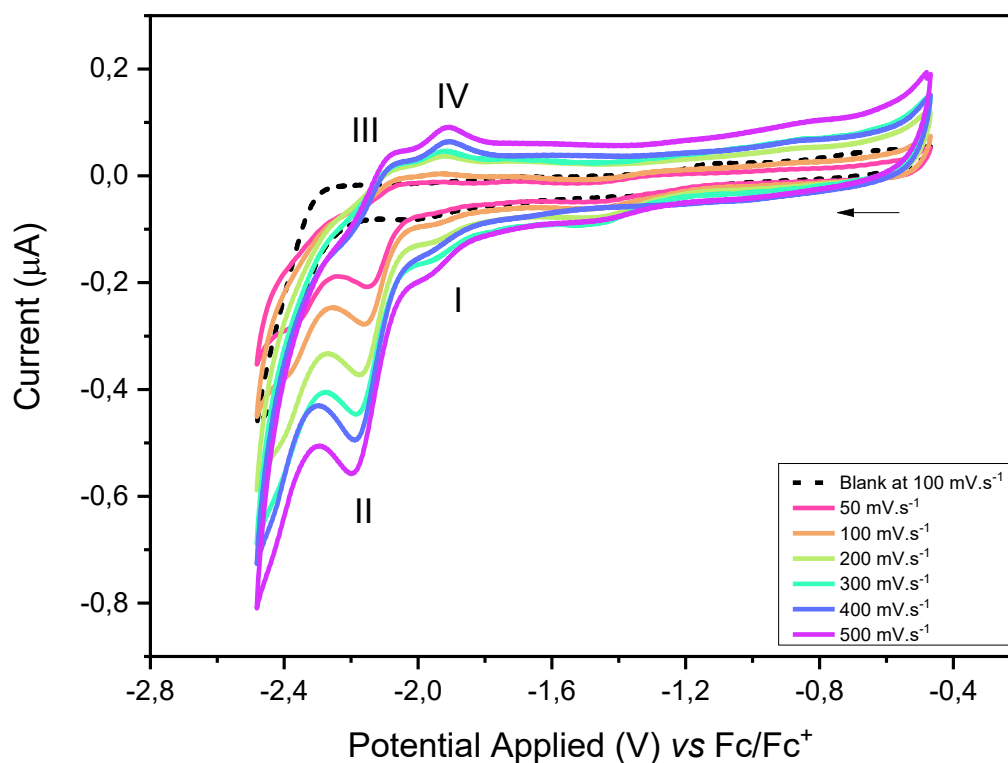
Unlike the scans in the anodic range, in the cathodic area it is clear that the reduction and oxidation peaks are dependent on the scan rate. On the cyclic voltammograms, the peak I appears at -1.95 V *vs* Fc/Fc⁺ and it is attributed to the trpy reduction. Theoretical calculations were performed for the reduced species

to verify the changes in the electron density as the reduction process takes place.

The SOMOs (Singly Occupied Molecular Orbital) orbitals are shown in Figure 21.

Figure 23. Orbitals SOMO-α and SOMO-β of [RuCl(trpy)(acpy)] reduced by one electron.

SOMO-α $\Delta G = 135,08$ kJ.mol^{-1} SOMO-β

-370,74 kJ.mol^{-1} -505,82 kJ.mol^{-1}
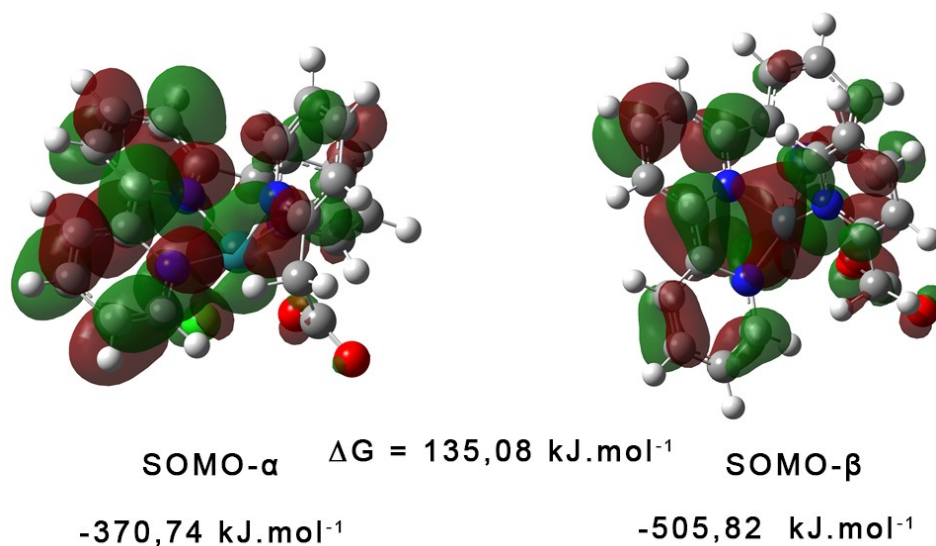
In this case, it is necessary to consider that there are two possible species due the doublet character of the one-electron reduction product. Based on the ΔG values, it is possible to notice that the SOMO-β is more stable than the SOMO-α. In both cases, the orbitals are centralized in the trpy ligand with some contribution of the d-orbitals in the metal center. Furthermore, spectroelectrochemical experiments were performed in 0.1 M of TBAPF$_6$ in anhydrous acetonitrile under an argon atmosphere and the genetared species *in situ* were monitored by UV-Vis, Figure 24.

Figure 24. Changes in the UV-Vis spectra of 0.1 mM [RuCl(trpy)(acpy)] during spectroelectrochemistry in 0.1 M TBAPF$_6$/CH$_3$CN applying -2.18 V *vs* Fc/Fc$^+$, $\Delta t = 10$ s.
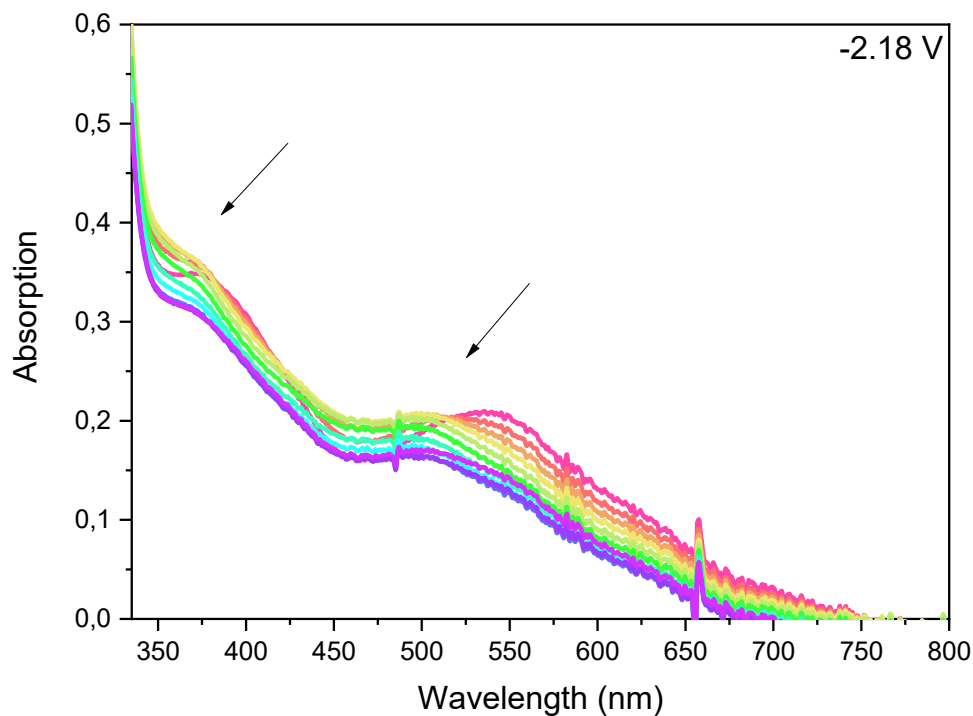
The increase of electron density in the trpy changes the character of the ligand from π-receptor to σ-donor. Therefore, it becomes more difficult to transfer electrons from the metal center to the ligand, resulting in a decrease of the MLCT absorption band simultaneously with a blue-shift in its maximum.

The peak II appears at 2.20 V *vs* Fc/Fc$^+$ and the orbitals of reduced species were obtained by TD-DFT, Figure 25.

Figure 25. Orbitals HOMO, SOMO-α and SOMO-β of [RuCl(trpy)(acpy)] reduced by two electrons.

HOMO

SOMO-α   ΔG = 18,3 kJ.mol^{-1} SOMO-β

-327,05 kJ.mol^{-1} -345,35 kJ.mol^{-1}
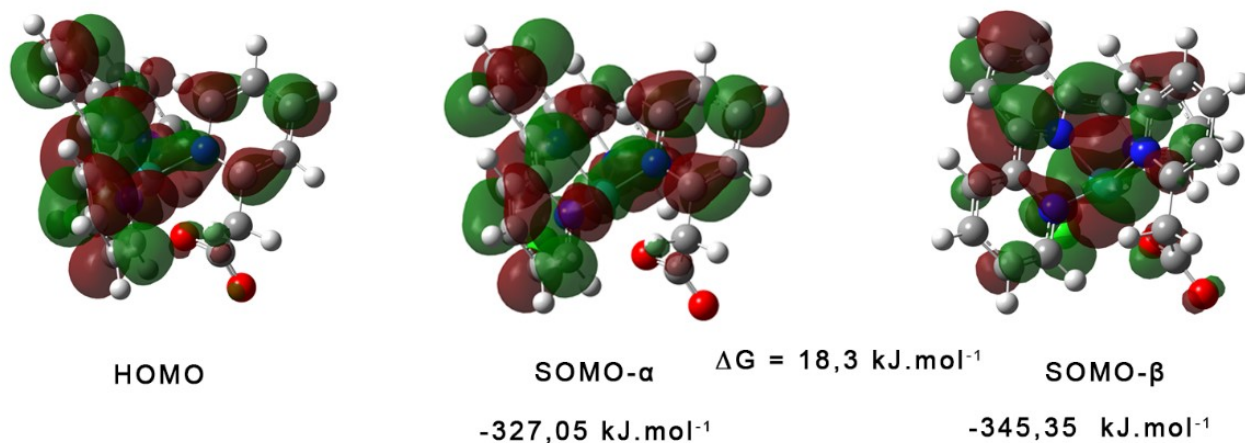
In this case, there are different possibilities of simulation of reduced species. The first one consists of a singlet (HOMO), and the other one, in a triplet (SOMO-α and SOMO-β). In all cases, the electron density is distributed over the trpy ligand and the d-orbitals of the metal center. In addition, there is also a contribution from the orbitals of acpy ligand. Espectroelectrochemical experiments were perfomed at this potential and are shown in Figure 26. It is possible to observe that after the second reduction there is an increase of absorption in the MLCT range. The electron density in the metal center is considerably increased, partially restablishing the MLCT band.

Figure 26. Changes in the UV-Vis spectra of 0.1 mM [RuCl(trpy)(acpy)] during spectroelectrochemistry in 0.1 M TBAPF$_6$/CH$_3$CN applying -2.48 V *vs* Fc/Fc$^+$, Δt = 10 s.
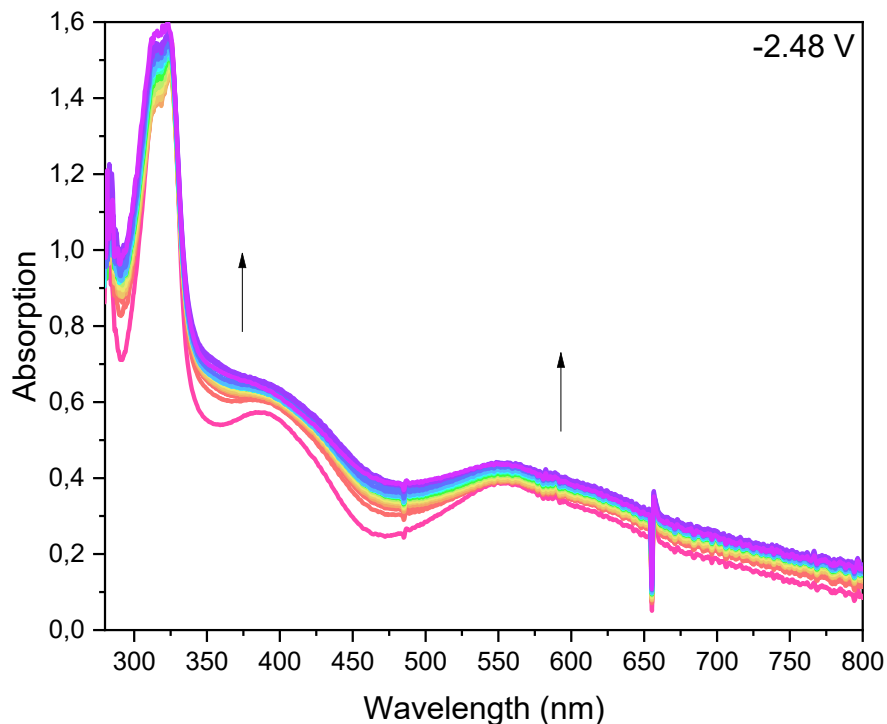
The peaks III and IV are related to the oxidation of the 1 or 2 e$^-$ reduced species and are only observed at fast scan rates, such as, 500, 400 and 300 mV s^{-1}. At lower scan rates, the peaks are not observed, which is an indication of a coupled chemical reaction following the electrochemical reduction steps. The coupled reaction step is probably the loss of the Cl$^-$ ligand to yield a penta-coordinated 18-electrons species. In order to check it, cyclic voltammetries at 1 V s^{-1} were perfomed, Figure 27.

Figure 27. Cyclic voltammetries of 1 mM [RuCl(trpy)(acpy)] in 0.1 M TBAPF$_6$/CH$_3$CN under argon atmosphere at 1 V s^{-1}
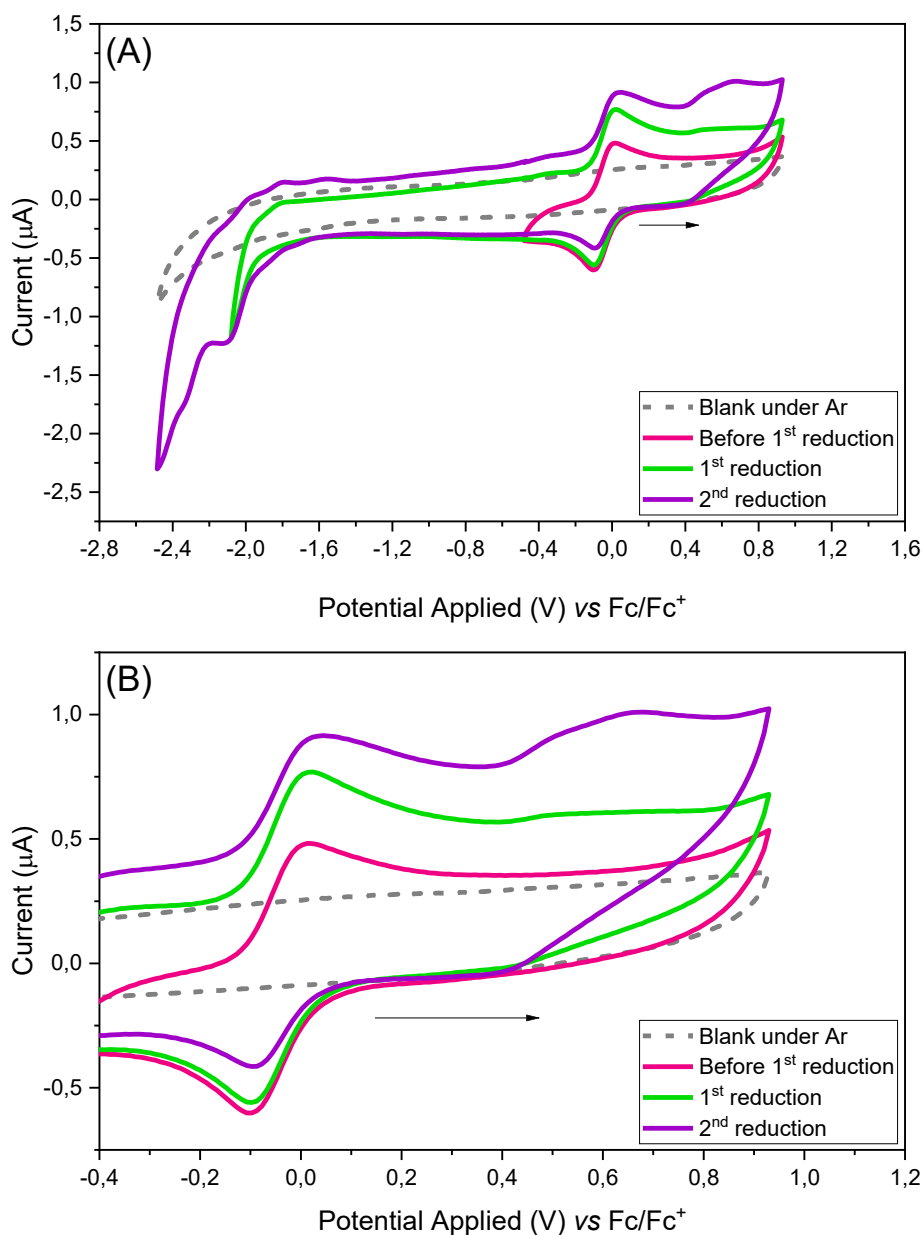
In Figure 27, just the second cycle of cyclic volttametries was taken to investigation. As the potential become more cathodic new peaks appear around 0.7 V and there is an increase of current. As the Cl$^-$ is a good σ-donor ligand, the electronic density over the metal center changes as the ligand is lost. This is

reflected in the oxidation potentials of the metal center suggesting that a new species is formed, probably the solvento complex and penta-coordinated 18-electrons species. In fact, DFT calculations for the reduced species indicate that the Ru-Cl bond distance increases in 3 and 10 pm as the parental complex is reduced by 1 or 2 e⁻, respectively, Table 6.

Table 6. Distance bond of reduced species obtaines by TD-DFT.

Electrons inserted in the structure	Ru-Cl (pm)	Ru-O (pm)	Ru-N$_{acpy}$ (pm)	Ru-N$_{1(trpy)}$ (pm)	Ru-N$_{2(trpy)}$ (pm)	Ru-N$_{3(trpy)}$ (pm)
0	237.152	204.538	204.004	199.381	187.817	200.901
1 (Doublet)	240.750	206.858	199.971	197.829	190.265	200.687
2 (Singlet)	247.117	208.518	194.925	197.153	192.241	197.679
2 (Triplet)	244.155	208.016	196.156	200.535	191.293	200.453

The formation of a penta-coordinated species after the second reduction was proposed based on previous reports for other ruthenium trpy-based complexes (WHITE; MAJI; OTT, 2014; KLEIN et al., 2017). So, the labilization of the chloride ligand is expected to yield a relatively stable 18-electrons penta-coordinated.

Data in Table 6 also evidences that the Ru-O bond becomes weaker as the metal center is reduced, which agrees well with the Pearson's acid base theory. As the complex is reduced, the Ru center becomes softer and the interaction with harder bases such as carboxylate groups decreases.

The cathodic behavior observed for the investigated complex shows some similarities with previous studies for other ruthenium trpy-based complexes. The

proposition that the first reduction occurs in the trpy ligand derives from the character of the polypyridyl ligand to act as a reservoir of electrons (ELGRISHI et al., 2014). Chen and collaborators reported that the first reduction occurs on the trpy ligand for the [Ru(CH$_3$CN)(trpy)(bpy)]$^{2+}$ complex at -1.34 V *vs* NHE (CHEN et al., 2011; CHEN et al., 2014). Johnson and collaborators reported the same behavior for the following complexes: [Ru(CH$_3$CN)(^{t}Bu$_3$tpy)(4,4'-dmbpy)]$^{2+}$ and [Ru(CH$_3$CN)(^{t}Bu$_3$tpy)(6-dmpy)]$^{2+}$ (^{t}Bu$_3$tpy = 4,4',4"-tri-*tert*-butyl-2,2':6,2"-terpyridine; 4,4'-dmbpy = 4,4'-dimethyl-2,2'-bipyridine; 6-mbpy= 6-methyl-2,2'-bipyridine), with the first reduction potentials at -1.78 V and -1.76 V *vs* Fc$^+$/Fc, respectively. (JOHNSON et al., 2016a; JOHNSON et al., 2016b). In Johnson's work this result is supported by DFT calculations, which show a LUMO orbital centered in the trpy ligand in both complexes, similarly to the computed for the [RuCl(trpy)(acpy)] complex.

For the second reduction, the literature usually describes it as the reduction of the second polypyridyl ligand, which in some cases is characterized as an irreversible process (SONDAZ et al., 2001; KOIZUMI; TOMON; TANAKA, 2003; GOZE et al., 2007; BREIVOGEL; KREITNER; HEINZE, 2014). An example of that is the [Ru(CH$_3$CN)(trpy)(bpy)]$^{2+}$ complex, whose second reduction has been reported to occur in the bpy ligand (CHEN et al., 2011; CHEN et al., 2014). Beyond the complexes reported by Chen and collaborators, other authors have reported the same behavior for other complexes containing different types of ligands (BERGER; MCMILLIN, 1988; ENGLAND et al., 2012; KLEIN et al., 2017; LEE et al., 2018). For example, Ghosh and collaborators reported a series of complexes based on the 4'-[4-(*tert*-butyl-phenyl)-1*H*-1,2,3-triazol-4-yl]-2,2':6',2"-terpyridine, for which it was observed that the first reduction happens in trpy

ligand, and the second one, in the bpy or the unmodified trpy ligand (GHOSH et al., 2020).

For [RuCl(trpy)(acpy)], reduction of the acpy ligand seems less accessible as there is no conjugation between the carboxylate group and the pyridyl ligand. So, the electron density remains concentrated in the trpy ligand. Following the labilization of the chloride ion, the Ru-O bond in the penta-coordinated species becomes weaker than that in the non-reduced species, which may allow an electrophilic attack by a suitable molecule.

4.4.   Electrocatalytic properties towards CO_2 electroreduction

The reduction of [RuCl(trpy)(acpy)] under CO_2 atmosphere leads to a considerable increase in the faradaic current consistent with a catalytic process, Figure 28.

Figure 28. Cyclic voltammetries of 1 mM [RuCl(trpy)(acpy)] in 0.1 M $TBAPF_6$/CH_3CN under argon and CO_2 atmosphere at 100 mV s^{-1}.
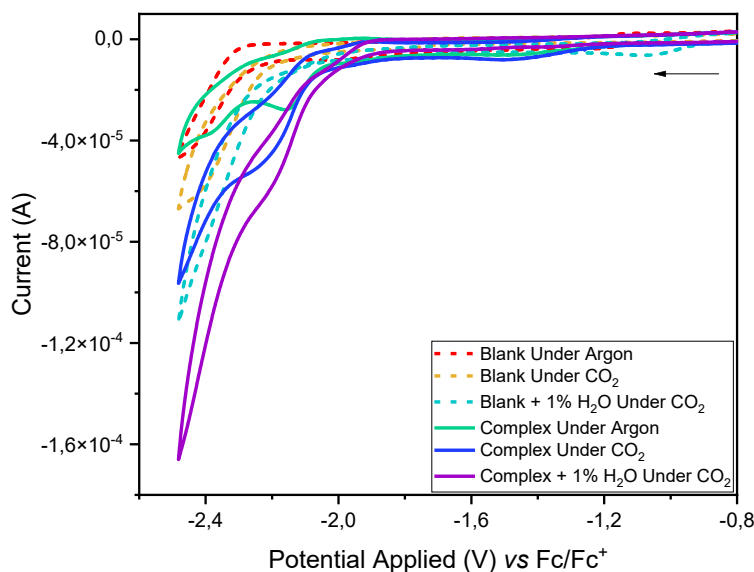
In the voltammograms of Figure 28 it is possible to observe that, comparing the electrochemical profiles under argon and CO_2, there is an increase in current, i.e., the complex is able to reduce CO_2 with an *onset* potential of -2.06 V *vs* Fc/Fc$^+$ in anhydrous conditions. In addition, in the presence of 1% water (v/v), in relation to the solvent, there is a small decrease in the *onset* potential to -2.0 V *vs* Fc/Fc$^+$. In both cases the *onset* occurs before the second reduction of complex. The interaction of [RuCl(trpy)(acpy)] with CO_2 was also observed by cyclic voltammetries, Figure 29.

Figure 29. Cyclic voltammetries of 1 mM [RuCl(trpy)(acpy)] in 0.1 M TBAPF$_6$/CH$_3$CN at 100 mV s^{-1} (A) under argon, (B) under CO_2 atmosphere and (C) under CO_2 considering first and second cycles.
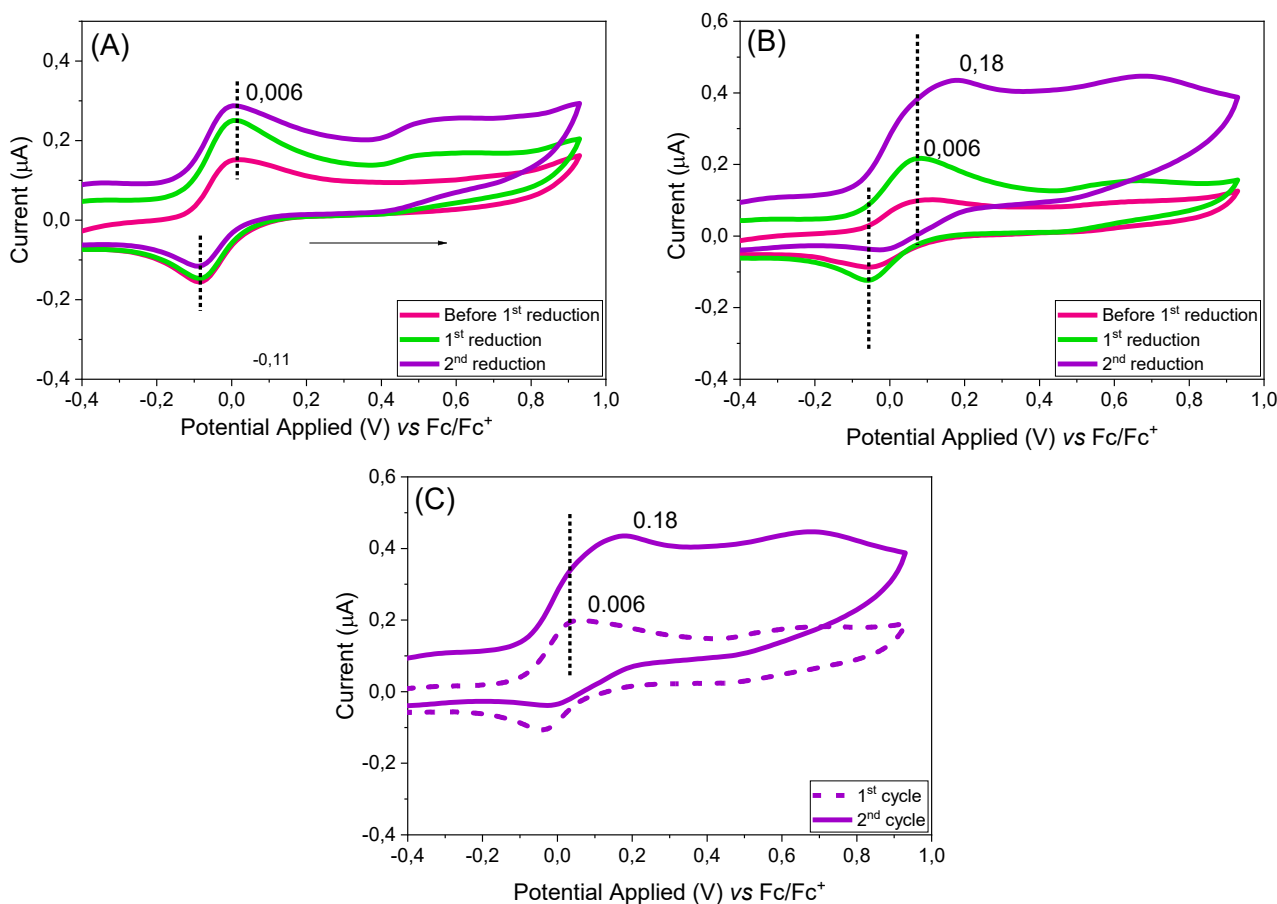
In Figure 29(A), the oxidation potential of couple $Ru^{II/III}$ under argon do not present any shifts even after the second reduction. Just a new peak around 0.7 V, described in the previous section as the formation of a new species after the loss of Cl^- ligand. Under CO_2 atmosphere, Figure 29(B), the oxidation potential peak of couple $Ru^{II/III}$ undergoes a shift from 0.006 to 0.18 V as clearly seen in Figure 29(C). this behavior suggests the interaction of CO_2 producing a new electroactive species during the catalytic process.

The catalytic constant (k_{cat}) was determined by Equation 3 (BARD; FAULKNER, 2002) and compared with other ruthenium complexes reported in the literature, Table 7.

$$i_c = nFA[Ru]\sqrt{k_{cat}D}$$ Equation 3

In the equation above, i_c corresponds to the catalytic peak current, n is the number of electrons involved in the process (n = 2), F is the Faraday constant (96485 C mol^{-1}), A is the electrode area (0.102 cm^2), [Ru] is the concentration of catalyst in solution, and D is the diffusion coefficient for Ru complexes ($\sim5.10^{-6}$ cm^2 s^{-1}) (CHEN et al., 2011; LEE et al., 2018).

Table 7. Electrocatalytic parameters for different ruthenium complexes.

Catalyst	Condition	k_{cat} (s^{-1})	Ref.
[RuCl(trpy)(acpy)]	0% H_2O/CH_3CN	1.5	This work
[Ru(trpy)(bpy)(CH$_3$CN)]$^{2+}$	0% H_2O/CH_3CN	5.5	(CHEN et al., 2011)
[Ru(trpy)(Mebim-py)(CH$_3$CN)]$^{2+}$	0% H_2O/CH_3CN	19.0	(CHEN et al., 2011)
[RuCl(trpy)(acpy)]	1% H_2O/CH_3CN	2.0	This work
[Ru(trpy)(bpy)(CH$_3$CN)]$^{2+}$	10% H_2O/CH_3CN	5.1	(CHEN et al., 2011)
[Ru(trpy)(pqn)(CH$_3$CN)]$^{2+}$	10% H_2O/CH_3CN	4.7	(LEE et al., 2018)

The determined catalytic rate constant (k_{cat}) obtained for [RuCl(trpy)(acpy)] is 1.5 s^{-1} in anhydrous conditions and 2.0 s^{-1} with 1% added water. As shown in Table 7, k_{cat} values obtained for the [RuCl(trpy)(acpy)] are lower when compared with other Ru^{II} complexes. This can be partially explained by the fact that, for the other complexes, the catalytic properties were evaluated for the solvento species. Thus, in the case of [RuCl(trpy)(acpy)], one limiting step would be the initial labilization of the chloride ligand before the CO_2 reduction. k_{cat} was also determined in the presence of D_2O in order to study an possible kinetic isotope effect (KIE). The k_{cat} obtained in D_2O was also 2.0 s^{-1}, Figure 30. This value suggest that the H_2O do not participate in the limiting step during the catalytic process.

Figure 30. Cyclic voltammetries of 1 mM [RuCl(trpy)(acpy)] in 0.1 M TBAPF$_6$/CH$_3$CN under CO$_2$ atmosphere at 100 mV s^{-1} in the presence of 1% H$_2$O or D$_2$O.
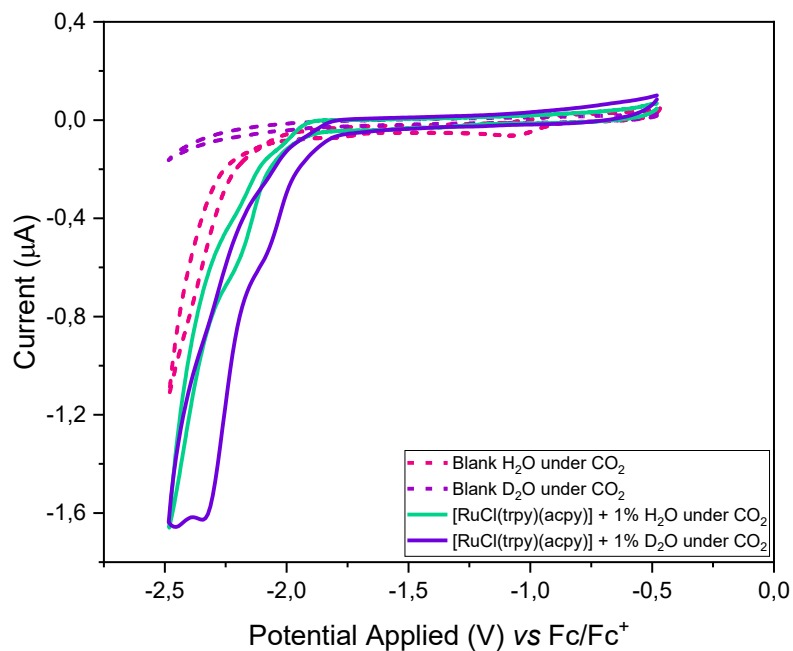
To check the catalyst efficiency and to obtain the Turnover Number (TON), bulk electrolysis experiments were perfomed in an H-cell as shown in Figure 31.

Figure 31. H-cell used in the bulk of electrolysis experiments.

     In this type of cell the electrodes are separated into two compartments. The purpose of this arrangement is to prevent the oxidation of reduced products on the counterelectrode. Bulk electrolysis experiments were perfomed using 1 mM of [RuCl(trpy)(acpy)] and 0.1 M of TBAPF$_6$ in acetonitrile. Control experiments were perfomed under the same conditions in the absence of CO_2 and also under CO_2 atmosphere and in the absence of the complex. Aliquotes of the catholyte headspace were collected during the experiments and analyzed by GC in order to identify and quantify the gases. CO was identified as the main reduction product, allowing for the determination of the turnover number (TON) as a function of time under different conditions, Figure 31. For reference, the well-know Lehn's CO_2 reduction catalyst *fac*-[ReCl(CO)$_3$(bpy)] (HAWECKER; LEHN; ZIESSEL, 1983; 1986) was evaluated in the same conditions. The value of

TON$_{CO}$ in these conditions reported by Franco and collaborators was 16 (FRANCO et al., 2015).

Figure 32. TON$_{CO}$ production as a function of time obtained by bulk electrolysis, applied potential: -2.18 V vs Fc/Fc$^+$, 1 mM [RuCl(trpy)(acpy)] and [ReCl(CO)$_3$(bpy)] in 0.1 M TBAPF$_6$/CH$_3$CN.
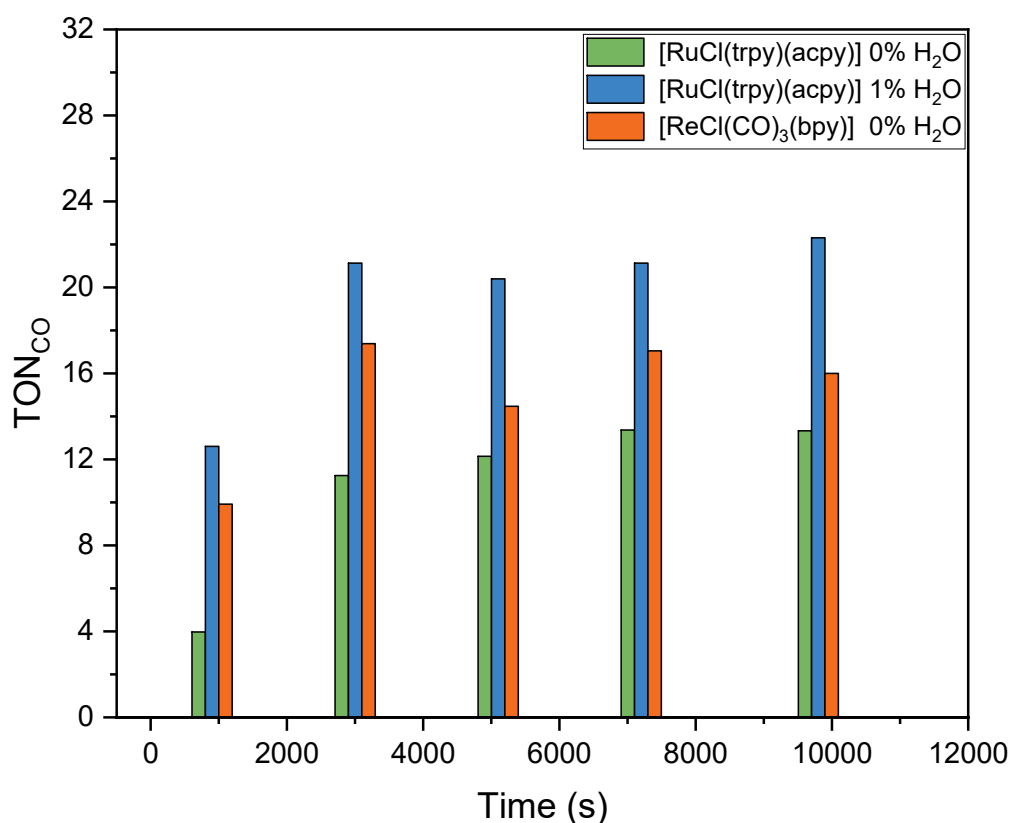
For the control experiments, i.e., in the absence of CO$_2$ or [RuCl(trpy)(acpy)] under argon, no CO was detected. For *fac*-[ReCl(CO)$_3$(bpy)], the TON$_{CO}$ was 15 ± 3, in line with the literature values. For the [RuCl(trpy)(acpy)] under anhydrous conditions, the CO production achieved a TON$_{CO}$ of 12 ± 1 after 3000 s, while in the presence of 1% water the TON$_{CO}$ was 21 ± 1. Trace amounts of H$_2$ were detected during the experiments in non-anydrous conditions with TON

<1. Moreover, in order to investigate if other species were formed during the electrolysis, aliquotes of the catholyte in all conditions were collected and basified with KOH 6 M, pH = 8.0. After this, the solvent was rotaevaporated, D_2O was added to the residue and the resulting solution analyzed by ^{1}H NMR, Figure 32.

Figure 33. Bulk of electrolysis at -2.18 V vs Fc/Fc+, 1 mM [RuCl(trpy)(acpy)] in 0.1 M TBAPF$_6$/CH$_3$CN.
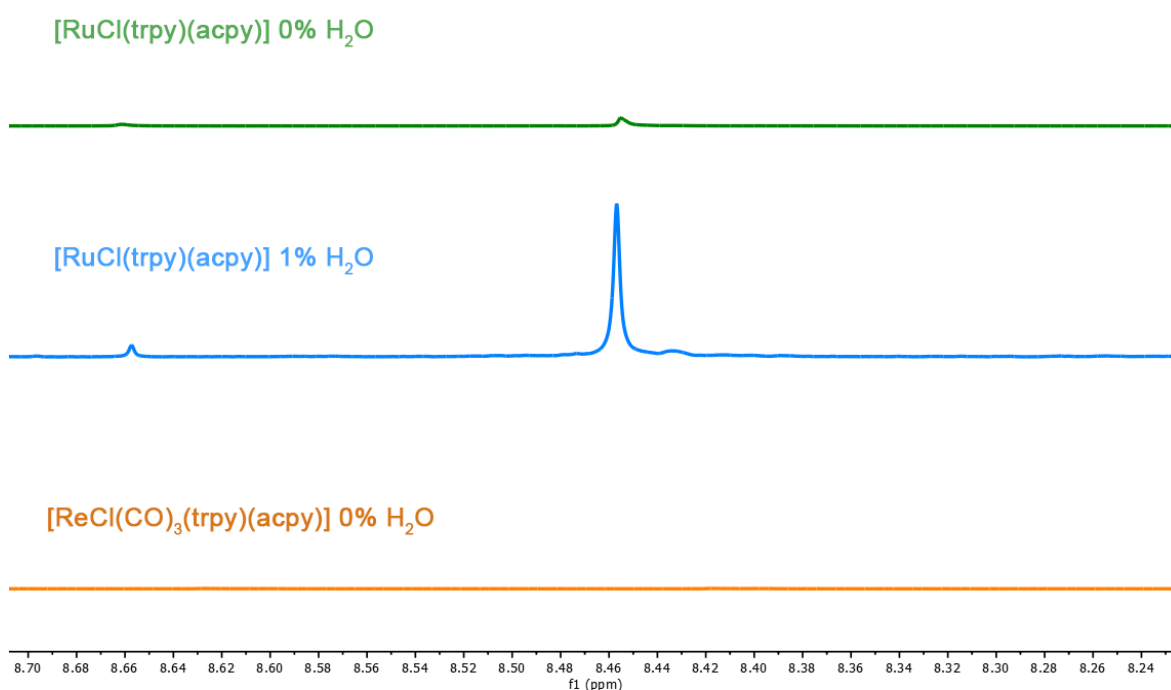
In the ^{1}H NMR data it is possible to observe that in the presence of water a singlet at 8.46 pm was detected, being attributed to formate ($HCOO^-$) as reported elsewhere (HUFF; SANFORD, 2013). The TON_{HCOO^-} achieved in this condition was 7.

Comparing the efficiency of the catalytic processes for different complexes is not an easy task. The reason for that is different conditions are applied in different studies and they have distinct influences on the overall catalytic

efficiency. Table 8 lists different ruthenium trpy-based complexes under different conditions with the respective TONs and Faradaic efficiency (FE). The faradaic effiency was determined according to Equation 4.

$$FE_{CO} = \frac{nFy}{Q}$$ Equation 4

The FE_{CO} correlates the experimental production of CO, $HCOO^-$ and H_2 with the overall charge that went through the electrochemical cell. In Equation 4, n represents the number of electrons involved in the CO_2 reduction to CO or $HCOO^-$, n = 2, F is the Faraday constant (96485 $C.mol^{-1}$), y is the number of mols of products formed and Q is the charge in the system through electrolysis.

Table 8. TON_{CO} and faradaic efficiencies for different ruthenium complexes.

Catalyst	Condition	E_{app} (V)	TON		FE		
			CO	$HCOO^-$	CO	$HCOO^-$	H_2
[RuCl(trpy)(acpy)]	0% H_2O/CH_3CN	-2.18	12	0	89%	-	<1%
[Ru(trpy)(bpy)(CH_3CN)]$^{2+}$ [a]	0% H_2O/CH_3CN	-2.00	5	-	76%	-	-
[RuCl(trpy)(acpy)]	1% H_2O/CH_3CN	-2.18	21	7	76%	20%	2%
[Ru(trpy)(bpy)(CH_3CN)]$^{2+}$ [b]	10% H_2O/CH_3CN	-1.68	7	-	90%	-	0.5%
[Ru(trpy)(Mebim-py)(CH_3CN)]$^{2+}$ [c]	5% H_2O/CH_3CN	-1.95	30	-	87%	-	-
[Ru(trpy)(pqn)(CH_3CN)]$^{2+}$ [d]	10% H_2O/CH_3CN	-1.70	2	<1	56%	7%	0.5%

[a](CHEN et al., 2011); [b](CHEN et al., 2014); [c](GONELL et al., 2019); [d](LEE et al., 2018).

Under anhydrous conditions, it is possible to compare the complex containing the bpy ligand and the new complex, [RuCl(trpy)(acpy)]. The latter exhibits a TON_{CO} almost two times higher than $[Ru(trpy)(bpy)(CH_3CN)]^{2+}$, showing that the new complex is more stable than the previous one. The comparison of TON_{CO} in the presence of water reveals that [RuCl(trpy)(acpy)] presents a higher TON_{CO} than $[Ru(trpy)(bpy)(CH_3CN)]^{2+}$ and $[Ru(trpy)(pqn)(CH_3CN)]^{2+}$.

For [RuCl(trpy)(acpy)], in the presence of water, the FE_{CO} decreases when compared to that in anhydrous conditions, from 89% to 76%. It can be explained by the production of formate which have a $FE_{HCOO^-} = 20\%$. Small amounts of H_2 were also identified. In anhydrous conditions the values obtained were smaller than 5 µmol, and with 1% of water 8 µmol. These values represents a $FE_{H_2} < 1\%$ in anhydrous conditions and 2% in the presence of water.

Clearly, the catalytic properties of [RuCl(trpy)(acpy)] are naturally influenced by the ligands. Partial labilization of acpy can be an important factor to explain the product selectivity and the electrocatalytic activity itself. Understanding such influence requires the analysis of the reaction mechanisms involved in CO_2 reduction mediated by coordination compounds. Several mechanistic propositions are described in the literature as summarized by Gonell and colleagues (GONELL et al., 2019), Figure 34.

Figure 34. Proposed mechanisms for CO_2 electroreduction by ruthenium catalysts.
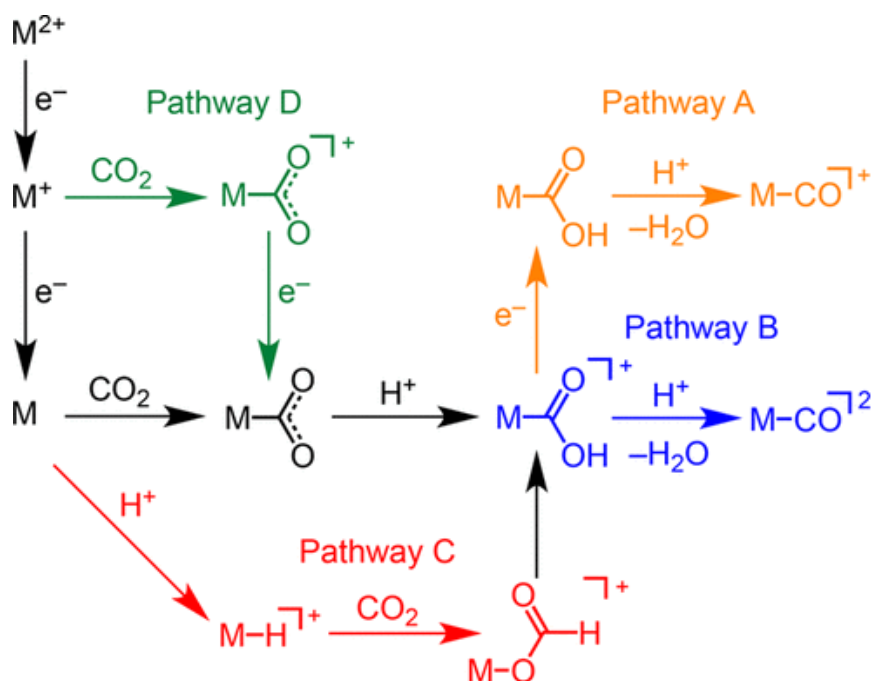
In general, most of the proposed mechanisms in the literature involve the CO_2 coordination after 1 or 2 e^- reduction, as shown in the pathways A to D. Despite this, some differences should be highlighted. For example, in pathway A after coordination of CO_2 to the metal center, the substrate undergoes protonation with a subsequent reduction before the protonolysis, releasing water and producing the M-CO complex, which further releases CO. This pathway is usually reported for Re(I) and Mn(I) systems and, in rare cases, for Ru(II) systems (SAMPSON et al., 2014; MIN et al., 2016; CLARK et al., 2018; GONELL et al., 2019).

Pathway B is the most common mechanism for ruthenium complexes, in which, following CO_2 coordination, there are two subsequent protonations releasing water and forming the M-CO complex (ISHIDA; TANAKA; TANAKA, 1987; CHEN et al., 2014; GONELL et al., 2019). Pathway C involves the

formation of a metal-hydride intermediate, which reacts with CO_2 to produce metallocarboxylate. This intermediate can yield formate or rearrange to release CO as in pathway B (MACHAN; SAMPSON; KUBIAK, 2015). The mechanism D is similar to A and B, but in it, CO_2 coordination occurs after the first reduction potential. After this, the reaction follows the same behavior observed in the other pathways (JOHNSON et al., 2016b; LEE et al., 2018).

For the [RuCl(trpy)(acpy)] complex, spectroelectrochemical experiments in the IR region were perfomed in order to identify possible reaction intermediates. Some probes in the [RuCl(trpy)(acpy)] were selected to be monitored, particularly the C=O and C=C bonds from de acpy and trpy ligand respectively. In this system, however, limitations in the spectroscopic window may restrict the data collection. The solvent absorption for example must be taken under consideration in order to observe spectroscopic changes in these stretchings. Firstly, dichloromethane was chosen as solvent due its spectral window from 1800 to 1500 cm^{-1}. The first experiment was performed under argon, Figure 35.

Figure 35. Changes in the FTIR spectra of 1 mM [RuCl(trpy)(acpy)] during the spectroelectrochemistry in 0.1 M TBAPF$_6$/CH$_2$Cl$_2$ varying potential under argon atmosphere Δt = 1.5 min.
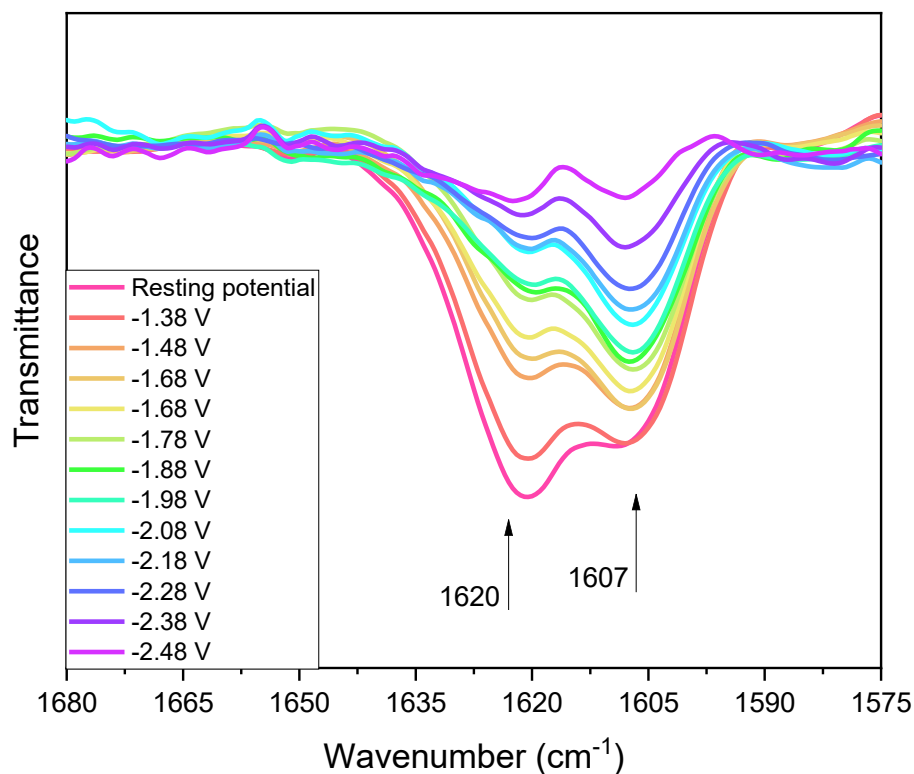
Under argon atmosphere, Figure 35, it is possible to observe that the stretchings at 1620 and 1607 cm^{-1} are shifted to higher wavenumbers when compared to the FTIR spectra in solid state, section 4.1, which can be related to the interaction with solvent molecules. As cathodic potentials are applied, it is possible to observe a decrease in the intensities and a small displacement of these stretchings. As described in section 4.1, these absorption bands are attributed to the C=C stretchings from aromatic ligands, in the trpy ligand, with a contribuition of C=O stretching from the acpy group. Trpy reduction would decrease the intensity of C=C stretching peaks, while changes in the electron

density of the metal center would shift the C=O stretching peak of the coordinate carboxylate group. Thus, the observed changes in Figure 35 are in agreement with the attributions made by electrochemistry, i.e., first reduction is trpy-centered following by reduction of the metal center.

The spectroelectrochemical experiments were also performed in acetonitrile. In anhydrous acetonitrile the experimental spectroscopic window was from 2200 to 1650 cm^{-1}. The C=C and C=O stretchings for [RuCl(trpy)(acpy)] would be expected around 1600 cm^{-1}. In this range, the solvent have a stronger absorption which not allow to see clearly any stretchings, as can be observed by the spectra in Appendix D. When 1% H$_2$O is added, the spectroscopic window is even smaller, from 1900 to 1750 cm^{-1}. In this case the water have a stronger absorption above 2000 cm^{-1} and at 1650 cm^{-1} which even with background subtraction or baseline correction, a more profound analysis could not be carried out. We have then employed D$_2$O instead of H$_2$O to expand the spectroscopic window.

In the presence of D$_2$O the useful spectroscopic window under argon atmosphere was from 2100 to 1600 cm^{-1}. So, in Figure 36 some changes during the spectroelectrochemical experiments with 1% D$_2$O under argon can be observed.

Figure 36. Changes in the FTIR spectra of 1 mM [RuCl(trpy)(acpy)] during the spectroelectrochemistry in 0.1 M TBAPF$_6$/CH$_3$CN with 1% of D$_2$O varying potential under argon atmosphere $\Delta t = 1.5$ min.
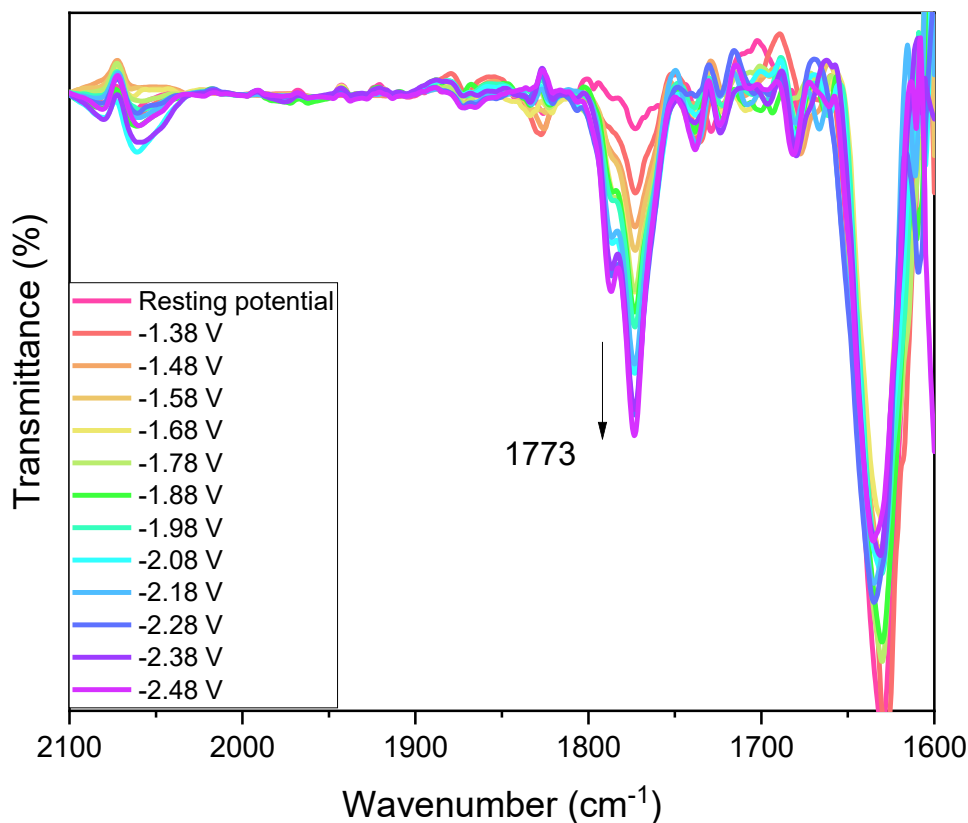
In Figure 36, in the presence of 1% D$_2$O and under argon, a new stretching at 1773 cm^{-1} can be observed as cathodic potentials are applied to the complex solution. When compared to the FTIR of the free acpy ligand, described in the section 4.1, it is possible to observe that this stretching seems to be the correspondent to the C=O of carboxylate group. This new stretching at 1773 cm^{-1} just occurs in the presence of D$_2$O, i.e., in anhydrous acetonitrile this behavior was not observed. It suggests a partial labilization of acpy can occur in presence of water and allowing one or two electron reduction of [RuCl(trpy)(acpy)].

In order to identify possible key intermediates during the catalytic process, the spectroelectrochemical experiments were also performed in the presence of CO_2. Iniatially, the experiments were performed in dichloromethane, Figure 37.

Figure 37. Changes in the FTIR spectra of 1 mM [RuCl(trpy)(acpy)] during the spectroelectrochemistry in 0.1 M $TBAPF_6/CH_2Cl_2$ varying potential under CO_2 atmosphere $\Delta t = 1.5$ min.
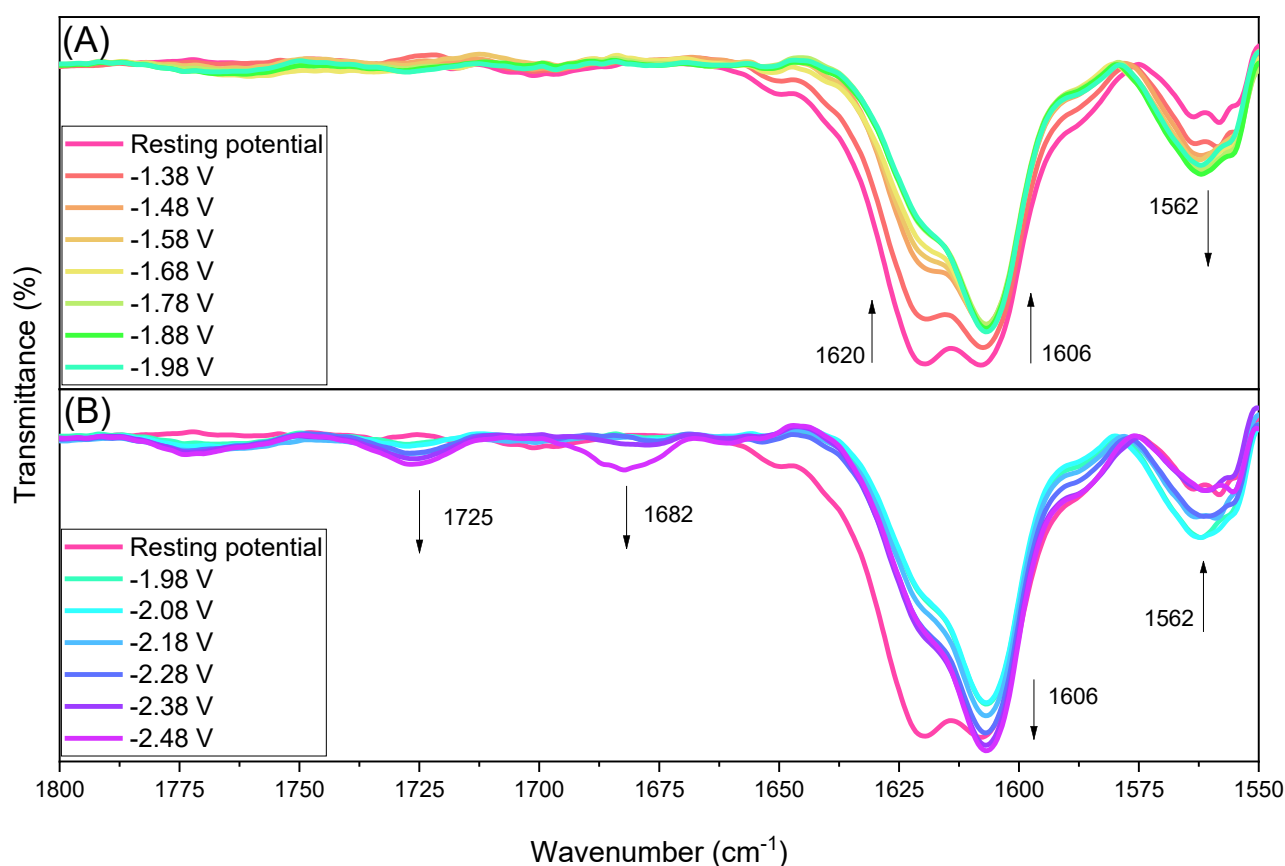
In Figure 37(A), it is possible to observe that, under a CO_2 atmosphere the stretchings at 1620 and 1607 cm^{-1} follow the same behavior as under argon atmosphere, Figure 35. In addition to this, a new stretching at 1562 cm^{-1} can be clearly seen. This range is known for asymmetrical stretchings for carboxylate

anions (SILVERSTEIN; WEBSTER; KIEMLE, 2005), which may arise the formation of $Ru-CO_2$ bond.

As the applied cathodic potential is increased, Figure 37(B), it is possible to observe that, after the first reduction potential, the intensity of the stretching at 1606 cm^{-1} increases. Concomitantly, the stretching at 1562 cm^{-1} decreases and two new small stretches are observed at 1725 and 1682 cm^{-1}, respectively. These new bands are observed when CO_2 is present, and this spectral region corresponds to typical ν(C=O) and ν(C-O) stretching modes in different configurations (SILVERSTEIN; WEBSTER; KIEMLE, 2005; NAKAMOTO, 2009). Therefore, we can tentatively attribute such peaks to the possible reaction intermediates formed by the interaction between CO_2 and the reduced metal complex species. In acetonitrile the same behavior was observed, Figure 38, but in this solvent the spectroscopic window is reduced in relation to CH_2Cl_2 inhibiting any observation below 1650 cm^{-1}. Two new stretchings at 1746 and 1682 cm^{-1} are observed as the potential become more cathodic, which correspond to the same stretchings observed in CH_2Cl_2.

Figure 38. Changes in the FTIR spectra of 1 mM [RuCl(trpy)(acpy)] during the spectroelectrochemistry in 0.1 M TBAPF$_6$/CH$_3$CN varying potential under CO$_2$ atmosphere Δt = 1.5 min.
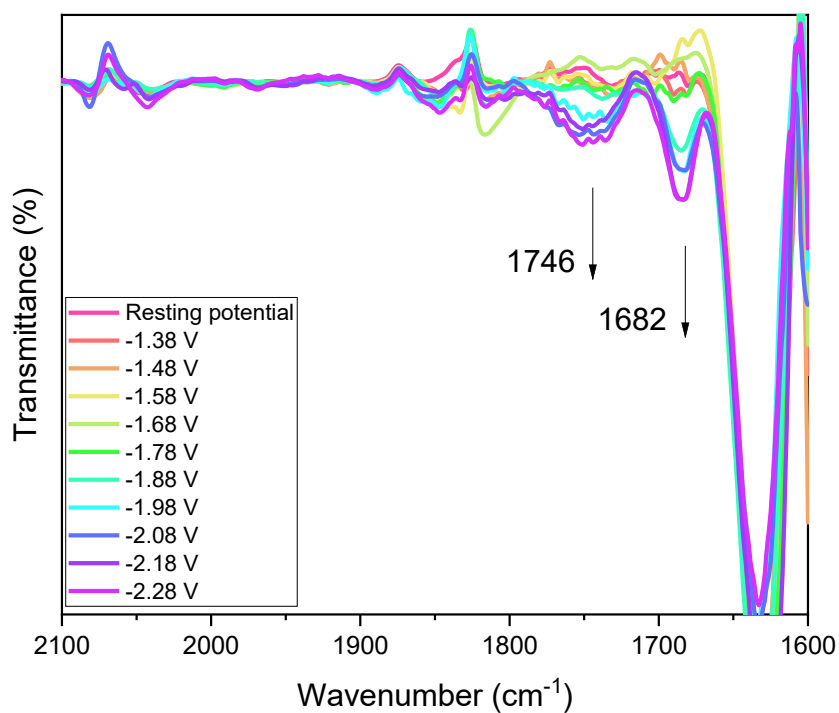

As reported earlier, in the presence of H$_2$O, the spectroscopic window is reduced to 1900 cm^{-1} and 1750 cm^{-1}. The same spectroscopic window was observed in the presence of CO$_2$, Appendix D. Thus, no additional stretching or shift could be observed in these conditions. In the presence of D$_2$O under CO$_2$ atmosphere new stretchings were observed, Figure 39.

Figure 39. Changes in the FTIR spectra of 1 mM [RuCl(trpy)(acpy)] during the spectroelectrochemistry in 0.1 M TBAPF$_6$/CH$_3$CN with 1% of D$_2$O varying potential under CO$_2$ atmosphere Δt = 1.5 min.
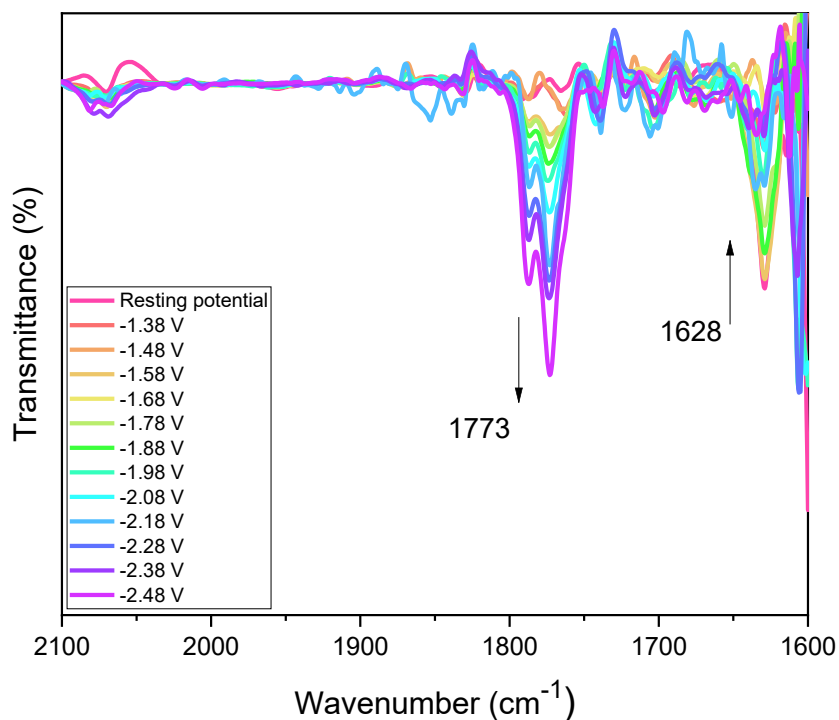
Under CO$_2$ and the presence of 1% of D$_2$O a new stretching at 1773 cm^{-1} was observed and the stretching at 1628 cm^{-1} decreased. The new stretching is just observed when water is added. The new stretching matches well with the stretching of C=O in the FTIR of the free acpy ligand. It suggest that a possible labilization of the carboxylate group occurs during the catalytic process in the presence of water. In addition, as the potential is increased and the stretching at 1773 cm^{-1} become more evident, the stretching at 1628 cm^{-1}, observed for the original complex, and attributed to the overlap between ν(C=O) and ν(C=C), decreases proportionaly. Similar behavior is observed under argon atmosphere,

however the relative intensity of the peak at 1773 cm^{-1} is smaller in relation to that at 1628 cm^{-1}. Thus, it seems the presence of CO_2 favors the formation of the species responsible for the stretching at 1773 cm^{-1}, i.e., the partial labilization of the acpy ligand.

The spectroelectrochemical behavior observed for the investigated complex shows some similarities with previous studies for other ruthenium trpy-based complexes. Particularly, the stretching at 1682 cm^{-1} under CO_2 observed in Figures 37(B) and 38, appears after the second reduction potential of the complex and coincides with previous literature data for Ru-COO$^-$ species (CHEN et al., 2011). In Chen's work, a stretching peak appears around 1675 cm^{-1} after the second reduction potential for the [Ru(trpy)(bpy)(CH$_3$CN)]$^{2+}$ complex under CO_2 atmosphere, which was attributed to the Ru-COO$^-$ species (CHEN et al., 2011). Moreover, the same behavior had been observed by Tanaka et al (NAGAO; MIZUKAWA; TANAKA, 1994). After the second reduction a new stretching was observed at 1653 cm^{-1}, but in this case, it was attributed to the formation of the species Ru-COOH (NAGAO; MIZUKAWA; TANAKA, 1994).

Following the formation of Ru-COO$^-$ or Ru-COOH species, Ru-CO can be generated as result of a condensation, which will further release CO.

Furthermore, the new stretching at 1773 cm^{-1}, observed just in presence of D_2O, match with the spectra for the free acpy ligand and suggest that the partially labilized acpy ligand might be able to interact with CO_2 during the electrocatalytic process, probably with the intermediation of protons. Moreover, in the presence of water, formate is also produced, indicating a secondary pathway in the course of the reaction. As shown in the Figure 34, the production of formate is typically preceded by the formation of metal-hydride species. For

example, in the work of Machan and coworkers with the *trans*-[Ru(mesmbpy)(CO)$_2$Cl$_2$] complex (mesmbpy = 6,6′-dimesityl-2,2′-bipyridine), it was observed that under CO_2 atmosphere and in the presence of a Brønsted acid (phenol) formate was produced and new stretchings at 2050 and 1983 cm^{-1} were observed and attributed to the formation of a metal-hydride in the spectroelectrochemical experiments (MACHAN; SAMPSON; KUBIAK, 2015). This species promptly reacts with CO_2 to yield a formate-coordinated species, which finally releases formate to the reaction medium.

Therefore, as formate is also observed for our electrocatalyst, a possible metal-hydride intermediate can be considered, despite no experimental evidence for this intermediate could be observed. It is also clear that, in presence of water the partial labilization of the acpy ligand occurs, which is not observed in anhydrous conditions and such configuration should be involved in the reduction of CO_2 to formate instead of CO. Based on our experimental observations and previous studies in the literature, a mechanism for CO_2 reduction mediated by [RuCl(trpy)(acpy)] can be proposed and is summarized in Figure 40.

Figure 40. Proposed mechanism for CO_2 reduction mediated by [RuCl(trpy)(acpy)].
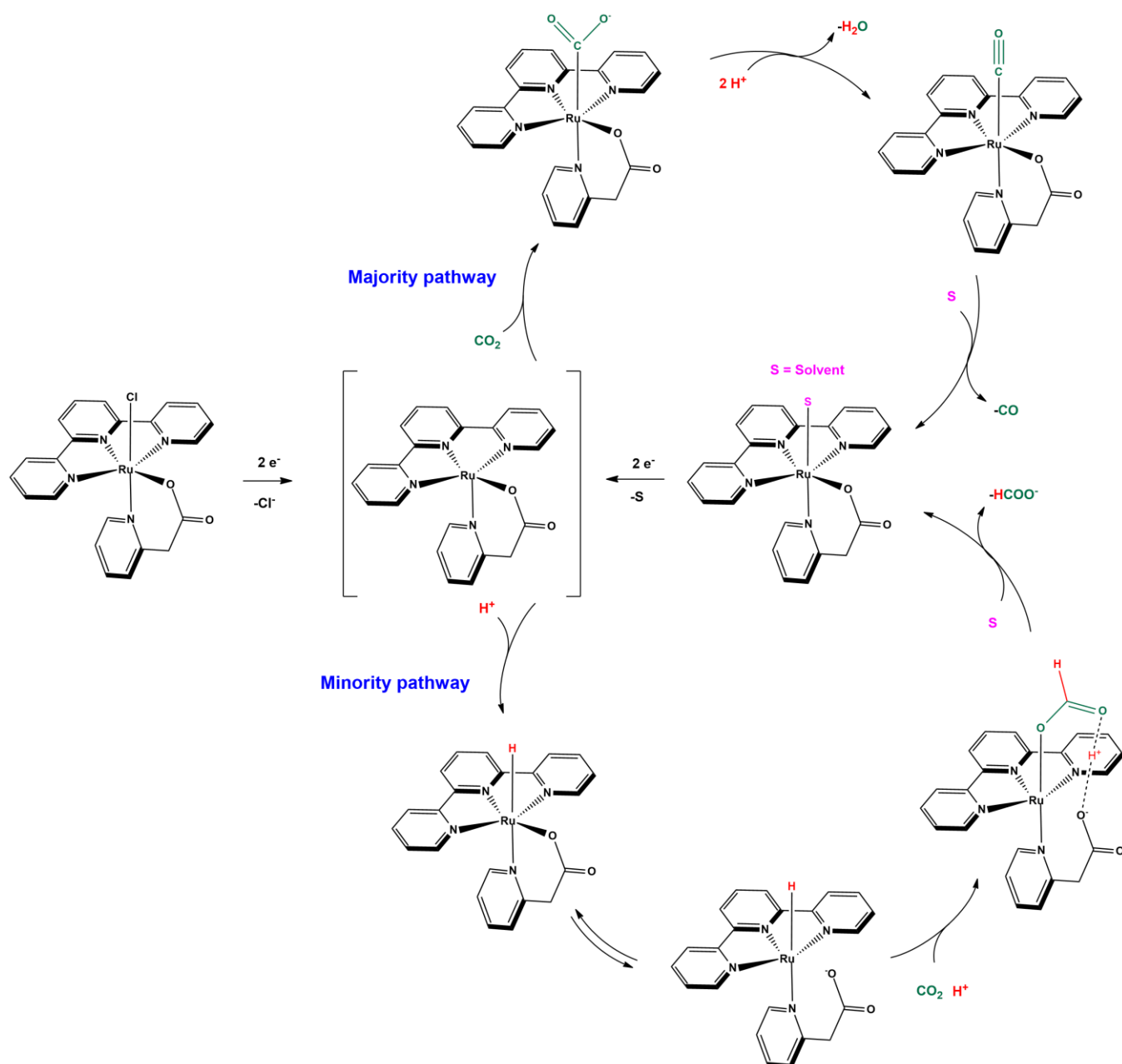
As summarized in Figure 40, initially the complex is reduced in 2e⁻ and the loss of Cl⁻ occurs yielding a pentacoordinated 18e⁻ species. The conclusion that the chloride ligand is lost during the reduction process is supported by the cyclic voltammetries at slow scan rates and are corroborated by the increase of Ru-Cl bond distance bond observed in the theoretical calculations. In the cyclic

voltammetries, after the second reduction, a new peak in the anodic range is observed suggesting that a new species is formed. After it, the mechanism of CO_2 reduction can follow two different pathways. The majoritarian pathway leads to the formation of CO and occurs both in the presence and in the absence of water as Brønsted acid. The minoritarian pathway leads to formation of formate and occurs only in the presence of water. In the former, the first reaction step involves the activation of the CO_2 molecule by the pentacoordinated $2e^-$ reduced complex to yield a metallocarboxylate complex, $Ru\text{-}COO^-$. The formation of this intermediated is corroborated by spectroelectrochemical experiments in dichloromethane and acetonitrile in which a new stretching appear at 1682 cm^{-1}. No spectroscopic evidence for the labilization of the acpy ligand is observed in this condition. The following step is the subsequent protonation of CO_2 releasing water, which gives the metal-carbonyl complex, Ru-CO. The increase in the TON_{CO} when water is added to the system (even activating the minoritarian pathway) corroborates for this proposition. The resulting Ru-CO complex is unstable in relation to the original complex, so one can expect the release of CO and coordination of a solvent molecule closing the catalytic cycle.

The suggested minoritarian pathway seems to be activated in the presence of water and involves the direct reaction of the $2e^-$ reduced pentacoordinated species with water to yield a metal-hydride complex, Ru-H. Despite no experimental evidence could found for the formation of this intermediate, it has been proposed in the literature (MACHAN; SAMPSON; KUBIAK, 2015) as a necessary step to porduce formate from CO_2. The available experimental data reveal that the presence of water triggers the partial labilization of the acpy ligand through the carboxylate group. In the spectroelectrochemical

experiments in the presence of D_2O, a new stretching is observed at 1773 cm^{-1} under argon and CO_2. This stretching matches with the C=O vibration observed for the carboxylate group of the non-coordinatinated acpy. We can expect that the carboxylate anion close to the coordination sphere can take part in different interactions (hydrogen bondings), favoring the formation of Ru-OCHO species, which will finally realease HCOO$^-$. This behavior was just observed in the presence of water, which suggests that the chelate breakdown just occurs in this condition. It also agrees well with the Pearson's theory for soft and hard acid/bases as the reduction of the metal center should destabilize the Ru-O bond. The reaction pathway shown in the Figure 40 involving the partial labilization of the acpy ligand is one among several possible alternatives considering the interaction of CO_2, Ru-H and the free carboxylate anion. DFT calculations can possibly indicate the most favorable one from an energetic point of view, since the experimental detection of such species is quite difficult.

The present results evidence how changes in the coordination sphere in conjunction with the physico-chemical conditions can drive the activity and selectivity of Ru-based CO_2 reduction catalysts. In particular, the presence of the acpy ligand plays an important rule, firstly modulating the oxidation/reduction potentials, and more importantly, offering the possibility of multiple reaction pathways due its partial labilization during the catalytic cycle. Continous investigations with increase amounts of water, or even employing different Brønsted acids may allow to optimize the TON and even triggers the formation of formate as major reduction product instead of CO.

5.   CONCLUSIONS

The new [RuCl(trpy)(acpy)] complex was successfully synthesized and characterized by different spectroscopic techniques, such as ^{1}H NMR, FTIR and UV-Vis absorption, which was further rationalized based on TD-DFT calculations. Different from its analog, $[Ru(bpy)_2(acpy)]^+$, the [RuCl(trpy)(acpy)] complex does not react with molecular oxygen, a stable compound at mild conditions.

The electrochemical experiments at anodic potentials revealed a peak at 0.006 V *vs* Fc/Fc^+ corresponding to the $Ru^{II/III}$ pair as evidenced by the decrease in the MLCT absorption during the spectroelectrochemical experiments. In cathodic potentials, the first reduction is trpy-based and the second one is concentrated in the metal center. These observations were proven by spectroelectrochemical experiments in the UV-Vis region, in which, a decrease in MLCT is firstly observed followed by a blue-shift. Moreover after the second reduction the MLCT absorption slighthly increases indicating an enhancement in the electron density in the metal center. At this point, chloride ligand is lost forming a pentacoordinated species, as observed by cyclic voltammetries experiments.

The new complex showed a catalytic activity with TON_{CO} = 12 in anhydrous conditions and TON_{CO} = 21 when 1% H_2O is added. These values are in the average of those reported for other ruthenium trpy-based complexes. Some insights about the mechanism were gained, for instance, that the chloride ligand is lost during the catalytic process, giving a site for CO_2 coordination. Also, the intermediate $Ru-COO^-$ was detected by spectroelectrochemical experiments in the IR range. In addition, the acpy ligand is partially labilized in the presence of water and triggers the formation of formate from CO_2. The main objectives of the

work were fulfilled as fundamental spectroelectrochemical studies were carried out and allow the unveiling of some the reaction steps involved in the CO_2 reduction by the new proposed complex.

6. REFERENCES

ABAD, A.; ALMELA, C.; CORMA, A.; GARCÍA, H. Efficient chemoselective alcohol oxidation using oxygen as oxidant. Superior performance of gold over palladium catalysts. **Tetrahedron,** v. 62, n. 28, p. 6666-6672, 2006. doi: <https://doi.org/10.1016/j.tet.2006.01.118>.

ADENIYI, A. A.; AJIBADE, P. A. Exploring the ruthenium-ligands bond and their relative properties at different computational methods. **Journal of Chemistry,** v. 2016, p. 1-15, 2016. doi: <https://doi.org/10.1155/2016/3672062>.

AGARWAL, J.; SHAW, T. W.; SCHAEFER, H. F.; BOCARSLY, A. B. Design of a catalytic active site for electrochemical CO_2 reduction with Mn(I)-tricarbonyl species. **Inorganic Chemistry,** v. 54, n. 11, p. 5285-5294, 2015. doi: <https://doi.org/10.1021/acs.inorgchem.5b00233>.

AKHADE, S. A.; LUO, W.; NIE, X.; BERNSTEIN, N. J.; ASTHAGIRI, A.; JANIK, M. J. Poisoning effect of adsorbed CO during CO_2 electroreduction on late transition metals. **Physical Chemistry Chemical Physics,** v. 16, n. 38, p. 20429-20435, 2014. doi: <http://dx.doi.org/10.1039/C4CP03340J>.

ALIG, L.; FRITZ, M.; SCHNEIDER, S. First-row transition metal (de)hydrogenation catalysis based on functional pincer ligands. **Chemical Reviews,** v. 119, n. 4, p. 2681-2751, 2019. doi: <https://doi.org/10.1021/acs.chemrev.8b00555>.

ANDREIADIS, E. S.; CHAVAROT-KERLIDOU, M.; FONTECAVE, M.; ARTERO, V. Artificial photosynthesis: from molecular catalysts for light-driven water splitting to photoelectrochemical cells. **Photochemistry and Photobiology,** v. 87, n. 5, p. 946-964, 2011. doi: <https://doi.org/10.1111/j.1751-1097.2011.00966.x>.

ARENDS, I.; KODAMA, T.; SHELDON, R. **Ruthenium catalysts and fine chemistry**: Springer Science & Business Media, 2004, v.11

ATILHAN, S.; PARK, S.; EL-HALWAGI, M. M.; ATILHAN, M.; MOORE, M.; NIELSEN, R. B. Green hydrogen as an alternative fuel for the shipping industry. **Current Opinion in Chemical Engineering,** v. 31, p. 1-8, 2021. doi: <https://doi.org/10.1016/j.coche.2020.100668>.

AYE, G. C.; EDOJA, P. E. Effect of economic growth on CO_2 emission in developing countries: Evidence from a dynamic panel threshold model. **Cogent Economics & Finance,** v. 5, n. 1, p. 1-22, 2017. doi: <https://doi.org/10.1080/23322039.2017.1379239>.

BARBER, J. Photosynthetic energy conversion: natural and artificial. **Chemical Society Reviews,** v. 38, n. 1, p. 185-196, 2009. doi: <http://dx.doi.org/10.1039/B802262N>.

BARD, A. J.; FAULKNER, L. R. **Fundamentals and Applications, New York: Wiley, 2001**: Springer, 2002

BARROS, C. L.; DE OLIVEIRA, P. J. P.; JORGE, F. E.; CANAL NETO, A.; CAMPOS, M. Gaussian basis set of double zeta quality for atoms Rb through Xe: application in non-relativistic and relativistic calculations of atomic and molecular properties. **Molecular Physics,** v. 108, n. 15, p. 1965-1972, 2010. doi: <https://doi.org/10.1080/00268976.2010.499377>.

BASSO, L.; CROTWELL, A.; DOLMAN, H.; GATTI, L.; GERBIG, C.; GRIFFITH, D.; HALL, B.; JORDAN, A.; KRUMMEL, P.; LEUENBERGER, M.; LOH, Z.; MIKALOFF-FLETCHER, S.; SAWA, Y.; SCHIBIG, M.; TARASOVA, O.; TURNBULL, J.; VERMEULEN, A. The state of greenhouse gases in the atmosphere based on global observations through 2020. **World Meteorological Organization,** v. 17, p. 1-10, 2021. doi: <https://library.wmo.int/doc_num.php?explnum_id=10904>.

BERARDI, S.; DROUET, S.; FRANCÀS, L.; GIMBERT-SURIÑACH, C.; GUTTENTAG, M.; RICHMOND, C.; STOLL, T.; LLOBET, A. Molecular artificial photosynthesis. **Chemical Society Reviews,** v. 43, n. 22, p. 7501-7519, 2014. doi: <http://dx.doi.org/10.1039/C3CS60405E>.

BERGER, R. M.; MCMILLIN, D. R. Localized states in reduced and excited-state ruthenium(II) terpyridyls. **Inorganic Chemistry,** v. 27, n. 23, p. 4245-4249, 1988. doi: <https://doi.org/10.1021/ic00296a032>.

BOUTIN, E.; MERAKEB, L.; MA, B.; BOUDY, B.; WANG, M.; BONIN, J.; ANXOLABÉHÈRE-MALLART, E.; ROBERT, M. Molecular catalysis of CO_2 reduction: recent advances and perspectives in electrochemical and light-driven processes with selected Fe, Ni and Co aza macrocyclic and polypyridine complexes. **Chemical Society Reviews,** v. 49, n. 16, p. 5772-5809, 2020. doi: <http://dx.doi.org/10.1039/D0CS00218F>.

BREIVOGEL, A.; KREITNER, C.; HEINZE, K. Redox and photochemistry of *bis*(terpyridine)ruthenium(II) amino acids and their amide conjugates – from understanding to applications. **European Journal of Inorganic Chemistry,** v. 2014, n. 32, p. 5468-5490, 2014. doi: <https://doi.org/10.1002/ejic.201402466>.

CHANG, X.; WANG, T.; GONG, J. CO_2 photo-reduction: insights into CO_2 activation and reaction on surfaces of photocatalysts. **Energy & Environmental Science,** v. 9, n. 7, p. 2177-2196, 2016. doi: <https://doi.org/10.1039/C6EE00383D >.

CHATTERJEE, D.; SENGUPTA, A.; MITRA, A. Synthesis, characterization and reactivity of a novel ruthenium(II) complex containing polypyridyl ligand. **Polyhedron,** v. 26, n. 1, p. 178-183, 2007. doi: <https://doi.org/10.1016/j.poly.2006.08.005>.

CHEN, Z.; CHEN, C.; WEINBERG, D. R.; KANG, P.; CONCEPCION, J. J.; HARRISON, D. P.; BROOKHART, M. S.; MEYER, T. J. Electrocatalytic reduction of CO_2 to CO by polypyridyl ruthenium complexes. **Chemical Communications,**

v. 47, n. 47, p. 12607-12609, 2011. doi: <http://dx.doi.org/10.1039/C1CC15071E>.

CHEN, Z.; KANG, P.; ZHANG, M.-T.; MEYER, T. J. Making *syngas* electrocatalytically using a polypyridyl ruthenium catalyst. **Chemical Communications,** v. 50, n. 3, p. 335-337, 2014. doi: <http://dx.doi.org/10.1039/C3CC47251E>.

CHOWDHURY, A. D.; DAS, A.; K, I.; MOBIN, S. M.; LAHIRI, G. K. Isomeric complexes of [Ru^{II}(trpy)(L)Cl] (trpy = 2,2′:6′,2″-terpyridine and HL = quinaldic acid): Preference of isomeric structural form in catalytic chemoselective epoxidation process. **Inorganic Chemistry,** v. 50, n. 5, p. 1775-1785, 2011. doi: <https://doi.org/10.1021/ic102195w>.

CLARK, M. L.; CHEUNG, P. L.; LESSIO, M.; CARTER, E. A.; KUBIAK, C. P. Kinetic and mechanistic effects of bipyridine (bpy) substituent, labile ligand, and Brønsted acid on electrocatalytic CO_2 reduction by Re(bpy) complexes. **ACS Catalysis,** v. 8, n. 3, p. 2021-2029, 2018. doi: <https://doi.org/10.1021/acscatal.7b03971>.

COLLOMB-DUNAND-SAUTHIER, M.-N.; DERONZIER, A.; ZIESSEL, R. Electrocatalytic reduction of carbon dioxide with mono (bipyridine) carbonylruthenium complexes in solution or as polymeric thin films. **Inorganic Chemistry,** v. 33, n. 13, p. 2961-2967, 1994. doi: <https://doi.org/10.1021/ic00091a040>.

COSTENTIN, C.; ROBERT, M.; SAVÉANT, J.-M.; TATIN, A. Efficient and selective molecular catalyst for the CO_2-to-CO electrochemical conversion in water. **Proceedings of the National Academy of Sciences,** v. 112, n. 22, p. 6882-6886, 2015. doi: <https://doi.org/10.1073/pnas.1507063112>.

COSTENTIN, C.; SAVÉANT, J.-M. Towards an intelligent design of molecular electrocatalysts. **Nature Reviews Chemistry,** v. 1, n. 11, p. 0087, 2017. doi: <https://doi.org/10.1038/s41570-017-0087>.

D'ALESSANDRO, D. M.; USOV, P. M. Spectroelectrochemistry: A powerful tool for studying fundamental properties and emerging applications of solid-state materials including metal–organic frameworks. **Australian Journal of Chemistry,** v. 74, n. 2, p. 77-93, 2021. doi: <https://doi.org/10.1071/CH20301>.

DAS, B.; EZZEDINLOO, L.; BHADBHADE, M.; BUCKNALL, M. P.; COLBRAN, S. B. Strategic design of a ruthenium catalyst for both CO_2 reduction and H_2O oxidation: the electronic influence of the co-ligands. **Chemical Communications,** v. 53, n. 72, p. 10006-10009, 2017. doi: <https://doi.org/10.1039/C7CC06294J>.

DUAN, L.; BOZOGLIAN, F.; MANDAL, S.; STEWART, B.; PRIVALOV, T.; LLOBET, A.; SUN, L. A molecular ruthenium catalyst with water-oxidation activity comparable to that of photosystem II. **Nature Chemistry,** v. 4, n. 5, p. 418-423, 2012. doi: <https://doi.org/10.1038/nchem.1301>.

ELGRISHI, N.; CHAMBERS, M. B.; ARTERO, V.; FONTECAVE, M. Terpyridine complexes of first row transition metals and electrochemical reduction of CO_2 to CO. **Physical Chemistry Chemical Physics,** v. 16, n. 27, p. 13635-13644, 2014. doi: <http://dx.doi.org/10.1039/C4CP00451E>.

ELGRISHI, N.; CHAMBERS, M. B.; WANG, X.; FONTECAVE, M. Molecular polypyridine-based metal complexes as catalysts for the reduction of CO_2. **Chemical Society Reviews,** v. 46, n. 3, p. 761-796, 2017. doi: <https://doi.org/10.1039/C5CS00391A>.

ELGRISHI, N.; ROUNTREE, K. J.; MCCARTHY, B. D.; ROUNTREE, E. S.; EISENHART, T. T.; DEMPSEY, J. L. A practical beginner's guide to cyclic voltammetry. **Journal of Chemical Education,** v. 95, n. 2, p. 197-206, 2018. doi: <https://doi.org/10.1021/acs.jchemed.7b00361>.

ENGLAND, J.; SCARBOROUGH, C. C.; WEYHERMÜLLER, T.; SPROULES, S.; WIEGHARDT, K. Electronic structures of the electron transfer series $[M(bpy)_3]_n$, $[M(tpy)_2]_n$, and $[Fe(tbpy)_3]_n$ (M = Fe, Ru; n = 3+, 2+, 1+, 0, 1−): A Mössbauer spectroscopic and DFT study. **European Journal of Inorganic Chemistry,** v. 2012, n. 29, p. 4605-4621, 2012. doi: <https://doi.org/10.1002/ejic.201200232>.

FAUSTINO, L. A.; SOUZA, B. L.; NUNES, B. N.; DUONG, A.-T.; SIELAND, F.; BAHNEMANN, D. W.; PATROCINIO, A. O. T. Photocatalytic CO_2 reduction by Re(I) polypyridyl complexes immobilized on niobates nanoscrolls. **ACS Sustainable Chemistry & Engineering,** v. 6, n. 5, p. 6073-6083, 2018. doi: <https://doi.org/10.1021/acssuschemeng.7b04713>.

FRANCO, F.; COMETTO, C.; GARINO, C.; MINERO, C.; SORDELLO, F.; NERVI, C.; GOBETTO, R. Photo- and electrocatalytic reduction of CO_2 by $[Re(CO)_3\{\alpha,\alpha'\text{-diimine-(4-piperidinyl-1,8-naphthalimide)}\}Cl]$ complexes. **European Journal of Inorganic Chemistry,** v. 2015, n. 2, p. 296-304, 2015. doi: <https://doi.org/10.1002/ejic.201402912>.

GHATAK, N.; CHAKRAVARTY, J.; BHATTACHARYA, S. Synthesis, characterization and cyclic voltammetric studies of monopicolinate complexes of ruthenium(II). **Transition Metal Chemistry,** v. 20, n. 2, p. 138-141, 1995. doi: <https://doi.org/10.1007/BF00167015>.

GHOSH, D.; KAJIWARA, T.; KITAGAWA, S.; TANAKA, K. Ligand-assisted electrochemical CO_2 reduction by Ru-polypyridyl vomplexes. **European Journal of Inorganic Chemistry,** v. 2020, n. 18, p. 1814-1818, 2020. doi: <https://doi.org/10.1002/ejic.202000259>.

GLIGORICH, K. M.; SIGMAN, M. S. Recent advancements and challenges of palladium(II)-catalyzed oxidation reactions with molecular oxygen as the sole oxidant. **Chemical Communications**, n. 26, p. 3854-3867, 2009. doi: <http://dx.doi.org/10.1039/B902868D>.

GONELL, S.; MASSEY, M. D.; MOSELEY, I. P.; SCHAUER, C. K.; MUCKERMAN, J. T.; MILLER, A. J. M. The *trans* effect in electrocatalytic CO_2 reduction: mechanistic studies of asymmetric ruthenium pyridyl-carbene catalysts. **Journal of the American Chemical Society,** v. 141, n. 16, p. 6658-6671, 2019. doi: <https://doi.org/10.1021/jacs.9b01735>.

GONELL, S.; ASSAF, E. A.; DUFFEE, K. D.; SCHAUER, C. K.; MILLER, A. J. M. Kinetics of the *trans* effect in ruthenium complexes provide insight into the factors that control activity and stability in CO_2 Electroreduction. **Journal of the American Chemical Society,** v. 142, n. 19, p. 8980-8999, 2020. doi: <https://doi.org/10.1021/jacs.0c02912>.

GONZÁLEZ-CASTAÑO, M.; DORNEANU, B.; ARELLANO-GARCÍA, H. The reverse water gas shift reaction: a process systems engineering perspective. **Reaction Chemistry & Engineering,** v. 6, n. 6, p. 954-976, 2021. doi: <http://dx.doi.org/10.1039/D0RE00478B>.

GOSWAMI, S.; MUKHERJEE, R.; CHAKRAVORTY, A. Chemistry of ruthenium. 12. Reactions of bidentate ligands with diaqua*bis*[2-(arylazo)pyridine]ruthenium(II) cation. Stereoretentive synthesis of *tris* chelates and their characterization: metal oxidation, ligand reduction, and spectroelectrochemical correlation. **Inorganic Chemistry,** v. 22, n. 20, p. 2825-2832, 1983. doi: <https://doi.org/10.1021/ic00162a012>.

GOZE, C.; SABATINI, C.; BARBIERI, A.; BARIGELLETTI, F.; ZIESSEL, R. Ruthenium−terpyridine complexes with multiple ethynylpyrenyl or ethynyltoluyl subunits: X-ray structure, redox, and spectroscopic properties. **Inorganic Chemistry,** v. 46, n. 18, p. 7341-7350, 2007. doi: <https://doi.org/10.1021/ic070149c>.

HAWECKER, J.; LEHN, J.-M.; ZIESSEL, R. Efficient photochemical reduction of CO_2 to CO by visible light irradiation of systems containing $Re(bipy)(CO)_3X$ or $Ru(bipy)_3^{2+}$–Co^{2+} combinations as homogeneous catalysts. **Journal of the Chemical Society, Chemical Communications**, n. 9, p. 536-538, 1983. doi: <http://dx.doi.org/10.1039/C39830000536>.

HAWECKER, J.; LEHN, J.-M.; ZIESSEL, R. Photochemical and electrochemical reduction of carbon dioxide to carbon monoxide mediated by (2,2′-bipyridine)tricarbonylchlororhenium(I) and related complexes as homogeneous catalysts. **Helvetica Chimica Acta,** v. 69, n. 8, p. 1990-2012, 1986. doi: <https://doi.org/10.1002/hlca.19860690824>.

HILDEBRANDT, D.; GLASSER, D.; HAUSBERGER, B.; PATEL, B.; GLASSER, B. J. Producing transportation fuels with less work. **Science,** v. 323, n. 5922, p. 1680-1681, 2009. doi: <https://doi.org/10.1126/science.1168455>.

HIMEDA, Y.; ONOZAWA-KOMATSUZAKI, N.; SUGIHARA, H.; KASUGA, K. Simultaneous tuning of activity and water solubility of complex catalysts by acid−base equilibrium of ligands for conversion of carbon dioxide. **Organometallics,** v. 26, n. 3, p. 702-712, 2007. doi: <https://doi.org/10.1021/om060899e>.

HORVÁTH, I. T.; KISS, G.; COOK, R. A.; BOND, J. E.; STEVENS, P. A.; RÁBAI, J.; MOZELESKI, E. J. Molecular engineering in homogeneous catalysis: One-phase catalysis coupled with biphase catalyst separation. The fluorous-soluble $HRh(CO)\{P[CH_2CH_2(CF_2)_5CF_3]_3\}_3$ hydroformylation system. **Journal of the American Chemical Society,** v. 120, n. 13, p. 3133-3143, 1998. doi: <https://doi.org/10.1021/ja9738337>.

HUFF, C. A.; SANFORD, M. S. Catalytic CO_2 hydrogenation to formate by a ruthenium pincer complex. **ACS Catalysis,** v. 3, n. 10, p. 2412-2416, 2013. doi: <https://doi.org/10.1021/cs400609u>.

HUSSAIN, I.; REHMAN, A. Exploring the dynamic interaction of CO_2 emission on population growth, foreign investment, and renewable energy by employing ARDL bounds testing approach. **Environmental Science and Pollution Research,** v. 28, n. 29, p. 39387-39397, 2021. doi: <https://doi.org/10.1007/s11356-021-13502-8>.

ISHIDA, H.; TANAKA, K.; TANAKA, T. Electrochemical CO_2 reduction catalyzed by ruthenium complexes $[Ru(bpy)_2(CO)_2]^{2+}$ and $[Ru(bpy)_2(CO)Cl]^+$. Effect of pH on the formation of CO and $HCOO^-$. **Organometallics,** v. 6, n. 1, p. 181-186, 1987. doi: <https://doi.org/10.1021/om00144a033>.

ISHIDA, H.; TANAKA, H.; TANAKA, K.; TANAKA, T. Selective formation of $HCOO^-$ in the electrochemical CO_2 reduction catalysed by $[Ru(bpy)_2(CO)_2]^{2+}$(bpy = 2,2′-bipyridine). **Journal of the Chemical Society, Chemical Communications**, n. 2, p. 131-132, 1987. doi: <http://dx.doi.org/10.1039/C39870000131>.

JAIN, I. P. Hydrogen the fuel for 21st century. **International Journal of Hydrogen Energy,** v. 34, n. 17, p. 7368-7378, 2009. doi: <https://doi.org/10.1016/j.ijhydene.2009.05.093>.

JAKUBIKOVA, E.; CHEN, W.; DATTELBAUM, D. M.; REIN, F. N.; ROCHA, R. C.; MARTIN, R. L.; BATISTA, E. R. Electronic structure and spectroscopy of $[Ru(tpy)_2]^{2+}$, $[Ru(tpy)(bpy)(H_2O)]^{2+}$, and $[Ru(tpy)(bpy)(Cl)]^+$. **Inorganic Chemistry,** v. 48, n. 22, p. 10720-10725, 2009. doi: <https://doi.org/10.1021/ic901477m>.

JOHNSON, B. A.; AGARWALA, H.; WHITE, T. A.; MIJANGOS, E.; MAJI, S.; OTT, S. Judicious ligand design in ruthenium polypyridyl CO_2 reduction catalysts to enhance reactivity by steric and electronic effects. **Chemistry A European Journal,** v. 22, n. 42, p. 14870-14880, 2016a. doi: <https://doi.org/10.1002/chem.201601612>.

JOHNSON, B. A.; MAJI, S.; AGARWALA, H.; WHITE, T. A.; MIJANGOS, E.; OTT, S. Activating a low overpotential CO_2 reduction mechanism by a strategic ligand modification on a ruthenium polypyridyl catalyst. **Angewandte Chemie International Edition,** v. 55, n. 5, p. 1825-1829, 2016b. doi: <https://doi.org/10.1002/anie.201508490>.

JORGE, F. E.; NETO, A. C.; CAMILETTI, G. G.; MACHADO, S. F. Contracted Gaussian basis sets for Douglas–Kroll–Hess calculations: Estimating scalar relativistic effects of some atomic and molecular properties. **The Journal of Chemical Physics,** v. 130, n. 6, p. 064108, 2009. doi: <https://doi.org/10.1063/1.3072360>.

KAMDAR, J. M.; GROTJAHN, D. B. An overview of significant achievements in ruthenium-based molecular water oxidation catalysis. **Molecules,** v. 24, n. 3, p. 494, 2019. doi: <https://doi.org/10.3390/molecules24030494>.

KANEGA, R.; ERTEM, M. Z.; ONISHI, N.; SZALDA, D. J.; FUJITA, E.; HIMEDA, Y. CO_2 hydrogenation and formic acid dehydrogenation using Ir catalysts with amide-based ligands. **Organometallics,** v. 39, n. 9, p. 1519-1531, 2020. doi: <https://doi.org/10.1021/acs.organomet.9b00809>.

KÄRKÄS, M. D.; VERHO, O.; JOHNSTON, E. V.; ÅKERMARK, B. Artificial photosynthesis: Molecular systems for catalytic water oxidation. **Chemical Reviews,** v. 114, n. 24, p. 11863-12001, 2014. doi: <https://doi.org/10.1021/cr400572f>.

KHAN, M. K.; KHAN, M. I.; REHAN, M. The relationship between energy consumption, economic growth and carbon dioxide emissions in Pakistan. **Financial Innovation,** v. 6, n. 1, p. 1, 2020. doi: <https://doi.org/10.1186/s40854-019-0162-0>.

KIM, W.; EDRI, E.; FREI, H. Hierarchical inorganic assemblies for artificial photosynthesis. **Accounts of Chemical Research,** v. 49, n. 9, p. 1634-1645, 2016. doi: <https://doi.org/10.1021/acs.accounts.6b00182>.

KLEIN, J.; STUCKMANN, A.; SOBOTTKA, S.; SUNTRUP, L.; VAN DER MEER, M.; HOMMES, P.; REISSIG, H.-U.; SARKAR, B. Ruthenium complexes with strongly electron-donating terpyridine ligands: effect of the working electrode on electrochemical and spectroelectrochemical properties. **Chemistry A European Journal,** v. 23, n. 50, p. 12314-12325, 2017. doi: <https://doi.org/10.1002/chem.201701431>.

KNÖR, G. Recent progress in homogeneous multielectron transfer photocatalysis and artificial photosynthetic solar energy conversion. **Coordination Chemistry Reviews,** v. 304-305, p. 102-108, 2015. doi: <https://doi.org/10.1016/j.ccr.2014.09.013>.

KOIZUMI, T.-A.; TOMON, T.; TANAKA, K. Terpyridine-analogous (N,N,C)-tridentate ligands: Synthesis, structures, and electrochemical properties of ruthenium(II) complexes bearing tridentate pyridinium and pyridinylidene ligands. **Organometallics,** v. 22, n. 5, p. 970-975, 2003. doi: <https://doi.org/10.1021/om020637m>.

KOK, B.; FORBUSH, B.; MCGLOIN, M. Cooperation of charges in photosynthetic O_2 evolution-I. A linear four step mechanism. **Photochemistry and Photobiology,** v. 11, n. 6, p. 457-475, 1970. doi: <https://doi.org/10.1111/j.1751-1097.1970.tb06017.x>.

KOPPENOL, W. H.; RUSH, J. D. Reduction potential of the carbon dioxide/carbon dioxide radical anion: a comparison with other C1 radicals. **The Journal of Physical Chemistry,** v. 91, n. 16, p. 4429-4430, 1987. doi: <https://doi.org/10.1021/j100300a045>.

KREIMEYER, A. New directions in industrial chemical research as reflected in Angewandte Chemie. **Angewandte Chemie International Edition,** v. 52, n. 1, p. 147-154, 2013. doi: <https://doi.org/10.1002/anie.201208912>.

KREJČIK, M.; DANĚK, M.; HARTL, F. Simple construction of an infrared optically transparent thin-layer electrochemical cell: Applications to the redox reactions of ferrocene, $Mn_2(CO)_{10}$ and $Mn(CO)_3$(3,5-di-t-butyl-catecholate). **Journal of Electroanalytical Chemistry and Interfacial Electrochemistry,** v. 317, n. 1, p. 179-187, 1991. doi: <https://doi.org/10.1016/0022-0728(91)85012-E>.

LAURENCZY, G.; DYSON, P. J. Homogeneous catalytic dehydrogenation of formic acid: progress towards a hydrogen-based economy. **Journal of Brazilian Chemical Society,** v. 25, p. 2157-2163, 2014. doi: <https://doi.org/10.5935/0103-5053.20140235>.

LEE, S. K.; KONDO, M.; NAKAMURA, G.; OKAMURA, M.; MASAOKA, S. Low-overpotential CO_2 reduction by a phosphine-substituted Ru(II) polypyridyl complex. **Chemical Communications,** v. 54, n. 50, p. 6915-6918, 2018. doi: <http://dx.doi.org/10.1039/C8CC02150C>.

LLOBET, A.; DOPPELT, P.; MEYER, T. J. Redox properties of aqua complexes of ruthenium(II) containing the tridentate ligands 2,2':6',2"-terpyridine and tris(1-pyrazolyl)methane. **Inorganic Chemistry,** v. 27, n. 3, p. 514-520, 1988. doi: <https://doi.org/10.1021/ic00276a016>.

LOGEMANN, M.; WOLF, P.; LOIPERSBÖCK, J.; SCHRADE, A.; WESSLING, M.; HAUMANN, M. Ultra-low temperature water–gas shift reaction catalyzed by homogeneous Ru-complexes in a membrane reactor – membrane development and proof of concept. **Catalysis Science & Technology,** v. 11, n. 4, p. 1558-1570, 2021. doi: <http://dx.doi.org/10.1039/D0CY02111C>.

LOUIS, H.; AKAKURU, O. U.; MONDAY, P.; FUNMILAYO, O. O. A review on the state-of-the-art advances for CO_2 electro-chemical reduction using metal complex molecular catalysts. **Eclética Química,** v. 44, n. 1, p. 11-39, 2019. doi: <https://doi.org/10.26850/1678-4618eqj.v44.1.2019.p11-39>.

MACHAN, C. W.; SAMPSON, M. D.; KUBIAK, C. P. A molecular ruthenium electrocatalyst for the reduction of carbon dioxide to CO and formate. **Journal of the American Chemical Society,** v. 137, n. 26, p. 8564-8571, 2015. doi: <https://doi.org/10.1021/jacs.5b03913>.

MÄGERLEIN, W.; DREISBACH, C.; HUGL, H.; TSE, M. K.; KLAWONN, M.; BHOR, S.; BELLER, M. Homogeneous and heterogeneous ruthenium catalysts in the synthesis of fine chemicals. **Catalysis Today,** v. 121, n. 1-2, p. 140-150, 2007. doi: <https://doi.org/10.1016/j.cattod.2006.11.024>.

MEYER, T. J.; HUYNH, M. H. V. The remarkable reactivity of high oxidation state ruthenium and osmium polypyridyl complexes. **Inorganic Chemistry,** v. 42, n. 25, p. 8140-8160, 2003. doi: <https://doi.org/10.1021/ic020731v>.

MIN, S.; RASUL, S.; LI, H.; GRILLS, D. C.; TAKANABE, K.; LI, L.-J.; HUANG, K.-W. Electrocatalytic reduction of carbon dioxide with a well-defined PN3−Ru pincer complex. **ChemPlusChem,** v. 81, n. 2, p. 166-171, 2016. doi: <https://doi.org/10.1002/cplu.201500474>.

MOHSIN, M.; ZHOU, P.; IQBAL, N.; SHAH, S. A. A. Assessing oil supply security of South Asia. **Energy,** v. 155, p. 438-447, 2018. doi: <https://doi.org/10.1016/j.energy.2018.04.116>.

MOHSIN, M.; KAMRAN, H. W.; ATIF NAWAZ, M.; SAJJAD HUSSAIN, M.; DAHRI, A. S. Assessing the impact of transition from nonrenewable to renewable energy consumption on economic growth-environmental nexus from developing Asian economies. **Journal of Environmental Management,** v. 284, p. 1-8, 2021. doi: <https://doi.org/10.1016/j.jenvman.2021.111999>.

MORIGAKII, M. K.; SILVA, E. M. D.; DE MELO, C. V.; PAVAN, J. R.; SILVA, R. C.; BIONDO, A.; FREITAS, J. C.; DIAS, G. H. Synthesis, characterization, DFT and TD-DFT study of the [Fe(mnt)(L)(t-BuNC)$_2$] octahedral complex (L= phen, bipy). **Química Nova,** v. 32, p. 1812-1817, 2009. doi: <https://doi.org/10.1590/S0100-40422009000700024>.

MOYER, B. A.; MEYER, T. J. Properties of the oxo/aqua system $(bpy)_2(py)RuO^{2+}/(bpy)_2(py)Ru(OH_2)^{2+}$. **Inorganic Chemistry,** v. 20, n. 2, p. 436-444, 1981. doi: <https://doi.org/10.1021/ic50216a024>.

MÜLLER, A. V.; GONCALVES, M. R.; RAMOS, L. D.; POLO, A. S.; FRIN, K. P. The importance of the ^{3}MLCT excited state of Ru(II), Re(I) and Ir(III) compounds on development of photosensors, oleds and CO_2 photoreduction. **Química Nova,** v. 40, p. 200-213, 2017. doi: <https://doi.org/10.21577/0100-4042.20160170>.

NAGAO, H.; MIZUKAWA, T.; TANAKA, K. Carbon-carbon bond formation in the electrochemical reduction of carbon dioxide catalyzed by a ruthenium complex. **Inorganic Chemistry,** v. 33, n. 15, p. 3415-3420, 1994. doi: <https://doi.org/10.1021/ic00093a033>.

NAKAMOTO, K. **Infrared and Raman spectra of inorganic and coordination compounds, part B: applications in coordination, organometallic, and bioinorganic chemistry**: John Wiley & Sons, 2009

NAKAMURA, G.; KONDO, M.; CRISALLI, M.; LEE, S. K.; SHIBATA, A.; FORD, P. C.; MASAOKA, S. Syntheses and properties of phosphine-substituted ruthenium(II) polypyridine complexes with nitrogen oxides. **Dalton Transactions,** v. 44, n. 39, p. 17189-17200, 2015. doi: <http://dx.doi.org/10.1039/C5DT02994E>.

NERI, G.; ALDOUS, I. M.; WALSH, J. J.; HARDWICK, L. J.; COWAN, A. J. A highly active nickel electrocatalyst shows excellent selectivity for CO_2 reduction in acidic media. **Chemical Science,** v. 7, n. 2, p. 1521-1526, 2016. doi: <http://dx.doi.org/10.1039/C5SC03225C>.

NGO, K. T.; MCKINNON, M.; MAHANTI, B.; NARAYANAN, R.; GRILLS, D. C.; ERTEM, M. Z.; ROCHFORD, J. Turning on the protonation-first pathway for electrocatalytic CO_2 reduction by manganese bipyridyl tricarbonyl complexes. **Journal of the American Chemical Society,** v. 139, n. 7, p. 2604-2618, 2017. doi: <https://doi.org/10.1021/jacs.6b08776>.

NILLES, C. K.; HERATH, H. N. K.; FANOUS, H.; UGRINOV, A.; PARENT, A. R. Electrochemical properties and C–H bond oxidation activity of $[Ru(tpy)(pyalk)Cl]^+$ and $[Ru(tpy)(pyalk)(OH)]^+$. **Dalton Transactions,** v. 47, n. 29, p. 9701-9708, 2018. doi: <http://dx.doi.org/10.1039/C8DT02260G>.

OLIVEIRA, A. M.; BESWICK, R. R.; YAN, Y. A green hydrogen economy for a renewable energy society. **Current Opinion in Chemical Engineering,** v. 33, p. 1-7, 2021. doi: <https://doi.org/10.1016/j.coche.2021.100701>.

OMRI, A.; DALY, S.; RAULT, C.; CHAIBI, A. Financial development, environmental quality, trade and economic growth: What causes what in MENA countries. **Energy Economics,** v. 48, p. 242-252, 2015. doi: <https://doi.org/10.1016/j.eneco.2015.01.008>.

PAL, D. B.; CHAND, R.; UPADHYAY, S. N.; MISHRA, P. K. Performance of water gas shift reaction catalysts: A review. **Renewable and Sustainable Energy Reviews,** v. 93, p. 549-565, 2018. doi: <https://doi.org/10.1016/j.rser.2018.05.003>.

PAUL, A.; BORRELLI, R.; BOUYANFIF, H.; GOTTIS, S.; SAUVAGE, F. Tunable redox potential, optical properties, and enhanced stability of modified ferrocene-based complexes. **ACS Omega,** v. 4, n. 12, p. 14780-14789, 2019. doi: <https://doi.org/10.1021/acsomega.9b01341>.

PAULA, M. M. D. S. **Sintese, caracterização e estudos eletroquimicos de complexos polipiridinicos de antenio (II), metaloporfirinas e seus aductos moleculares**. Universidade Federal de Santa Catarina, 1994.

PETERSON, A. A.; NØRSKOV, J. K. Activity descriptors for CO_2 electroreduction to methane on transition-metal catalysts. **The Journal of Physical Chemistry Letters,** v. 3, n. 2, p. 251-258, 2012. doi: <https://doi.org/10.1021/jz201461p>.

PRADO, F. S.; SOUSA, S. F.; MACHADO, A. E. H.; PATROCINIO, A. O. T. Influence of the protonatable site in the photo-induced proton-coupled electron transfer between rhenium (I) polypyridyl complexes and hydroquinone. **Journal of Brazilian Chemical Society,** v. 28, p. 1741-1751, 2017. doi: <https://doi.org/10.21577/0103-5053.20170022>.

RAINES, C. A. The Calvin cycle revisited. **Photosynthesis Research,** v. 75, n. 1, p. 1-10, 2003. doi: <https://doi.org/10.1023/A:1022421515027>.

RAMAKRISHNAN, S.; CHIDSEY, C. E. D. Initiation of the electrochemical reduction of CO_2 by a singly reduced ruthenium(II) bipyridine complex. **Inorganic Chemistry,** v. 56, n. 14, p. 8326-8333, 2017. doi: <https://doi.org/10.1021/acs.inorgchem.7b01004>.

RITCHIE, H.; ROSER, M. Energy. **Our World in Data**, 2020. doi: <https://ourworldindata.org/energy>.

ROHMANN, K.; KOTHE, J.; HAENEL, M. W.; ENGLERT, U.; HÖLSCHER, M.; LEITNER, W. Hydrogenation of CO_2 to formic acid with a highly active ruthenium acriphos complex in DMSO and DMSO/Water. **Angewandte Chemie International Edition,** v. 55, n. 31, p. 8966-8969, 2016. doi: <https://doi.org/10.1002/anie.201603878>.

SAMPSON, M. D.; NGUYEN, A. D.; GRICE, K. A.; MOORE, C. E.; RHEINGOLD, A. L.; KUBIAK, C. P. Manganese catalysts with bulky bipyridine ligands for the electrocatalytic reduction of carbon dioxide: Eliminating dimerization and altering catalysis. **Journal of the American Chemical Society,** v. 136, n. 14, p. 5460-5471, 2014. doi: <https://doi.org/10.1021/ja501252f>.

SAMPSON, M. D.; KUBIAK, C. P. Manganese electrocatalysts with bulky bipyridine ligands: utilizing lewis acids to promote carbon dioxide reduction at low overpotentials. **Journal of the American Chemical Society,** v. 138, n. 4, p. 1386-1393, 2016. doi: <https://doi.org/10.1021/jacs.5b12215>.

SCHAUB, T.; PACIELLO, R. A. A process for the synthesis of formic acid by CO_2 hydrogenation: Thermodynamic aspects and the role of CO. **Angewandte Chemie International Edition,** v. 50, n. 32, p. 7278-7282, 2011. doi: <https://doi.org/10.1002/anie.201101292>.

SCHMEIER, T. J.; DOBEREINER, G. E.; CRABTREE, R. H.; HAZARI, N. Secondary coordination sphere interactions facilitate the insertion step in an Iridium(III) CO_2 reduction catalyst. **Journal of the American Chemical Society,** v. 133, n. 24, p. 9274-9277, 2011. doi: <https://doi.org/10.1021/ja2035514>.

SCHMIDT, S. B.; HUSTED, S. The biochemical properties of manganese in plants. **Plants,** v. 8, n. 381, p. 1-15, 2019. doi: <https://doi.org/10.3390/plants8100381>.

SEU, C. S.; APPEL, A. M.; DOUD, M. D.; DUBOIS, D. L.; KUBIAK, C. P. Formate oxidation via β-deprotonation in $[Ni(P^{R2}N^{R'}_2)_2(CH_3CN)]^{2+}$ complexes. **Energy & Environmental Science,** v. 5, n. 4, p. 6480-6490, 2012. doi: <http://dx.doi.org/10.1039/C2EE03341K>.

SHAH, S. A. A.; ZHOU, P.; WALASAI, G. D.; MOHSIN, M. Energy security and environmental sustainability index of South Asian countries: A composite index approach. **Ecological Indicators,** v. 106, p. 105507, 2019. doi: <https://doi.org/10.1016/j.ecolind.2019.105507>.

SHEN, H.; PEPPEL, T.; STRUNK, J.; SUN, Z. Photocatalytic reduction of CO_2 by metal-free-based materials: Recent advances and future perspective. **RRL Solar,** v. 4, n. 8, p. 1900546, 2020. doi: <https://doi.org/10.1002/solr.201900546>.

SHERBORNE, J.; SCOTT, S. M.; GORDON, K. C. Spectroelectrochemical studies of some ruthenium(II) complexes with polypyridyl bridging ligands. **Inorganica Chimica Acta,** v. 260, n. 2, p. 199-205, 1997. doi: <https://doi.org/10.1016/S0020-1693(96)05567-3>.

SILVA, G. T. S. T.; LOPES, O. F.; DIAS, E. H.; TORRES, J. A.; NOGUEIRA, A. E.; FAUSTINO, L. A.; PRADO, F. S.; PATROCINIO, A. O. T.; RIBEIRO, C. Redução de CO_2 em hidrocarbonetos e oxigenados: fundamentos, estratégias e desafios. **Química Nova,** v. 44, n. 8, p. 963-9681, 2021. doi: <http://dx.doi.org/10.21577/0100-4042.20170745>.

SILVERSTEIN, R. M.; WEBSTER, F. X.; KIEMLE, D. **Spectrometric Identification of Organic Compounds, 7th Edition**: Wiley, 2005

SINOPOLI, A.; LA PORTE, N. T.; MARTINEZ, J. F.; WASIELEWSKI, M. R.; SOHAIL, M. Manganese carbonyl complexes for CO_2 reduction. **Coordination Chemistry Reviews,** v. 365, p. 60-74, 2018. doi: <https://doi.org/10.1016/j.ccr.2018.03.011>.

SKOOG, D.; WEST, D.; HOLLER, F.; CROUCH, S. J. P. S. P. **Fundamentos de química analítica.** : Cengage do Brasil, 2006

SONDAZ, E.; GOURDON, A.; LAUNAY, J.-P.; BONVOISIN, J. (Bipyridine)(terpyridine)(4-iodophenylcyanamide)ruthenium(II) complex: crystallography, electronic absorption spectroscopy, cyclic voltammetry and EPR measurements. **Inorganica Chimica Acta,** v. 316, n. 1, p. 79-88, 2001. doi: <https://doi.org/10.1016/S0020-1693(01)00382-6>.

SOUSA, S. F.; SAMPAIO, R. N.; BARBOSA NETO, N. M.; MACHADO, A. E. H.; PATROCINIO, A. O. T. The photophysics of *fac*-[Re(CO)$_3$(NN)(bpa)]$^+$ complexes: a theoretical/experimental study. **Photochemical & Photobiological Sciences,** v. 13, n. 8, p. 1213-1224, 2014. doi: <http://dx.doi.org/10.1039/C4PP00074A>.

SOUSA, S. F.; PATROCINIO, A. O. T. A química de coordenação e a produção de combustíveis solares. **Química Nova,** v. 37, n. 5, p. 886-895, 2014. doi: <https://doi.org/10.5935/0100-4042.20140140>.

SOUSA, S. F. **Síntese e caracterização de complexos polipiridínicos de Ru (II) com diferentes ligantes carboxilatos e avaliação da reatividade frente ao oxigênio molecular**. Instituto de Química, Universidade Federal de Uberlândia, 2019. 161 p.

SOUSA, S. F.; ERTEM, M. Z.; FAUSTINO, L. A.; MACHADO, A. E. H.; CONCEPCION, J. J.; MAIA, P. I. S.; PATROCINIO, A. O. T. Mechanistic investigation of the aerobic oxidation of 2-pyridylacetate coordinated to a Ru(II) polypyridyl complex. **Dalton Transactions,** v. 50, p. 15248-15259, 2021. doi: <http://dx.doi.org/10.1039/D1DT02461B>.

SOUZA, B. L.; FAUSTINO, L. A.; PRADO, F. S.; SAMPAIO, R. N.; MAIA, P. I. S.; MACHADO, A. E. H.; PATROCINIO, A. O. T. Spectroscopic characterization of a new Re(I) tricarbonyl complex with a thiosemicarbazone derivative: towards sensing and electrocatalytic applications. **Dalton Transactions,** v. 49, n. 45, p. 16368-16379, 2020. doi: <http://dx.doi.org/10.1039/D0DT01078B>.

STEYNBERG, A. P. Chapter 1 - Introduction to Fischer-Tropsch Technology. In: Steynberg, A. e Dry, M. (Ed.). **Studies in Surface Science and Catalysis**: Elsevier, 2004. v.152, p.1-63.

SULLIVAN, B. P.; CALVERT, J. M.; MEYER, T. J. *Cis-trans* isomerism in (trpy)(PPh$_3$)RuC12. Comparisons between the chemical and physical properties of a *cis-trans* isomeric pair. **Inorganic Chemistry,** v. 19, n. 5, p. 1404-1407, 1980. doi: <https://doi.org/10.1021/ic50207a066>.

SUN, Y.; BIGI, J. P.; PIRO, N. A.; TANG, M. L.; LONG, J. R.; CHANG, C. J. Molecular cobalt pentapyridine catalysts for generating hydrogen from water. **Journal of the American Chemical Society,** v. 133, n. 24, p. 9212-9215, 2011. doi: <https://doi.org/10.1021/ja202743r>.

SUNG, S.; KUMAR, D.; GIL-SEPULCRE, M.; NIPPE, M. Electrocatalytic CO_2 reduction by imidazolium-functionalized molecular catalysts. **Journal of the American Chemical Society,** v. 139, n. 40, p. 13993-13996, 2017. doi: <https://doi.org/10.1021/jacs.7b07709>.

TAKEDA, H.; KOIKE, K.; INOUE, H.; ISHITANI, O. Development of an efficient photocatalytic system for CO_2 reduction ssing rhenium(I) complexes based on mechanistic studies. **Journal of the American Chemical Society,** v. 130, n. 6, p. 2023-2031, 2008. doi: <https://doi.org/10.1021/ja077752e>.

TAKEUCHI, K. J.; SAMUELS, G. J.; GERSTEN, S. W.; GILBERT, J. A.; MEYER, T. J. Multiple oxidation states of ruthenium and osmium based on dioxo/diaqua couples. **Inorganic Chemistry,** v. 22, n. 9, p. 1407-1409, 1983. doi: <https://doi.org/10.1021/ic00151a033>.

TANAKA, K.; MORIMOTO, M.; TANAKA, T. J. C. L. The water gas shift reaction catalyzed by ruthenium carbonyl complexes. **Chemistry Letters,** v. 12, n. 6, p. 901-904, 1983. doi: <https://doi.org/10.1246/cl.1983.901>.

TANAKA, R.; YAMASHITA, M.; NOZAKI, K. Catalytic hydrogenation of carbon dioxide ssing Ir(III)−pincer complexes. **Journal of the American Chemical Society,** v. 131, n. 40, p. 14168-14169, 2009. doi: <https://doi.org/10.1021/ja903574e>.

TSIERKEZOS, N. G. Cyclic voltammetric studies of ferrocene in nonaqueous solvents in the temperature range from 248.15 to 298.15 K. **Journal of Solution Chemistry,** v. 36, n. 3, p. 289-302, 2007. doi: <https://doi.org/10.1007/s10953-006-9119-9>.

ULMER, U.; DINGLE, T.; DUCHESNE, P. N.; MORRIS, R. H.; TAVASOLI, A.; WOOD, T.; OZIN, G. A. Fundamentals and applications of photocatalytic CO_2 methanation. **Nature Communications,** v. 10, n. 1, p. 1-12, 2019. doi: <https://doi.org/10.1038/s41467-019-10996-2>.

VECCHI, V.; BARERA, S.; BASSI, R.; DALL'OSTO, L. Potential and challenges of improving photosynthesis in *Algae*. **Plants,** v. 9, n. 1, p. 1-25, 2020. doi: <https://doi.org/10.3390/plants9010067>.

WANG, W.; HIMEDA, Y.; MUCKERMAN, J. T.; MANBECK, G.; FUJITA, E. CO_2 hydrogenation to formate and methanol as an alternative to photo- and electrochemical CO_2 reduction. **Chemical Reviews,** v. 115, p. 12936-12973, 2015. doi: <https://doi.org/10.1021/acs.chemrev.5b00197>.

WHITE, T. A.; MAJI, S.; OTT, S. Mechanistic insights into electrocatalytic CO_2 reduction within $[Ru^{II}(tpy)(NN)X]^{n+}$ architectures. **Dalton Transactions,** v. 43, n. 40, p. 15028-15037, 2014. doi: <http://dx.doi.org/10.1039/C4DT01591F>.

YIN, W.-J.; WEN, B.; GE, Q.; LI, X.-B.; TEOBALDI, G.; LIU, L.-M. Activity and selectivity of CO_2 photoreduction on catalytic materials. **Dalton Transactions,** v. 49, n. 37, p. 12918-12928, 2020. doi: <http://dx.doi.org/10.1039/D0DT02651D>.

ZAFAR, M. W.; ZAIDI, S. A. H.; KHAN, N. R.; MIRZA, F. M.; HOU, F.; KIRMANI, S. A. A. The impact of natural resources, human capital, and foreign direct investment on the ecological footprint: The case of the United States. **Resources Policy,** v. 63, p. 101428, 2019. doi: <https://doi.org/10.1016/j.resourpol.2019.101428>.

ZHANG, B.; SUN, L. Artificial photosynthesis: opportunities and challenges of molecular catalysts. **Chemical Society Reviews,** v. 48, n. 7, p. 2216-2264, 2019. doi: <http://dx.doi.org/10.1039/C8CS00897C>.

ZHANG, R.-Z.; WU, B.-Y.; LI, Q.; LU, L.-L.; SHI, W.; CHENG, P. Design strategies and mechanism studies of CO_2 electroreduction catalysts based on coordination chemistry. **Coordination Chemistry Reviews,** v. 422, p. 1-28, 2020. doi: <https://doi.org/10.1016/j.ccr.2020.213436>.

ZHANG, S.; FAN, Q.; XIA, R.; MEYER, T. J. CO_2 reduction: From homogeneous to heterogeneous electrocatalysis. **Accounts of Chemical Research,** v. 53, n. 1, p. 255-264, 2020. doi: <https://doi.org/10.1021/acs.accounts.9b00496>.

ZHOU, S.; HAMBURGER, M. Formation of sodium cluster ions in electrospray mass spectrometry. **Rapid Communications in Mass Spectrometry,** v. 10, n. 7, p. 797-800, 1996. doi: <https://doi.org/10.1002/(SICI)1097-0231(199605)10:7%3C797::AID-RCM550%3E3.0.CO;2-7>.

7.   APPENDICES

APPENDIX A – Vibrational Spectroscopy

Figure A- 1. FTIR spectrum of trpy.
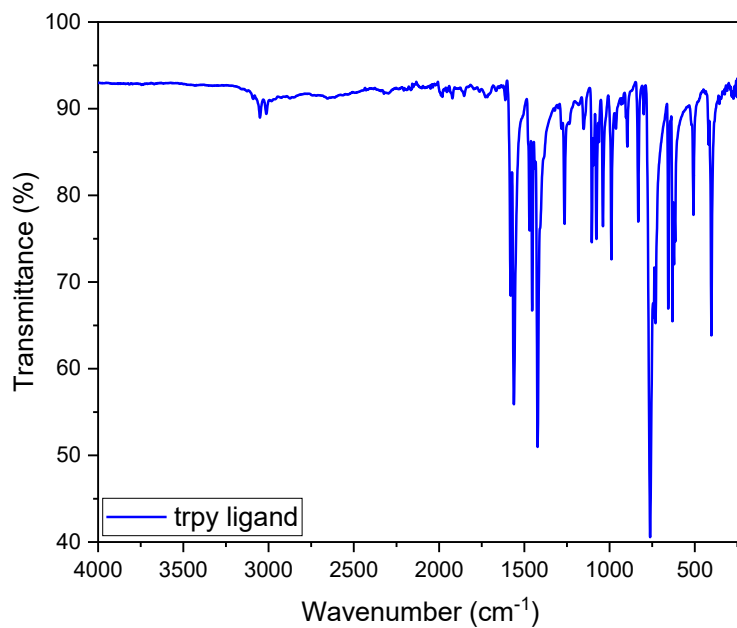
Figure A- 2. FTIR spectrum of acpy.
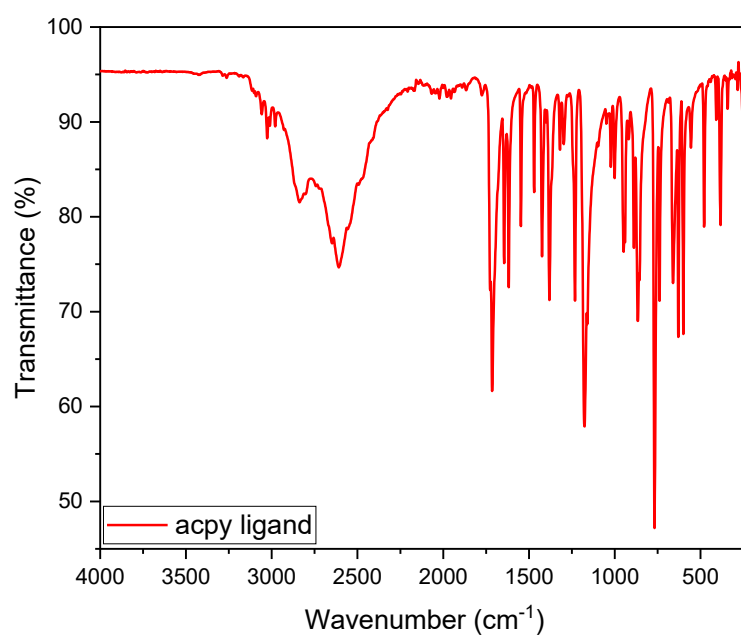
Figure A- 3. FTIR spectrum of [RuCl$_3$(trpy)].
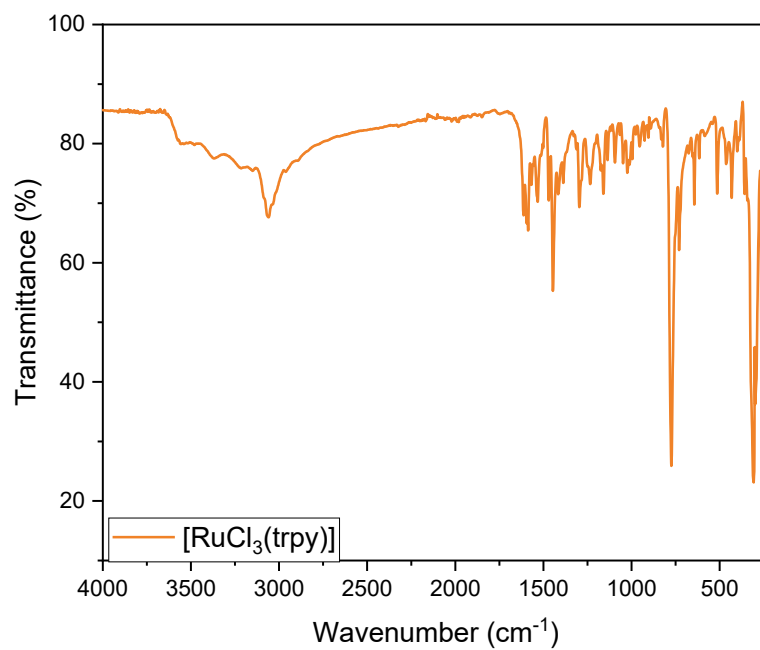
Figure A- 4. FTIR spectrum of [RuCl(trpy)(acpy)].
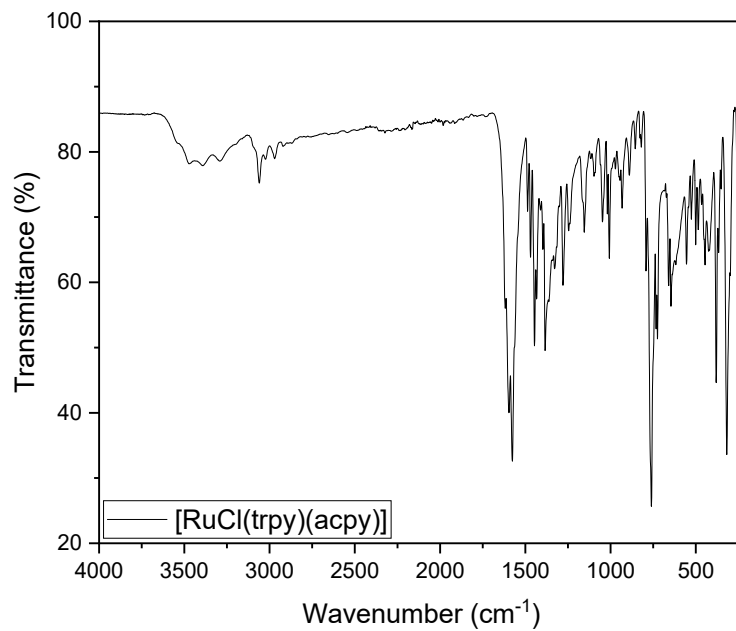
APPENDIX B – Cyclic and Differential Pulse Voltammetry

Figure B- 1. Differential pulse voltammogram of 1 mM [RuCl(trpy)(acpy)], 0.1 M TBAPF$_6$/CH$_3$CN under argon atmosphere.
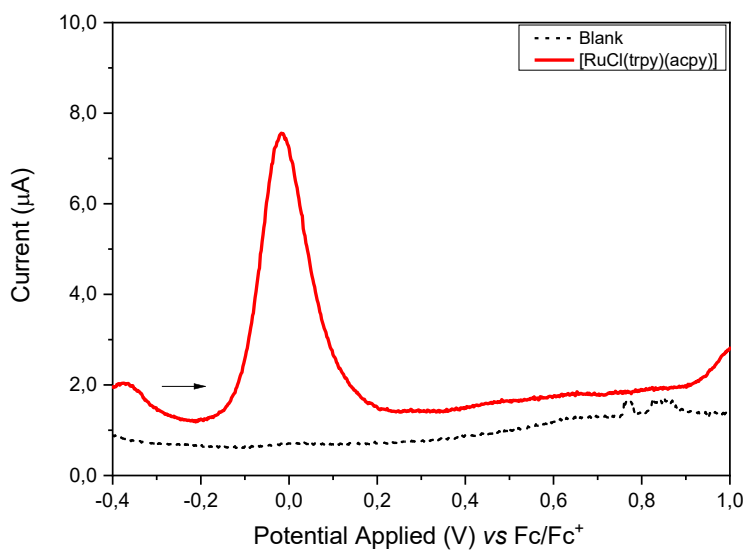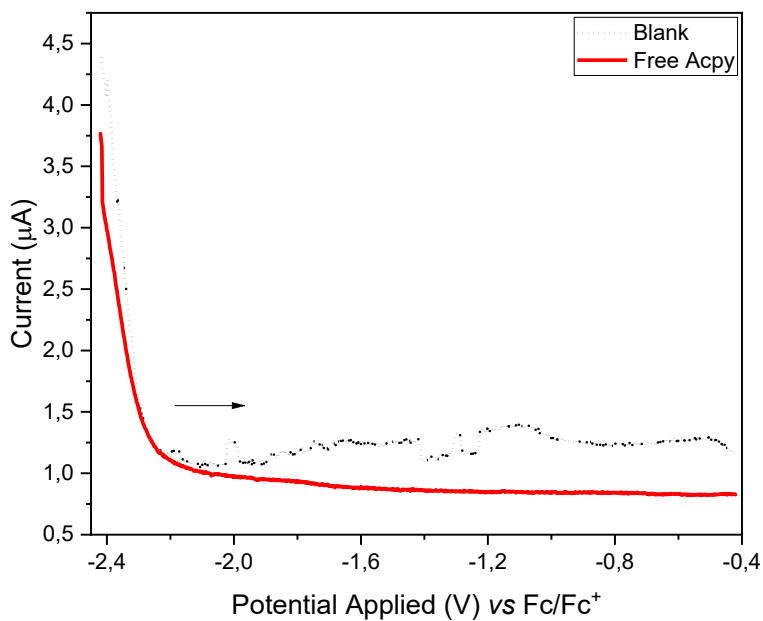

Figure B- 2. Differential pulse voltammogram of 1 mM [RuCl(trpy)(acpy)], 0.1 M TBAPF$_6$/CH$_3$CN under argon atmosphere.
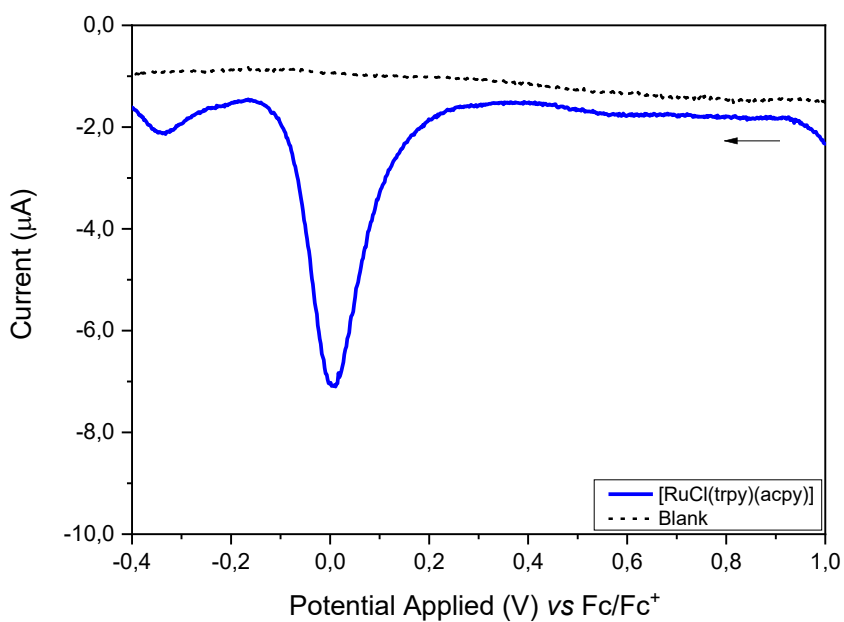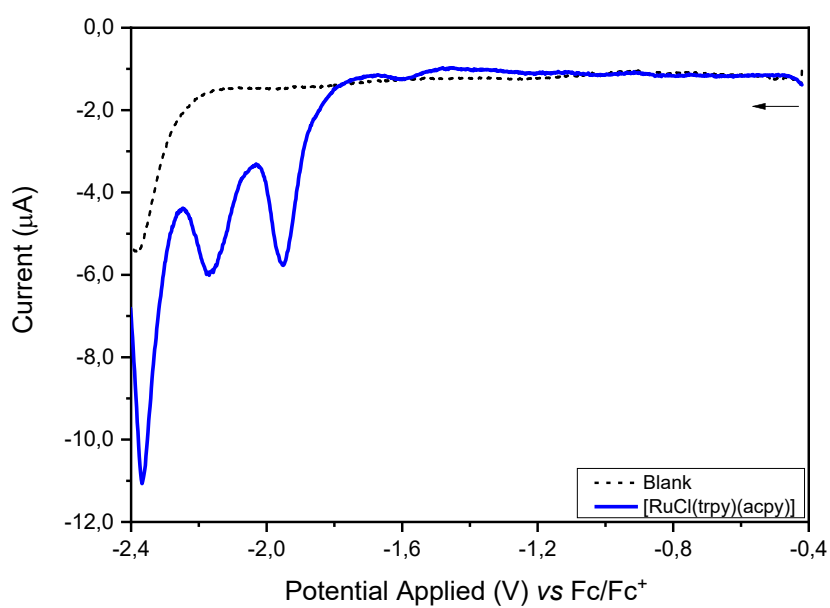
Figure B- 3. Cyclic voltammetries of 1 mM acpy ligand, 0.1 M TBAPF$_6$/CH$_3$CN under argon atmosphere at differents scan rates.
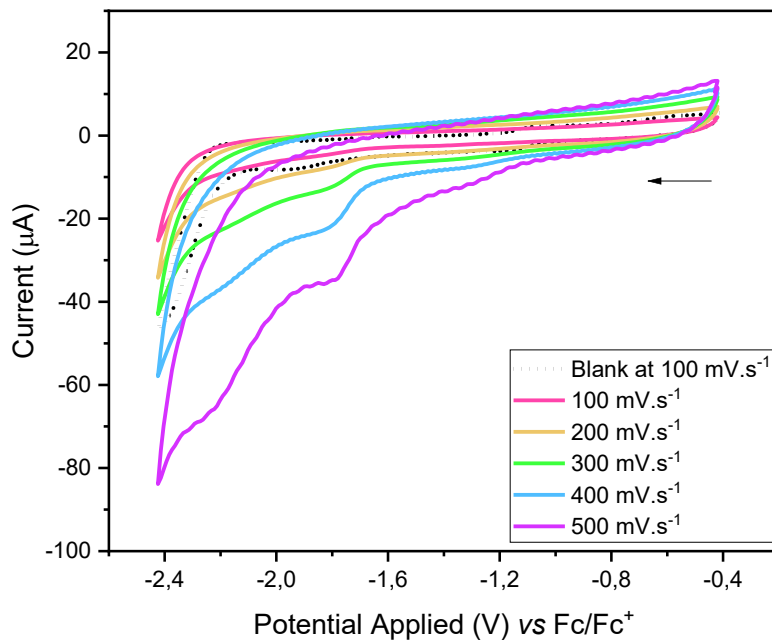
Figure B- 4. Differential pulse voltammogram of 1 mM acpy ligand, 0.1 M TBAPF$_6$/CH$_3$CN under argon atmosphere.
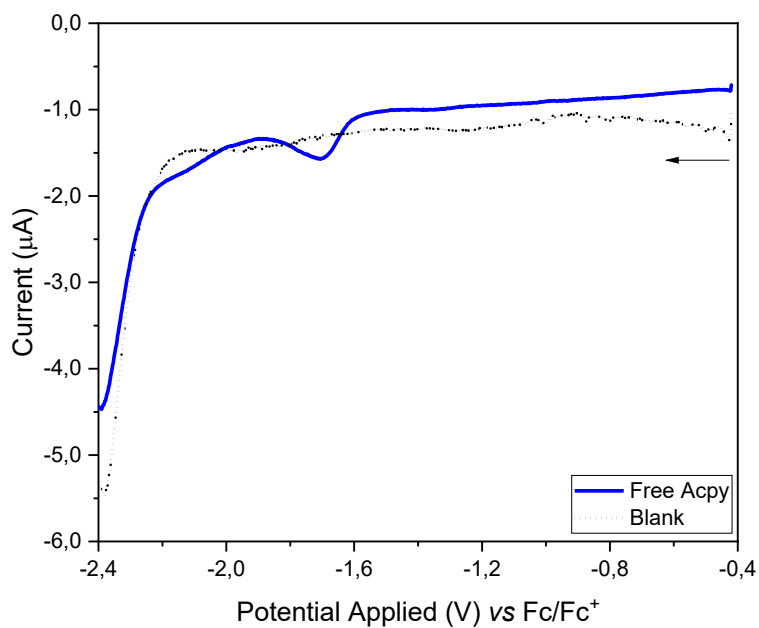
Figure B- 5. Differential pulse voltammogram of 1 mM acpy ligand, 0.1 M TBAPF$_6$/CH$_3$CN under argon atmosphere.

Figure B- 6. Differential pulse voltammogram of 1 mM [RuCl(trpy)(acpy)], 0.1 M TBAPF$_6$/CH$_3$CN under argon atmosphere.

Figure B- 7. Differential pulse voltammogram of 1 mM [RuCl(trpy)(acpy)], 0.1 M TBAPF$_6$/CH$_3$CN under argon atmosphere.
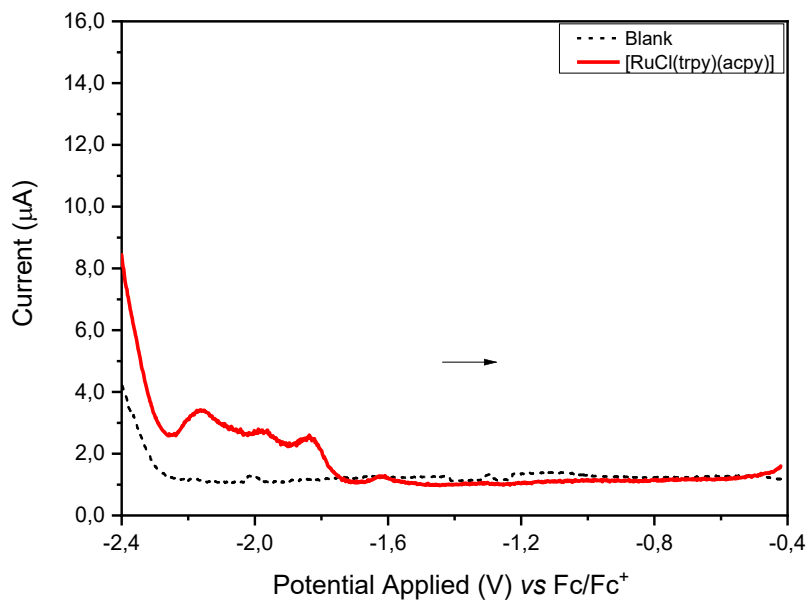

Figure B- 8. Cyclic voltammetries of 1 mM [RuCl(trpy)(acpy)], 0.1 M of TBAPF$_6$ in anhydrous CH$_3$CN under CO$_2$ atmosphere at differents scan rates.
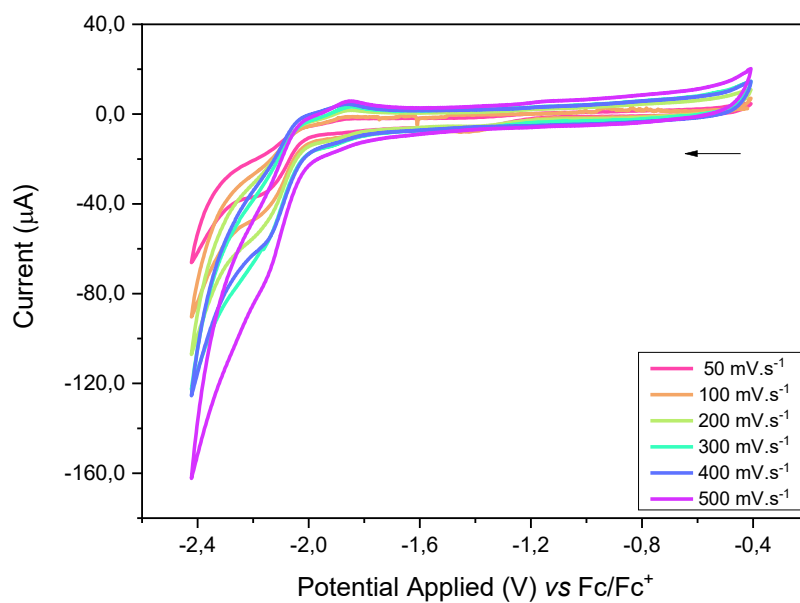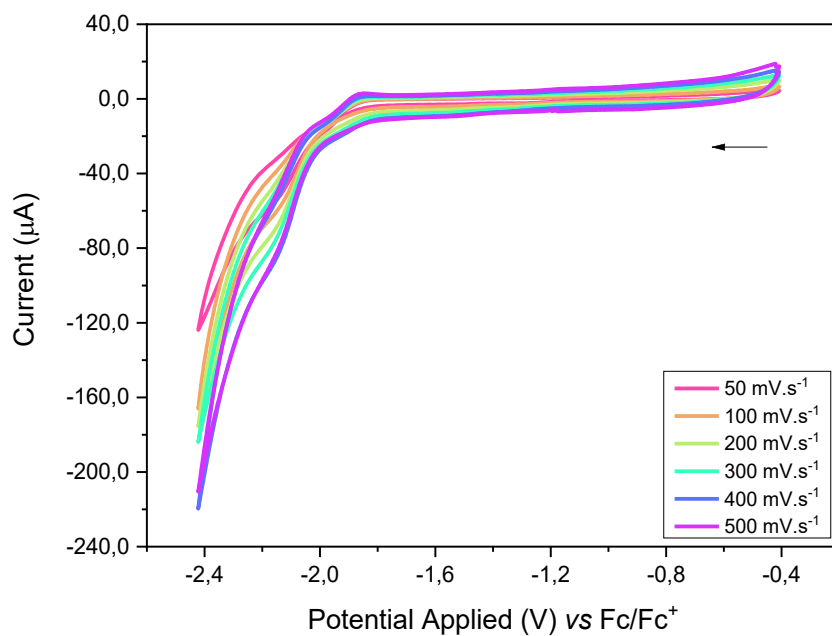
Figure B- 9. Cyclic voltammetries of 1 mM [RuCl(trpy)(acpy)], 0.1 M of TBAPF$_6$/CH$_3$CN and 1% H$_2$O, under CO$_2$ atmosphere in differents scan rates.

APPENDIX C – Theoretical calculations
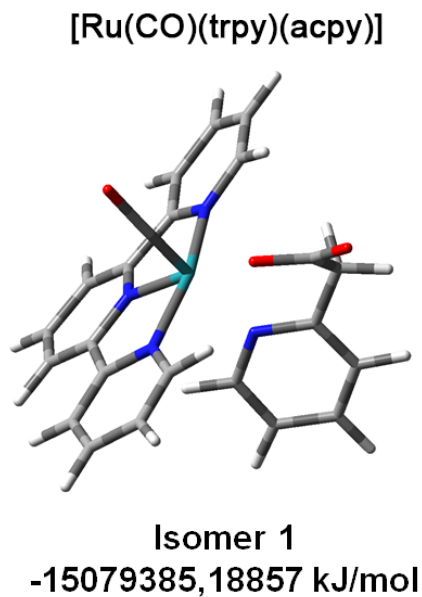
Figure C- 1. Isomer 1 for [Ru(CO)(trpy)(acpy)].

[Ru(CO)(trpy)(acpy)]

Isomer 1
-15079385,18857 kJ/mol

Figure C- 2. Isomer 2 for [Ru(CO)(trpy)(acpy)].

[Ru(CO)(trpy)(acpy)]
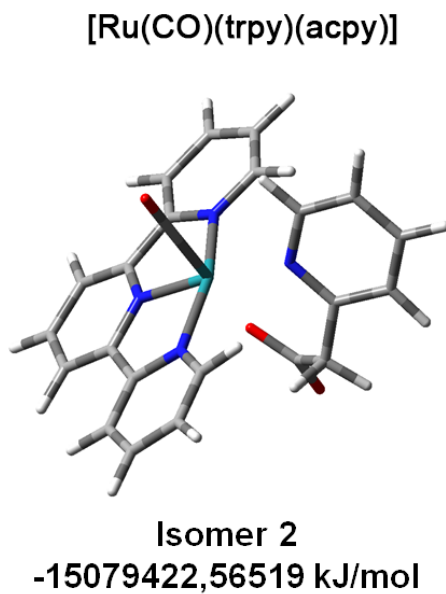
Isomer 2
-15079422,56519 kJ/mol

Figure C- 3. Theoretical eletronic spectra of [RuCl(trpy)(acpy)] reduced in 1e⁻ in acetonitrile.
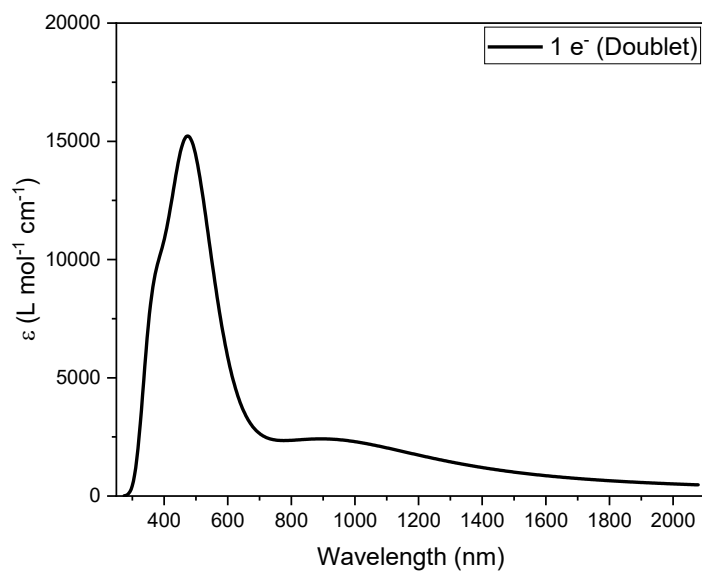

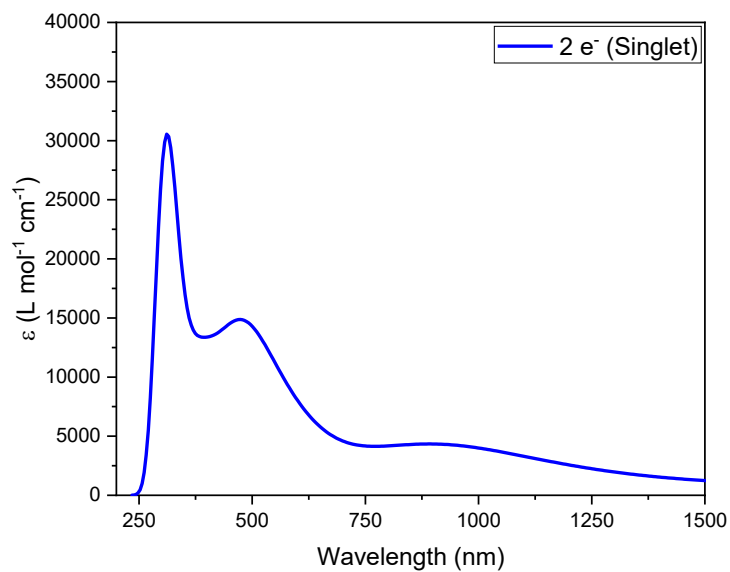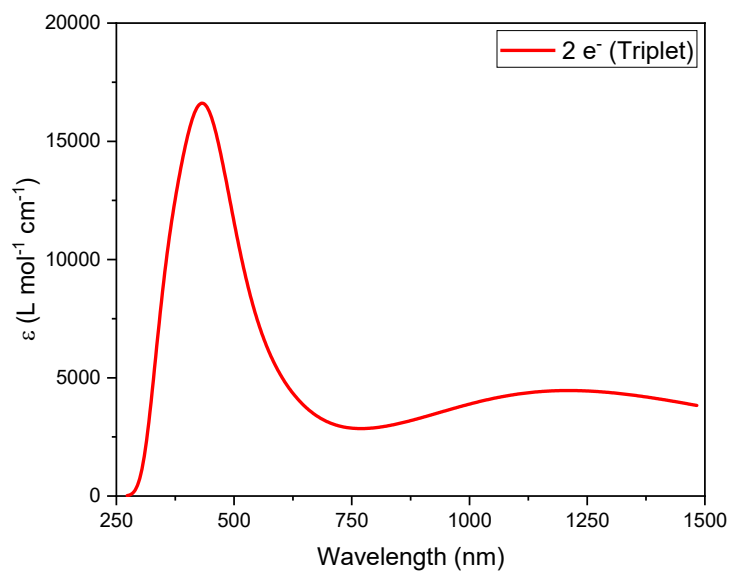**Figure C- 4.** Theoretical eletronic spectra of [RuCl(trpy)(acpy)] reduced in 2e⁻ in acetonitrile

Figure C- 5. Theoretical eletronic spectra of [RuCl(trpy)(acpy)] reduced in 2e⁻ in acetonitrile.

APPENDIX D – Spectroelectrochemistry

Figure D- 1. Changes in the FTIR spectra of 1 mM [RuCl(trpy)(acpy)] during the spectroelectrochemistry in 0.1 M TBAPF$_6$/CH$_3$CN varying potential under argon atmosphere Δt = 1.5 min.

Figure D- 2. Changes in the FTIR spectra of 1 mM [RuCl(trpy)(acpy)] during the spectroelectrochemistry in 0.1 M TBAPF$_6$/CH$_3$CN varying potential under argon atmosphere and 1% H$_2$O Δt = 1.5 min.
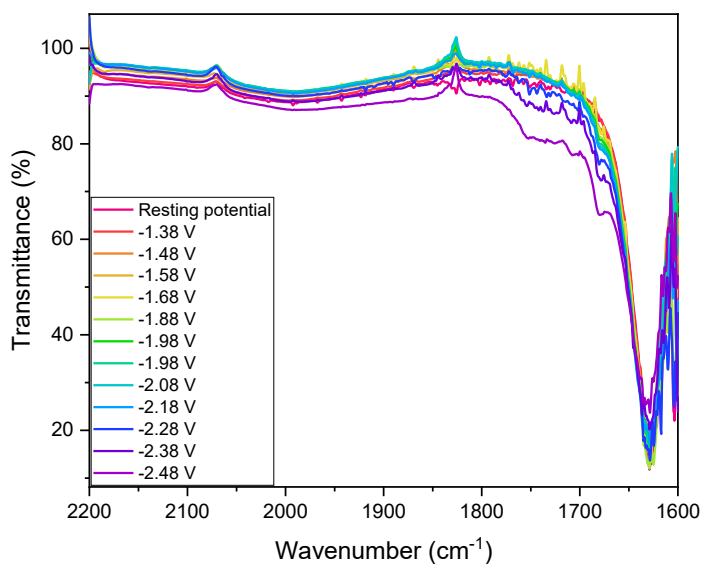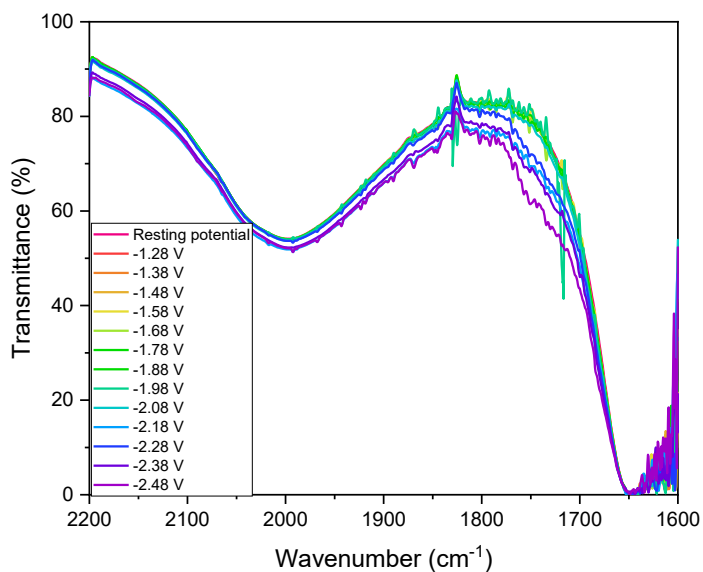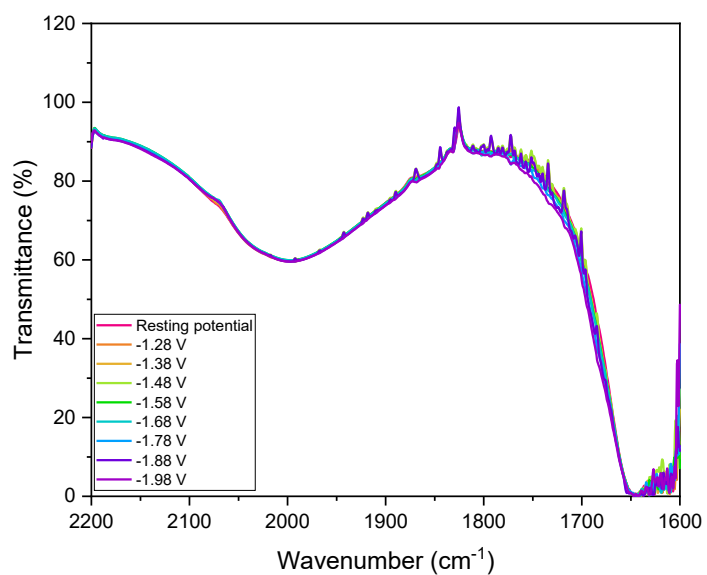
Figure D- 3. Changes in the FTIR spectra of 1 mM [RuCl(trpy)(acpy)] during the spectroelectrochemistry in 0.1 M TBAPF$_6$/CH$_3$CN varying potential under CO$_2$ atmosphere and 1% H$_2$O Δt = 1.5 min.

CURRICULUM VITAE

LEANDRO AUGUSTO FAUSTINO

leandro3378@hotmail.com
Uberlândia – MG / Brazil

Education

B.Sc. (**2016**) Chemistry, Universidade Federal de Uberlândia, 2016.

M.Sc. (**2018**) Chemistry, Universidade Federal de Uberlândia with Professor Antônio Otávio de Toledo Patrocínio. Dissertation title: "Propriedades fotoquímicas do complexo *fac*-[Re(CO)$_3$(dcbH$_2$)(*trans*-stpy)]$^+$".

Research Internship

December **2019** to August **2020** – Artificial Photosynthesis Group, Brookhaven National Laboratory, under supervision of Dr. Javier J. Concepcion. (CAPES: 88887.374340/2019-00)

Publications – Journal Articles

1. SOUSA, SINVAL F.; ERTEM, MEHMED Z.; <u>FAUSTINO, LEANDRO A.</u>; MACHADO, ANTONIO EDUARDO. H.; CONCEPCION, JAVIER J.; MAIA, PEDRO I. S.; PATROCINIO, ANTONIO OTAVIO T. Mechanistic investigation of the aerobic oxidation of 2-pyridylacetate coordinated to a Ru(II) polypyridyl complex. **DALTON TRANSACTIONS**, v. 50, p. 15248, **2021**.

2. SILVA, GELSON; LOPES, OSMANDO; DIAS, EDUARDO; TORRES, JULIANA; NOGUEIRA, ANDRÉ; <u>FAUSTINO, LEANDRO</u>; PRADO, FERNANDO; PATROCÍNIO, ANTÔNIO; RIBEIRO, CAUE. Redução de CO$_2$ em hidrocarbonetos e oxigenados: fundamentos, estratégias e desafios. **QUIMICA NOVA**, v. 44, p. 963, **2021**.

3. SOUZA, BRENO L.; <u>FAUSTINO, LEANDRO A.</u>; PRADO, FERNANDO S.; SAMPAIO, RENATO N.; MAIA, PEDRO I. S.; MACHADO, ANTONIO EDUARDO H.; PATROCINIO, ANTONIO OTAVIO T. Spectroscopic characterization of a new Re(I) tricarbonyl complex with a thiosemicarbazone derivative: towards sensing and electrocatalytic applications. **DALTON TRANSACTIONS**, v. 49, p. 16368, **2020**.

4. <u>FAUSTINO, LEANDRO A.</u>; HORA MACHADO, ANTONIO EDUARDO; PATROCINIO, ANTONIO OTAVIO T. Photochemistry of *fac*-[Re(CO)$_3$(dcbH$_2$)(*trans*-stpy)]$^+$: New insights on the isomerization mechanism of coordinated stilbene-like Ligands. **INORGANIC CHEMISTRY**, v. 57, p. 2933, **2018**.

5. <u>FAUSTINO, LEANDRO A</u>; SOUZA, BRENO L; NUNES, BARBARA N; DUONG, ANH-THU; SIELAND, FABIAN; BAHNEMANN, DETLEF W.; PATROCINIO, ANTONIO OTAVIO TOLEDO. Photocatalytic CO$_2$ reduction by Re(I) polypyridyl complexes immobilized on niobates nanoscrolls. **ACS Sustainable Chemistry & Engineering**, v. 6, p. 6073, **2018**.

Publications – Book Chapters

1. NUNES, BARBARA N.; <u>FAUSTINO, LEANDRO A.</u>; MULLER, ANDRESSA V.; POLO, ANDRE S.; PATROCINIO, ANTONIO OTAVIO T. Nb$_2$O$_5$ dye-sensitized solar cells. Nanomaterials for Solar Cell Applications. 1 ed.: **Elsevier**, **2019**, p. 287-322.

Abstracts in scientific meetings

1. <u>FAUSTINO, L. A.</u>; CONCEPCION, JAVIER; HORA MACHADO, ANTONIO EDUARDO; PATROCINIO, A. O. T. A new ruthenium(II) complex as electrocatalyst for CO$_2$ reduction. I Wokshop do Grupo de Materiais Inorgânicos do Triângulo, Uberlândia-MG, **2021**.

2. LUNA, E. T. M.; ZANATTO, L. S.; <u>FAUSTINO, LEANDRO A.</u>; PATROCINIO, A. O. T. Caracterização espectroscópica de um complexo polipiridínico de Ru(II) contendo os ligantes 2,2'-bipiridina e α-oxo-2-piridilacetato. XXXIII Encontro Regional da Sociedade Brasileira de Química, Uberlândia-MG, **2019**.

3. <u>FAUSTINO, L. A.</u>; SOUZA, BRENO L.; NUNES, BARBARA N ; DUONG, ANH-THU; SIELAND, FABIAN; BAHNEMANN, DETLEF W.; PATROCINIO, A. O. T. Photocatalytic CO_2 Reduction by Re(I) Polypyridyl Complexes Immobilized on Niobates Nanoscrolls. XIX Brazillian Meeting on Inorganic Chemistry, Fortaleza-CE, **2018**.

4. <u>FAUSTINO, L. A.</u>; PRADO, F. S.; SOUSA, S. F.; PATROCINIO, A. O. T. Propriedades espectroscópicas de complexos tricarbonílicos de Re(I) com os ligantes 2,2'-bipiridina e ácido 4,4'-dicarboxílico-2,2'-bipiridina. XXX Encontro da Sociedade Brasileira de Química, Uberlândia-MG, **2016**.

5. PRADO, F. S.; SOUZA, S. F.; FAUSTINO, L. A.; PATROCINIO, A. O. T. Estudo da supressão da luminescência do complexo *fac*-[Re(CO)₃(bpy)py]⁺ utilizando hidroquinona e 4-cianofenol. XXX Encontro da Sociedade Brasileira de Química, Uberlândia-MG, **2016**.

6. <u>FAUSTINO L. A.</u>; LACERDA, V. P. B.; PATROCINIO, A. O. T. Síntese do actinômetro tris-(oxalato)ferrato(III) de potássio e calibração de sistema fotoquímico. XXIX Encontro Regional da Sociedade Brasileira de Química, Belo Horizonte-MG, **2015**.

7. <u>FAUSTINO, L. A.</u>; SANTANA, L. K.; FREITAS, L. L.; CANOBRE, S. C.; AMARAL, F. A. Obtenção de compósito de ppi com HDL Co-Al-Cl obtido pelo método de co-precipitação à pH constante e variável à partir de baterias de íons-lítio descartadas. XXI Congresso da Sociedade Iberoamericana de Eletroquímica, La Serena, **2014**.

8. <u>FAUSTINO, L. A.</u>; AMARAL, F. A. Reprocessamento de material catódico para a obtenção de hidróxidos duplos lamelares HDL Co-Al-Cl a partir de baterias de íons lítio pelo método de co-precipitação em pH constante. I Encontro de Iniciação Científica e Tecnológica da UFU, Uberlândia, **2014**.

9. <u>FAUSTINO, L. A.</u>; FREITAS, L. L.; SANTANA, L. K.; CANOBRE, S. C.; AMARAL, F. A. Síntese de Hidróxido Duplo Lamelar via co-precipitação a pH variável a partir de baterias de íons lítio, XVII Encontro Regional da Sociedade Brasileira de Química, São João del-Rei-MG, **2013**.

Oral presentation in scientific meeting

1. <u>FAUSTINO, L. A.</u>; CONCEPCION, JAVIER; HORA MACHADO, ANTONIO EDUARDO; PATROCINIO, A. O. T. A new ruthenium(II) complex as electrocatalyst for CO_2 reduction. I Wokshop do Grupo de Materiais Inorgânicos do Triângulo, Uberlândia-MG, **2021**.

Scientific divulgation

1. FAUSTINO, L. A. Oportunidades para mestrandos, doutorandos e doutores no exterior. VI Workshop de Pós-graduação em Química, Uberlândia, **2019**.

Teaching

1. Teaching assistant – Experimental Chemistry II. Universidade Federal de Uberlândia, June – December **2016**.
2. Teaching assistant - Mathematics for deaf students. Universidade Federal de Uberlândia, April – June, **2017**.
3. Teaching assistant – Inorganic Chemistry III. Universidade Federal de Uberlândia, February – June, **2019**.

Organization of scientific events

1. II Semana da Química UFU. Universidade Federal de Uberlândia, July 21-24, **2014**.